PERFORMANCE COMPARISON OF BRBFS DESIGNED USING DIFFERENT RESPONSE MODIFICATION FACTORS

A THESIS SUBMITTED TO
THE GRADUATE SCHOOL OF NATURAL AND APPLIED SCIENCES
OF
MIDDLE EAST TECHNICAL UNIVERSITY

BY

TUĞBERK GÜNER

IN PARTIAL FULFILLMENT OF THE REQUIREMENTS
FOR
THE DEGREE OF MASTER OF SCIENCE
IN
CIVIL ENGINEERING

SEPTEMBER 2020

Approval of the thesis:

PERFORMANCE COMPARISON OF BRBFS DESIGNED USING DIFFERENT RESPONSE MODIFICATION FACTORS

submitted by **TUĞBERK GÜNER** in partial fulfillment of the requirements for the degree of **Master of Science** i**n Civil Engineering, Middle East Technical University** by,

Prof. Dr. Halil Kalıpçılar
Dean, Graduate School of **Natural and Applied Sciences** _____

Prof. Dr. Ahmet Türer
Head of the Department, **Civil Engineering** _____

Prof. Dr. Cem Topkaya
Supervisor, **Civil Engineering, METU** _____

Examining Committee Members:

Prof. Dr. Murat Altuğ Erberik
Civil Engineering, METU _____

Prof. Dr. Cem Topkaya
Civil Engineering, METU _____

Prof. Dr. Eray Baran
Civil Engineering, METU _____

Prof. Dr. Alp Caner
Civil Engineering, METU _____

Assoc. Prof. Dr. Alper Aldemir
Civil Engineering, Hacettepe University _____

Date: 02.09.2020

I hereby declare that all information in this document has been obtained and presented in accordance with academic rules and ethical conduct. I also declare that, as required by these rules and conduct, I have fully cited and referenced all material and results that are not original to this work.

Name, Last name : Tuğberk Güner

Signature :

ABSTRACT

PERFORMANCE COMPARISON OF BRBFS DESIGNED USING DIFFERENT RESPONSE MODIFICATION FACTORS

Güner, Tuğberk
Master of Science, Civil Engineering
Supervisor : Prof. Dr. Cem Topkaya

September 2020, 114 pages

In this study, buckling restrained braced frames (BRBFs) designed with various response modification factors were examined by numerical analysis and their performances were compared using the next-generation performance assessment approach. Three, six, and nine-story archetypes (low to medium-rise) with response modification factors in the range of 1 to 8 were designed using ASCE7-16, AISC 341-16, and AISC 360-16 specifications. A total of 24 archetypes were analyzed using nonlinear dynamic analysis procedures by subjecting them to both MCE and DBE level ground motions. The ground motion histories were acquired from the FEMA P-695 Far-Field record-set and scaled according to the requirements of the FEMA P-695 methodology. FEMA P-58 methodology was utilized to assess performance. For performance evaluation; peak and residual interstory drift ratios and peak story accelerations were determined and converted to performance quantification values by using the Performance Assessment Calculation Tool (PACT), which is supplied as a part of FEMA P-58 methodology. The probabilistic distributions of repair cost and repair time, unsafe placard probability, and irreparable residual drift probability were obtained, and a comparative study of response modification factors in terms of these results was conducted. The results showed that designing BRBFs using lower response factors increases post-

earthquake performance until the point where acceleration governed nonstructural damages surpass the structural damages. An ideal response factor is proposed herein based on the consequence measures. The study was complemented by investigating the behavior of self-centering BRBFs and comparing their performance with those of conventional BRBFs.

Keywords: Buckling restrained braced frames; response modification factor; next-generation performance assessment; FEMA P-58; self-centering.

ÖZ

FARKLI TAŞIYICI SİSTEM DAVRANIŞ KATSAYISI İLE TASARLANMIŞ BURKULMASI ÖNLENMİŞ ÇAPRAZLI ÇERÇEVELERİN PERFORMANSININ KARŞILAŞTIRILMASI

Güner, Tuğberk
Yüksek Lisans, İnşaat Mühendisliği
Tez Yöneticisi: Prof. Dr. Cem Topkaya

Eylül 2020, 114 sayfa

Bu çalışmada, farklı taşıyıcı sistem davranış katsayısı ile tasarlanmış burkulması önlenmiş çaprazlı çerçeveler (BÖÇÇ), nümerik analiz ile incelenmiş ve performansları yeni nesil performans değerlendirme yaklaşımı kullanılarak karşılaştırılmıştır. Sistem davranış katsayısı 1 ile 8 arasında olan üç, altı ve dokuz katlı prototip yapılar (az-orta katlı yapılar), ASCE7-16, AISC 341-16, ve AISC 360-16 şartnameleri kullanılarak tasarlanmışlardır. Toplamda 24 prototip yapı, doğrusal olmayan dinamik analiz prosedürü ile 50 yılda aşılma olasılığı %2 ve %10 olan yer hareketlerine tabi tutularak analiz edilmiştir. Yer hareketi kayıtları, FEMA P-695 uzak alan kayıt setinden alınıp FEMA P-695 metodolojisinin gerekliliklerine göre ölçeklendirilmiştir. Performansı belirlemek için FEMA P-58 metodolojisinden yararlanılmıştır. Performans değerlendirmesi için, maksimum ve kalıcı ötelenme oranları ve maksimum kat ivmeleri belirlenip FEMA P-58 metodolojisinin bir parçası olarak verilen Performance Assessment Calculation Tool (PACT) ile performans değerlerine dönüştürülmüştür. Onarım maliyeti ve süresinin olasılıksal dağılımları, ağır hasar olasılığı ve onarılamaz kalıcı ötelenme olasılığı değerleri elde edilerek bu değerler ile taşıyıcı sistem davranış katsayıları arasında karşılaştırmalı çalışma yapılmıştır. Sonuçlar, BÖÇÇ'lerin daha düşük sistem davranış katsayısı ile

tasarlanmasının, deprem sonrası performansını, ivmeye bağlı yapısal olmayan hasarların yapısal hasarlardan baskın çıktığı noktaya kadar arttırdığını göstermiştir. Sonuçlar dikkate alınarak ideal sistem davranış katsayısı önerilmiştir. Çalışma, kendinden merkezleyen burkulması önlenmiş çaprazlı çerçevelerin davranışlarının incelenmesi ve performanslarının geleneksel BÖÇÇ'ler ile karşılaştırılması ile zenginleştirilmiştir.

Anahtar Kelimeler: Burkulması önlenmiş çaprazlı çerçeveler; sistem davranış katsayısı; yeni nesil performans değerlendirme; FEMA P-58; kendinden merkezleme

To my family

ACKNOWLEDGMENTS

I would like to thank my supervisor Prof. Dr. Cem Topkaya, for his patience, wisdom, constant support, and encouragement throughout the research and writing of this thesis. He steered me in the right direction whenever he thought I needed it. It was an honor to work with him.

Special thanks to my friends A. Burak Ayaz, Yunus E. Balcıoğlu, and Mehmet Yalçın for their friendship throughout the completion of this thesis. They have been a great source of moral support and advice. I would also like to thank, Muammer Akca, Salih C. Rakıcı, Hasan Korkmaz, L. Kerem Dumanay, and many others for their fellowship during my years in Ankara.

My deepest gratitude goes to my family as I am forever indebted to them for giving me the opportunities that made me who I am today. I want to express my sincere thanks to my mother Fürüzan Güner and my father İsmail Güner for the encouragement and love they have given me my whole life. I would also like to thank the rest of my family for raising me and guiding me.

I would like to express special thanks to my little sister, Talia Ecem Güner, for her endless love. It is my greatest desire to show her the same support later on in life during her better and bigger accomplishments.

A heartfelt thanks go to my girlfriend Kübra Karataş, for her love and being my biggest supporter. I am grateful for her guidance and comments, for all the late nights and early mornings, for being my editor and proofreader and for being with me when I was only thinking about boring engineering stuff. She is my other half and the love of my life.

This study was supported through grant number 217M414 from the Scientific and Technological Council of Turkey (TÜBİTAK). The support during my study is acknowledged as well.

TABLE OF CONTENTS

LIST OF TABLES

TABLES

LIST OF FIGURES

FIGURES

LIST OF ABBREVIATIONS

ABBREVIATIONS

AISC:	American Institute of Steel Construction
ASCE:	American Society of Civil Engineers
ATC:	Applied Technology Council
BFRP:	Basalt fiber-reinforced polymers
BRBs:	Buckling Restrained Braces
BRBFs:	Buckling Restrained Brace Frames
DBE:	Design Basis earthquake
ELF:	Equivalent Lateral Force method
FF:	Far Field
FEMA:	Federal Emergency Management Agency
IDR:	Interstory Drift Ratio
LRFD:	Load & Resistance Factor Design
MCE:	Maximum considered earthquake
R-IDR:	Residual interstory drift ratio
SC-BRBs:	Self-Centering Buckling Restrained Braces
SC-BRBFs:	Self-Centering Buckling Restrained Brace Frames
SDC:	Seismic Design Category
SFRS:	Seismic Force Resisting System
SMA:	Shape Memory Alloy

LIST OF SYMBOLS

SYMBOLS

A_{sc}:	The design BRB core area
$A_{sc,min}$:	The minimum required BRB core area
C:	Cost of BRB, $
$C_{d:}$	Deflection amplification factor
D:	Dead load, kN
E:	Earthquake load
F:	Required strength of BRB core, kN
F_a:	Short-period site coefficient
F_v:	Long-period site coefficient
Fy:	Yield strength, MPa
F_{ysc}:	The yield strength of the BRB core
L:	Live load
L_B:	Required length of BRB, m
P_{max}:	The maximum compression strength of BRB at specific strain value
P_{sc}:	The critical axial load on BRB
R:	Response modification coefficient
S_1:	Spectral response acceleration parameter at a period of 1s
S_{D1}:	Design spectral response acceleration parameter at a period of 1 s
S_{DS}:	Design Spectral response acceleration parameter at short periods
S_{M1}:	Spectral response acceleration parameter at a period of 1s adjusted for site class effects
S_{MS}:	Spectral response acceleration parameter at short periods adjusted for site class effects
S_S:	Spectral response acceleration parameter at short periods
T_{max}:	The maximum tension strength of BRB at specific strain value

T_y:	The Tension yield strength of BRB
α:	The ratio of the yielding length to the total length of a BRB
β:	Compression over-strength adjustment factor
ε_{br}:	The expected design brace axial strain
Ω:	Overstrength Factor
θ :	The brace angle measured with respect to a horizontal axis
θ_s:	Elastic interstory drift angle
ω:	Strain-hardening adjustment factor

CHAPTER 1

INTRODUCTION

1.1 General

The consequences of earthquakes, such as lateral displacements, cause important concerns for engineers. Thus, for many years, conventional braces have been used commonly for damage and displacement control of structures. However, after severe earthquakes and detailed experiments all around the world, the poor performance of the conventional concentrically braced frames (CBF) caused significant concern among the engineers. CBFs displayed limited ductility due to a number of nonductile modes such as connection failure, brace fracture. Furthermore, even when these modes do not arise, CBFs tend to exhibit strength loss under cyclic loading, a situation that can create soft story mechanisms (Sabelli, 2008). The reason for the strength loss is that braces exhibit unsymmetrical and complex hysteretic behavior due to strength deterioration in compression (Sabelli, Mahin and Chang, 2003). This behavior creates substantial energy absorption capacity loss in the lateral resisting system.

In order to overcome these limitations, a more ductile version of braced frames was developed, which is called a Special Concentrically Braced Frame (SCBF). The main aim of this system is to provide ductile system performance through a combination of cyclic brace buckling and tensile yielding. The provisions about the SCBFs encourages engineers to design for the expected yield mechanism of the structure by using the requirements for minimum design strength of elements based on the maximum brace tension and compression forces, and the maximum difference between tension and compression, which anticipated due to buckling. These requirements lead to a significant increase in the cost of the design of connections, columns, and beams.

As a result of the problems mentioned above, a better and symmetric hysteretic behavior, preventing the buckling of the brace in compression, was suggested by researchers. As a result, buckling restrained braces (BRBs) were developed. Rather than design for the excessive differences in brace compression and tension strengths, the problem is solved by the introduction of a brace that exhibits symmetrical hysteretic behavior. A BRB is designed to resist stresses in its steel core while an encasement, which is designed to take no axial stresses, provides resistance to buckling of the core by confinement. This sleeve effectively reduces the slenderness of the core to zero. Consequently, the steel core of the BRB can yield in compression, similar to its tension yielding.

1.2 Development of BRBs

Lateral force resisting systems that uses BRBs, i.e., Buckling restrained braces frame (BRBF) systems, instead of conventional braces were found out to be very effective in dissipating seismic energy in structures since BRBs show the same deformation model in both compression and tension loading cycles with very high energy absorption capacities by non-degrading plastic behavior (Naghavi *et al.*, 2019). Fig. 1.1 shows the hysteretic behavior advantage of BRBs in contrast to conventional braces. Due to enhanced seismic behavior, BRBs are widely used for seismic absorption devices in modern structures, and a lot of research work has been performed in Japan and the rest of Asia (Xie, 2005). Details of the findings were summarized and reported by Uang and Nakashima (2004).

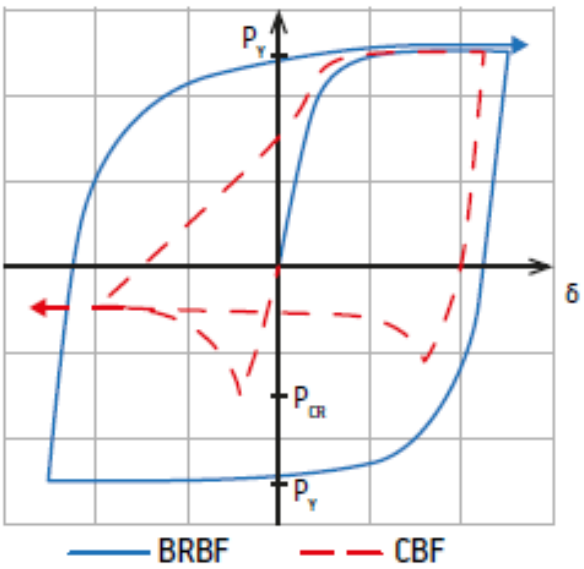

Figure 1.1. Comparison of Hysteretic behaviors (Star Seismic Europe Ltd.)

The first buckling restrained concept appeared in the 1970s; however, limited experimental success was reported. The first successful BRB was achieved by Fujimoto and his team in 1988, and one year later first project application was established. These BRBs were applied to steel frame office buildings in Tokyo in 1990 (Fujimoto *et al.*, 1990), see Fig. 1.2. After this point, the popularity of BRB increased rapidly, and through the 1990s, BRBs were applied to approximately 160 buildings in Japan. Moreover, as a result of perfect energy dissipation capacities, BRBs were also employed as an energy dissipating elastoplastic damper in structures. In 2005, buckling restrained braces were first included in US seismic provisions. Through the following years, BRBs popularity increased significantly, and research and applications can be found in Japan, Taiwan, China, USA, Canada, Turkey, Iran, Italy, and many other countries (Takeuchi and Wada, 2018). Recent BRB application in Turkey, Izmir is given in Fig. 1.3.

Figure 1.2. The first BRBF application in 1989 (Takeuchi and Wada, 2018)

Figure 1.3. Core Brace BRB Application, Folkart Towers, Izmir, Turkey (*Core Brace*)

Typical BRBs include two main parts, the inner steel core and surrounding encasing member. The core carries axial loads and dissipates energy. The core of

BRB generally consists of two parts; nonyielding parts, which are the two outer parts, and yielding part (center part), see Fig. 1.4. The nonyielding (elastic) parts are designed to always stay in elastic limits. The encasing provides lateral support to the core and prevents it from buckling by applying confinement pressure, and force it to buckle at higher modes. As a critical point, the transmission of axial loads to the encasement must be prevented. For this purpose, a low friction interface and sufficient gap for lateral expansion of core due to the Poisson effect must be provided to the design of encasement. The encasement member of BRBs are generally assumed to not carry any axial load, i.e., they are not designed for carrying any axial load. However, in reality, it is impossible to eliminate all stresses on the encasement under compression due to friction and Poisson's effect. For these reasons, BRBs generally have a compression strength higher than their tensile strength.

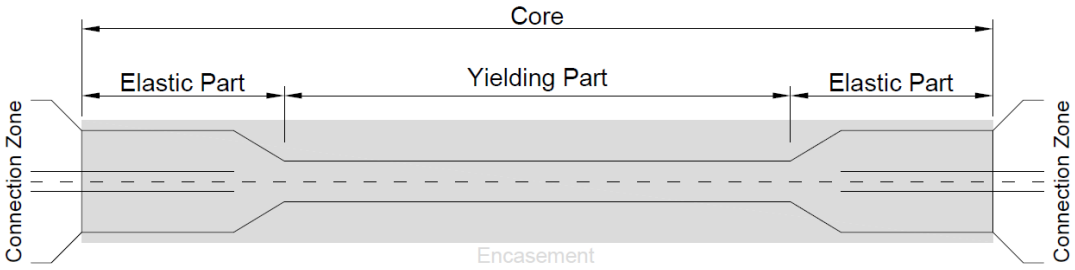

Figure 1.4. Sections of BRBs

According to the restraining mechanism, BRBs can be divide into two main categories; one is restrained by steel tubes filled by mortar or concrete, and the other one is pure steel, i.e., All-Steel BRBs, see Fig. 1.5. Experimental tests on both mortar-filled BRBs (Black, Makris and Aiken, 2004; Tremblay et al., 2006; Fahnestock, Ricles and Sause, 2007) and All-Steel BRBs (Eryasar and Topkaya, 2010; Bozkurt and Topkaya, 2016; Dehghani and Tremblay, 2018) demonstrated the great energy dissipation capacity and efficiency of BRBs for both approaches.

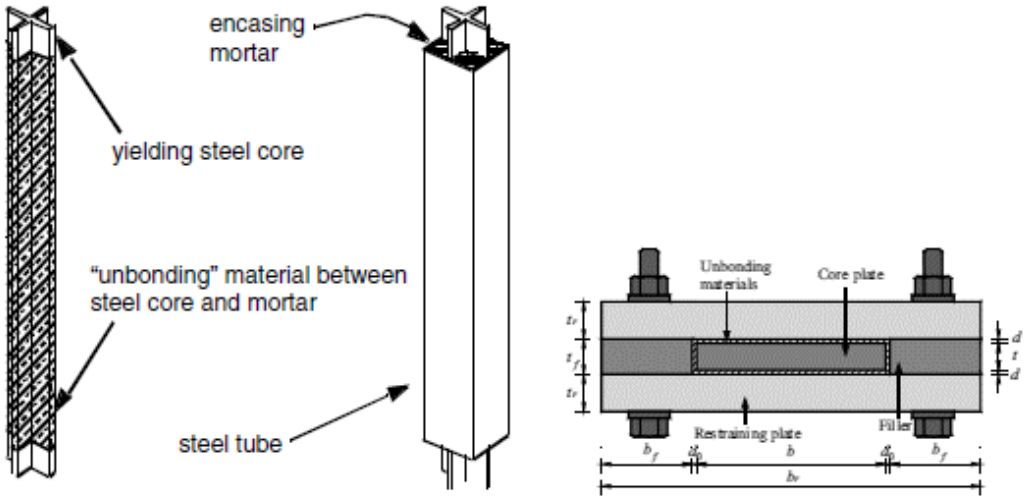

Figure 1.5. Types of BRBs: (a) Mortal Filled BRB, (b) All-Steel BRB

Steel Encased BRBs have many advantages over mortar filled ones, such as being light-weight, simple, and quickly produced since no mortar setting is necessary. The restraining section can be made by welded or bolted connections. The challenge in the All-Steel BRBs is the minimization of the friction between restraining and core plate. The friction is one of the most important concepts in BRB performance since friction can transfer axial loads to the casing, and cause global buckling of BRB or can cause an excessive increase in compressive strength.

1.3 Design of BRBFs

Designing BRBFs carefully with expertise provides a lateral force-resisting system that can convert the essential ductility of steel into system ductility, which consequently controls the response of the structure against severe earthquakes.

As in the case of conventional brace frame systems, many brace configurations are possible, Fig. 1.6. In this study, the inverted V-bracing (chevron) configuration was considered for every BRBF design. The reasons for this decision were explained in the design chapter.

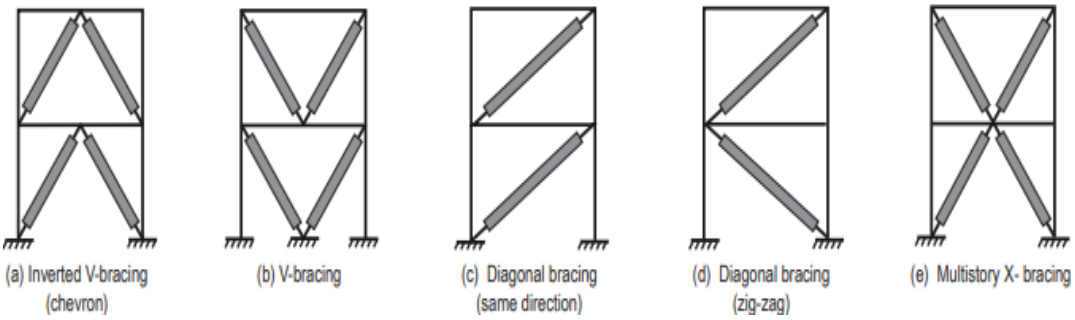

Figure 1.6. Common BRB configurations

According to the AISC Seismic Provisions for Structural Steel Buildings (AISC 341)(American Institute of Steel Construction, 2016a), in the design of BRBF structures, the inelastic deformations under the design earthquake must occur primarily as BRB yielding in tension and compression. Truss analysis is acceptable for determining the axial seismic forces on braces. In addition to forces, strain demands on BRBs due to deformations must be determined. In the code, deformations were defined as the story drift of at least 2% of the story height or two times the design story drift. After axial load and strain demands of BRBs are determined, BRBs shall be designed, tested, and detailed. The required strength of columns, beams, struts, and connections shall be determined using capacity-limited design procedures. A detailed procedure can be found in the AISC Seismic Design Manual (American Institute of Steel Construction, 2012).

In the design of BRBFs, in order to acquire lateral forces in basic level, the equivalent lateral force method might be adopted in accordance with code limitations. In this procedure, in order to count the nonlinear deformations, response modification factor (R), overstrength factor (Ω), and deflection amplification factor (C_d) were introduced to the force and deformation demands, Fig. 1.7. These factors were developed for many types of lateral force resisting systems by researchers and generally differ from one specification to another across the world. In ASCE 7-16 (American Society of Civil Engineers, 2017a), for BRBFs; R, Ω, and C_d values are given as 8, 2.5, and 5, respectively. As mentioned, due to capacity-limited design principles, the design of BRBF is directly related to the axial load and deformations

of BRBs, therefore determining design demands are very crucial to acquire desired performance.

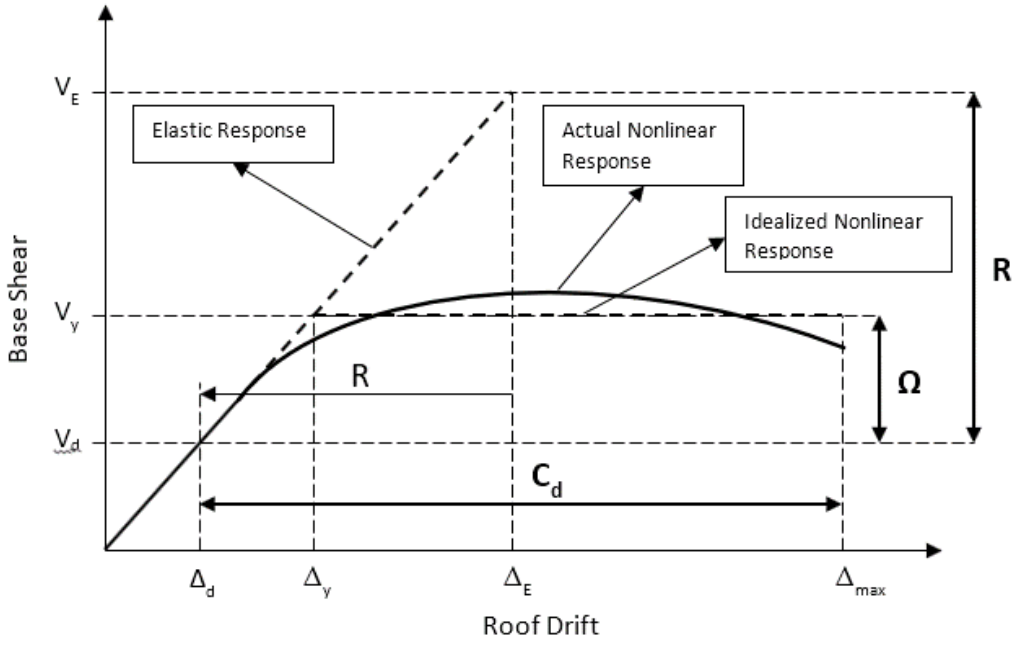

Figure 1.7. Inelastic Design Spectrum and Response Factors

1.4 Literature Survey on BRBFs

In this study, the effect of reducing the response modification factor (R-Factor) on the performance of BRBFs was investigated. For this purpose, 3-, 6- and 9-Story archetypes (low to medium-rise) with R-Factor in the range of 1 to 8 were designed and analyzed. In order to examine the effect of R-Factor in the design of BRBFs, many pieces of research were conducted. One of the prior studies on the effect of the response factor was conducted by Sabelli et.al. (2003). They conducted numerical investigations on 3 and 6 story archetypes by considering R = 6 and R = 8 in the calculations. Beside the R-Factor, they also examined the effect of the flexibility of beams, and the level of seismic hazard on the inelastic dynamic behavior of BRBFs. In the end, their extensive analytical seismic investigation on

BRBFs revealed that the response of BRBF was not sensitive to R-Factor selected in the range of 6 to 8.

One of the extensive investigations about the member and system behavior of BRBFs under seismic motion was conducted by Fahnestock et al. (2007a). They conducted a research program to find out the applicability of US provisions on the design of BRBFs. Nonlinear time-history analyses were conducted for both MCE and DBE seismic hazard levels. The findings reveal that using the equivalent lateral force method in the design process satisfies the LS (Life Safety) and NC (Non-collapse) performance levels. The authors recommended a reevaluation of response factors prescribed in ASCE7-05 (American Society of Civil Engineers, 2005). In brief, R=8 and C_d value equal to R-factor was suggested by authors.

Özkılıç et al. (2018) reported evaluation of seismic response factors for BRBFs using FEMA P695 methodology. In total, 24 archetypes were designed according to the US specifications, and they were examined using nonlinear dynamic analysis under DBE and collapse level ground motions. Their results indicated that current seismic response factors were adequate in terms of interstory drift and cumulative axial strain capacities, while maximum axial strain demands reach more than 2 times the axial strain capacity of the BRB. In addition, they recommended a C_d profile that varies along with the height, because findings pointed out that inelastic deflections were non-uniform over the height.

Asgarian and Shokrgozar (2009) examined the response factors of BRBFs using various heights and bracing configurations, including diagonal, split X, V, and Inverted V bracings and concluded that R factors range between 7 and 9.4. They suggested that the response modification factor, ductility ratio, and overstrength ratio for BRBF as 8.35, 5, and 1.67, respectively. As a side note, the reduction of overstrength and ductility factors were reported as the number of stories is increased. Similar research about BRBFs was also conducted by Mahmoudia and Zareea (2013), and they noted that as the height increase, both overstrength and response modification factors decrease, but their data could not converge on the conclusion

for the ductility factor. As a conclusion, ductility and overstrength factors were recommended as 4.7 and 1.9 for single bay and 8 and 2.4 for double bracing bay (Multi-Story X-Bracing) BRBFs. For the response modification factor, their results show significant variation (7 to 22); consequently, in order to acquire the R-Factor of the building, a detailed analysis was suggested.

Kim and Park (2009) showed that the response modification factor calculated for 4-story low-rise BRBFs is larger than the codified R factor while the ones for medium-rise structures are lower than the codified value. As a part of beta testing of the methodology given in Quantification of Building Seismic Performance Factors (FEMA P695) (Federal Emergency Management Agency, 2009), 10 archetype BRBFs with number of stories varying between 2 and 16 were investigated (NEHRP Consultants Joint Venture, 2010). The results revealed that all of the archetypes designed with the codified R=8 satisfied the performance objectives. A very detailed study was conducted by Bosco and Marino (2013) to develop a design procedure for BRBFs for possible adoption in Eurocode 8 (European Committee for Standardization, 2004). BRBF archetypes were designed with different response modification factors (behavior factors (q)) that varied between 2.5 and 6.5. The continuity condition of columns, design story drift angle, and the inclusion of P-Δ effects during the design stage were considered as the parameters. The value of q was developed as a continuous function of the assumed ductility capacity of the BRBs for cases with different column continuity conditions and the way in which P-Δ effects are accounted for during the design. Moni et al. (2016) studied BRBFs designed according to the Canadian provisions and concluded that R factors range between 4.8 and 6.0 and the codified value of 4.8 in the Canadian specification can be considered as a lower bound. Abou-Elfath et al. (2018) determined that the R factors range between 6.7 and 9.1 for BRBFs designed according to the Egyptian code.

As the literature on response factors of BRBFs suggests, researchers mainly focused on obtaining demand and capacity of members, such as interstory drift ratios

(IDR) and ductility demands, on getting the best performance and energy absorption capacity from the BRBFs. However, as the knowledge and experience on seismic resistant structures increase, the post-earthquake performance of buildings started to get more attention due to significant seismic losses. As a result, many investigations on residual interstory drift ratio (R-IDR) demands, which is one of the major indicators of seismic loss, were conducted by researchers. Erochko et al. (2011) conducted comparative research on residual drift response of SMRF and BRBF structures, with number of stories between 2 to 12. Their findings pointed out that while both lateral force-resisting systems exhibited similar peak IDRs, BRBF structures experienced larger residual drift ratios in comparison to SMRF buildings. The team also created a function to estimate R-IDRs. They concluded that, when 0.5% R-IDR represents total economic loss, BRBF buildings have a high probability of total economic loss after the design-based earthquake. Similar high residual drifts also presented by Fahnestock et al. (2007a) as mean R-IDRs of 0.9% for the DBE seismic hazard level and 2% for the MCE seismic hazard level. In order to investigate the source of residual deformation deficiency of BRBs, Mahdavipour, and Deylami (2014) investigated the effect of strain hardening ratio on residual deformations. Their results showed that while residual demands are very sensitive to strain hardening ratio, IDRs are not. Additionally, investigations to reduce the R-IDRs of BRBF structures were conducted. For instance, Kiggins and Uang (2006) conducted research to decrease the residual drifts on BRBFs by using them with SMRFs as dual systems. Their findings showed that although maximum IDRs were not affected significantly, due to selected SMRFs has very low lateral resisting in comparison to BRBF, a substantial reduction in residual drift was achieved. In recent years, in order to eliminate residual drifts in BRBFs, a new type of brace system which combines self-centering braces with BRBs is developed by researchers. The details about the self-centering BRBs are given in Chapter 6.

1.5 Performance Assessment

Existing seismic provisions are mostly aimed to control the lateral deformations; however, the parameters such as lateral deformations or seismic responses are commonly meaningless to investors and decision-makers because they prefer economic quantities rather than the dynamic response quantities (Guerrero *et al.*, 2017). At this point, converting response quantities to more comprehensible values such as costs plays important roles, and obtained values estimate the post-earthquake performance of a structure. Quantifying post-earthquake behavior in terms of cost and down-time makes the distinction between proposed lateral force-resisting systems clearer for decision-makers.

After severe earthquakes, as some of the buildings survive without collapse, significant damages and corresponding high repair costs could cause them to be demolish. Factors such as residual drift capacity, post-earthquake safety, an initial performance level with respect to design earthquake and repair (or retrofit) cost play an important role in the determination of the repairability of buildings (Polese, Di Ludovico and Prota, 2018). Therefore, predicting the true loss potential of buildings is a critical and complex procedure (Xu *et al.*, 2019).

In order to provide a systematical approach to seismic loss, performance-based design approaches were suggested. The main differences between performance-based design and code-based design are given in Table 1.1, which was prepared by FEMA. Currently, in the US, two generations of performance-based design approaches are available, as named first-generation and second-generation (Next-Generation). ASCE 41 (American Society of Civil Engineers, 2017b) and the performance evaluation part of ASCE 7 can be given as examples for the first-generation approach. As the demands on more detailed performance assessments increased, Federal Emergency Management Agency (FEMA) and Applied Technology Council (ATC) introduced a program to create a next-generation performance-based seismic design guideline in 2006 under ATC-58 project to expand the available procedures to improve and advance the available performance

evolution procedures (Federal Emergency Management Agency, 2006). As a product of this program, in the first phase, the next-generation performance-based design code FEMA P-58 was released by FEMA in 2012 and as a part of the second phase updated version of the code was published in 2018. In this study, the second phase FEMA P-58 (Federal Emergency Management Agency, 2018c), was used to acquire performance.

Table 1.1 Comparison of code-based and performance-based approaches (FEMA, 2018a)

Type of Loss	Code-Based Approach	Performance-Based Approach*
Structural Damage	Damage at or below a level expected to keep occupants safe in large earthquakes.	Evaluates and controls the likely extent of damage to the building structure.
Nonstructural Damage	Some components are designed to remain in position. Other components and contents are not regulated.	Evaluates and controls the likely extent of damage to a building's nonstructural elements and some contents.
Casualties, including Deaths and Injuries	In newer buildings, occupants are expected to be safe. Retrofits of existing buildings are intended to improve but not guarantee safety.	Evaluates and controls the likelihood of deaths or injuries due to building damage.
Financial Losses from Structural and Nonstructural Damage	Not evaluated.	Evaluates controls the likely expected direct dollar losses from damage.
Likelihood of Unsafe Placard	Not evaluated.	Evaluates and controls the likelihood of receiving a post-earthquake unsafe placard (red tag) that restricts entry and use.
Repair Time	Not evaluated.	Evaluates and controls the likely duration of repairs, a key factor in how long a building will be unusable after an earthquake, and the chance a building will need to be demolished.
Environmental Impacts	Not evaluated.	Evaluates and controls the likely carbon and energy impacts due to building repairs or demolition.

* *Note:* Only the FEMA P-58 methodology can estimate all the listed aspects of earthquake performance.

FEMA P-58 framework estimates the economic losses in four steps. As a first step, using computer analysis, the structural responses at different seismic hazard levels were determined. The procedure also includes a simplified methodology when detailed analyses are not possible. In the second step, expected damages to structural and nonstructural components were estimated based on fragility functions. In the

next step, economic consequences were evaluated using a set of consequence functions to translate damage to potential repair costs, times, and casualties. At the final step, the consequences of individual components were aggregated at the building level to obtain performance measures (Cardone and Perrone, 2015). The flowchart of the process, which was published by FEMA, is given in Fig 1.8.

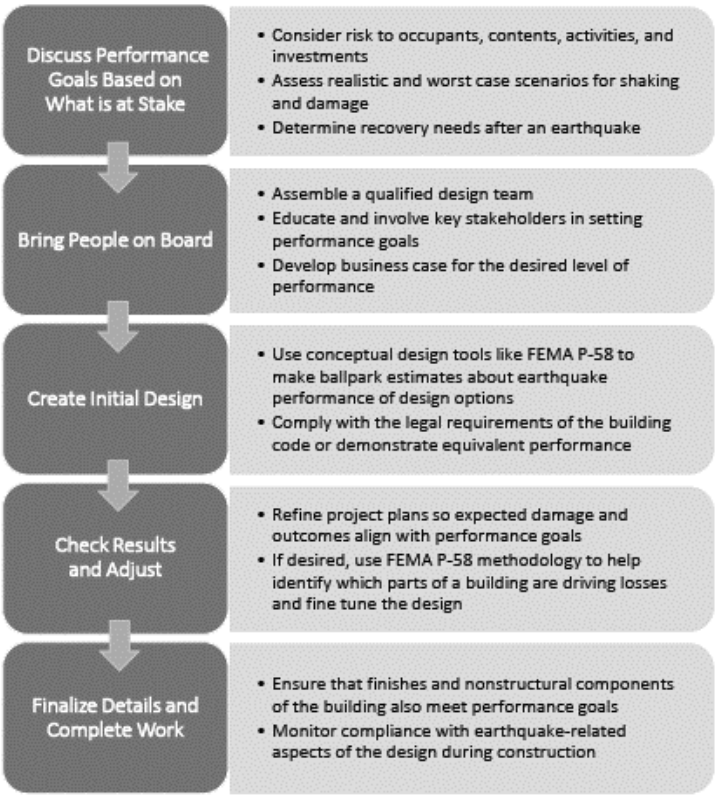

Figure 1.8. Flowchart of performance-based seismic design process

In terms of the first-generation performance evolution of BRBFs, Speicher, and Harris (2018) investigated the performance of BRBF buildings in accordance with ASCE 41. BRBF structures, which were designed using equivalent lateral force and response spectrum analysis procedures, were analyzed using linear and nonlinear material definitions under static and dynamic analysis procedures. The analyzed frames mostly satisfied the performance objectives of ASCE 41; however, 8 Story buildings and the base columns of structures showed deficiencies. One of the important findings was that the linear procedures produced less conservative results

in contrast to nonlinear procedures; consequently, refinement in ASCE 41 procedure suggested. At last, they determined that the unsatisfactory performance of braces in the nonlinear procedures was not caused by the proportioning of members due to distributed failures along with the height. This condition shows the difficulty of creating a relationship between the performance objectives of ASCE 41 and ASCE7.

Example applications of FEMA P-58 procedures on older R/C buildings can be found at the works of D. Cardone and G. Perrone (2015) and Romano et al. (2015). Zeng et al. (2016) conducted research on regional earthquake loss prediction and proposed a method to extend the economic loss prediction method of FEMA P-58 to regional earthquake loss prediction. Del Gobbo et al. (2018) assessed the seismic performance of Eurocode 8 compliant CBF buildings using FEMA P-58. Their results show that the repair cost calculations were sensitive to nonstructural quantities and nonstructural elements' seismic design categorization. As a result, they concluded that modern Eurocode drift limits do not account for acceleration sensitive damages. Jarrett et al. (2015) conducted an investigation on two new innovative structural seismic resisting systems using FEMA P-58 and FEMA P695 procedures. They determined the performance of archetypes under four different seismic hazard levels (Serviceability, DBE, MCE, and Near Collapse). They concluded that, at low ground motion intensities, the contributions to cost come mainly from the nonstructural fragilities while at higher intensities, more structural components would likely be damaged and contribute to the cost. Guerrero et al. (2017) evaluated the economic benefits of using BRBFs in hospitals, and the results showed that structures equipped with BRBs introduced lower expected losses and lifecycle costs in contrast to structures without BRBs.

In terms of deficiencies of the FEMA P-58, several studies were conducted. The work of Safiey et al. (2019) presented that the FEMA P-58 irreparability model often results in an overestimation of direct building losses due to demolish probability solely based on the residual drift. In contrast, the demolition of buildings is determined depending on factors such as structural, strategic, and financial decision variables. Additionally, research on the 2009 L'Aquila earthquake shows

that the predicted seismic performance quantities using FEMA P-58 have an error in the range of 30% to 48% when compared with the actual loss. This error was connected to the condition that no adjustment applied to local costs and since the consequence functions of FEMA P-58 are based on the data of building costs in Northern California in 2011 (Del Vecchio *et al.*, 2018).

1.6 Scope

The goal is to investigate and compare the performance of BRBF buildings with various R-factors by using next-generation performance approaches. The changes in initial cost and post-earthquake performance pointers such as repair costs, downtime and replacement probabilities, in other words, seismic loss parameters, were examined. The examination was conducted to reach the optimum performance from BRBFs in terms of minimum seismic loss and post-earthquake performance with minimal seismic demands and initial costs. Performance comparisons were done for both DBE (10% in 50 years) and MCE (2% in 50 years) seismic hazard levels to detect the impact of reducing R-Factor, while increasing initial cost for different earthquake intensities at the same time. The FEMA P-58 methodology was applied to assess the post-earthquake performance of 3-, 6- and 9- story BRBF archetypes. In total, 8 archetypes for 3 different height structures were designed with R-Factors in the range of 1 to 8. Each archetype was designed according to AISC 341-16 and ASCE 7-16 procedures. The AISC 360-16 (American Institute of Steel Construction, 2016b) procedure was acquired in necessary places. The design parameters were selected with the help of the FEMA P695 guideline. Due to the requirement of performance assessment, nonlinear dynamic analyses were conducted for ground motion set supplied by FEMA P695. A total of 44 ground motion history was scaled and applied to archetypes. Finally, the results were extensively discussed from the perspective of both the engineer and the decision maker, as suggested by FEMA P-58. In addition, performances of self-centering BRB frames were investigated and compared with conventional BRBFs.

CHAPTER 2

DESIGN OF ARCHETYPES

In this study, a total of 24 archetypes with different response factors (R=1, 2, 3,4,5,6,7,8) and the number of stories (3,6,9) were designed to obtain optimum post-earthquake performance. In the design process, the limitations and guidance of Minimum Design Loads and Associated Criteria for Buildings and Other Structures (ASCE 7-16), Seismic Provisions for Structural Steel Buildings (AISC 341-16) and Specification for Structural Steel Buildings (AISC 360-16) were used. One of the noteworthy decisions is that it was assumed that wind load did not govern against earthquake loads since the main aim is to compare post-earthquake performances. The maximum value of *R* was limited to 8, which is the recommended design value by ASCE7-16. Values greater than 8 may be considered as well; however, a complementary study based on FEMA P695 would need to be conducted to evaluate the collapse potential of systems with values higher than the codified value. Each archetype was optimized in order to obtain minimum structural weight and cost. Besides the core of BRBs, for all structural members, A992 grade steel (Fy = 345MPa) was used.

2.1 Description

Three, six, and nine-story archetypes were considered for this study since low and medium-rise structures were evaluated, and different story heights also represent the results for structures with different periods. The story heights were taken as 3.5m for all stories except the first floor, which was 4.3m. Fig. 2.1 presents the typical elevation plan for archetypes. It was assumed that columns were changed in every 3

stories as it is mostly applicable design procedure in the field. For simplicity, each individual archetype uses the same beam size. As a brace configuration, chevron bracing (inverted-V) was considered. This type of configuration was chosen to ensure that braces are strength controlled (Özkılıç, Bozkurt and Topkaya, 2018), and using diagonal BRB is not practical because of the wide span.

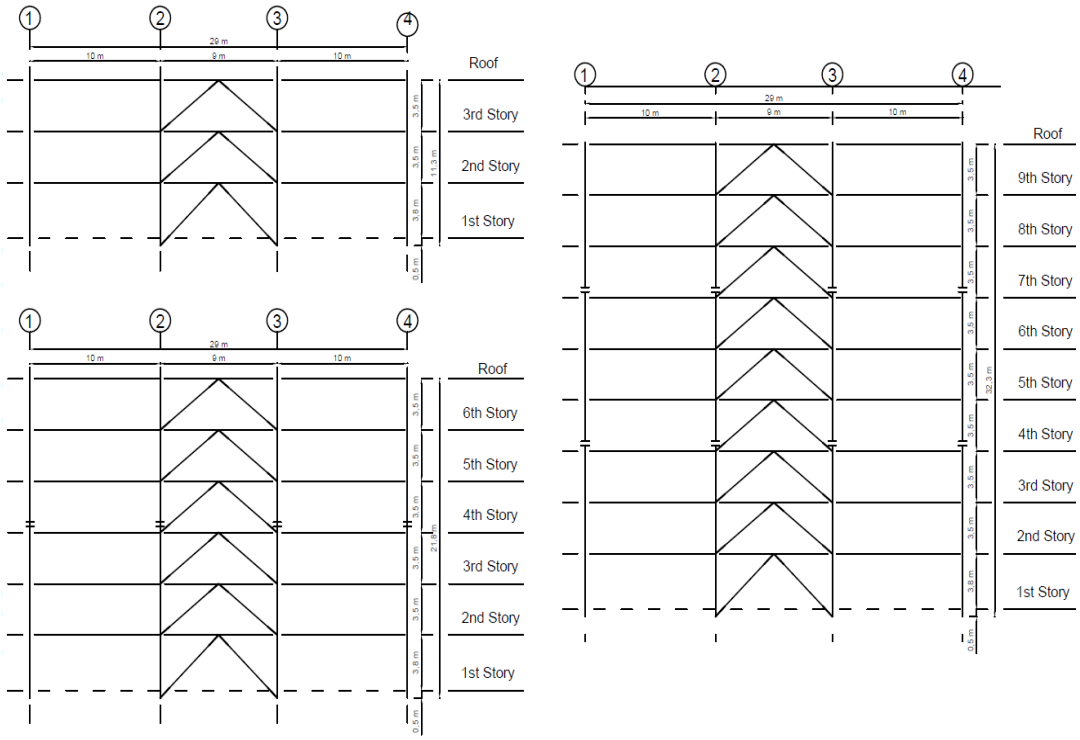

Figure 2.1. Elevation plan for archetypes

Regular square floor plan, shown in Fig. 2.2, with 29m side length, was used for all archetypes. In the design process, to ensure strength govern design of BRBs, wider BRB bay was required. As a result, the 9-meter bay was used for the BRBF application. For other bays, 10m width was adopted. Bay sizes were kept the same for both directions. Each archetype has four bays with chevron BRBF, two in the east-west direction, and two in the north-south direction. As a result of the square and symmetric floor plan, a single BRBF design was sufficient per archetype. Only

one BRBF was designed and analyzed per archetype, and results were interpreted for both directions.

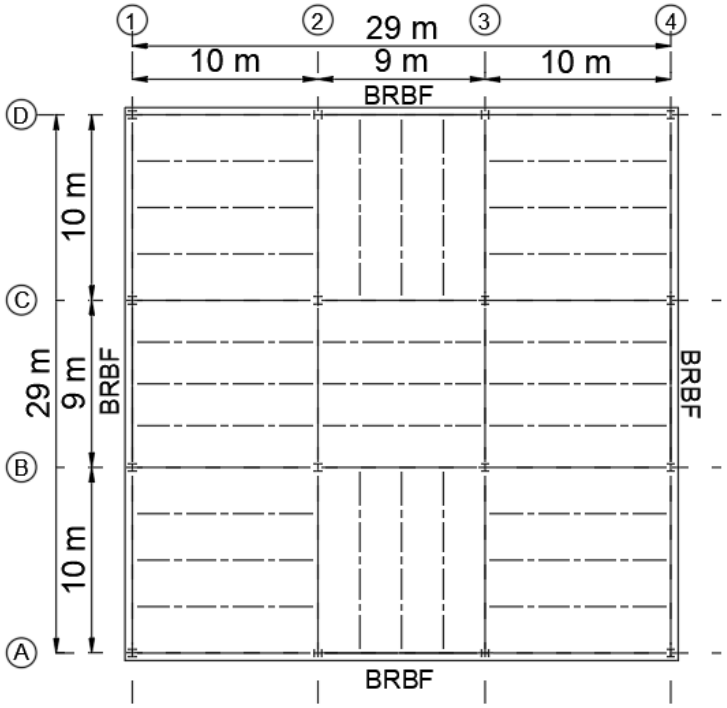

Figure 2.2. Floor plan

2.2 BRB Properties

In basic BRB design, a typical BRB core is composed of a yielding segment at the middle and two non-yielding segments at ends (see Fig. 2.3). The length of the yielding part depends on the required stiffness of brace and manufacturers' choice. For this study, the length of the yielding segment was considered as 2/3 of the total length of the BRB core. The BRB total length was considered as the distance between the nodes of beam-column-brace intersections. The non-yielding part of the core was considered as a cruciform shape with two times the area of yielding segment. The stiffness of BRB was computed using weighted averages of yielding and non-yielding parts of the core with respect to their length. For core plates of BRBs, S235 grade steel with a F_y = 235MPa was used. S235 grade is a common type of steel used in Europe.

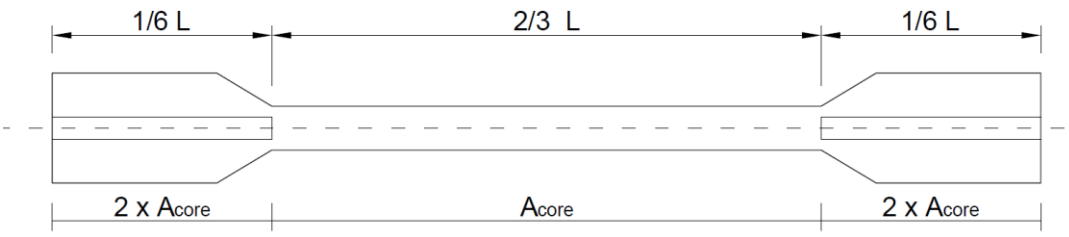

Figure 2.3. BRB core details

2.3 Overview of Design Approach

In the selection of the seismic hazard level, FEMA P695 methodology was utilized. Since in the methodology, different seismic design categories are available, to evaluate critical performance and with the reference of ASCE 41 performance evaluation procedure, SDC D_{max} seismic hazard level was selected for design procedures. This seismic level represents the highest seismic hazard level in the methodology. Furthermore, beta testing of the Methodology (NEHRP Consultants Joint Venture, 2010) on BRBFs showed that the response modification factor is governed by the SDC D_{max}, and the overstrength factor is governed by SDC D_{min} and lower seismic hazard levels. Since in this study, the response modification factor was considered, the selection of SDC D_{max} is suitable. Spectral response acceleration parameters for maximum considered earthquake (MCE) at SDC D_{max} and 5% damped case values are presented in Table 2.1. Adjusted values for both spectral response acceleration parameter at a short period (S_s) and spectral response acceleration parameter at a period of 1s (S_1) for default site class D is also presented. It must be noted that FEMA P695 guideline uses ASCE 7-05 site coefficients for earthquake demands, and these values were considered despite ASCE 7-16 was used for other parameters. For the seismic design of the structural system, as ASCE 7 defines the design-based earthquake (DBE), demands are taken as two-thirds of the MCE demands. The spectral accelerations for DBE and MCE are given in Fig 2.4.

In this study, the fundamental period of the building (T) is considered equal to C_u times the approximate fundamental period (T_a), where C_u coefficient is 1.4 for high seismic regions and T_a is defined in ASCE7-16 as a function of the type of SFRS and building height. The same approach is recommended in FEMA P695 for the design of archetypes. It should be noted that the $T=C_u \times T_a$ provides a non-conservative approach as the R factor is reduced. This assumption was adopted to avoid iterations in the design process and to prevent introducing an additional penalty for systems designed with reduced R factors.

Table 2.1 Design spectral acceleration values

	S_S (g)	F_a	S_{MS} (g)	S_{DS} (g)
SDC Dmax	1.5	1.0	1.5	1.0

	S_1(g)	F_v	S_{M1}(g)	S_{D1}(g)
SDC Dmax	0.6	1.5	0.9	0.6

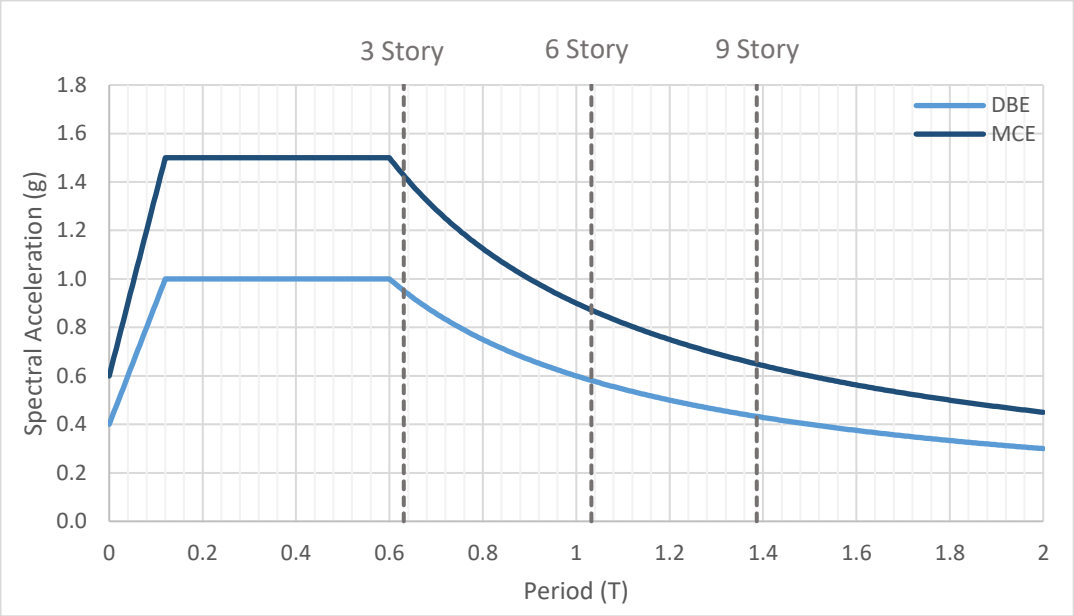

Figure 2.4. DBE and MCE spectrum

For the design of BRBFs, Equivalent Lateral Force (ELF) method was utilized. According to ASCE 7-16, the ELF method is permitted for structures with no structural irregularities and not exceeding 160 ft (48.8 m) in structural height. As the maximum structural height for considered archetypes is 32.3m, and no irregularity exists, the ELF method was applicable for all archetypes.

ASCE 7-16 recommended response modification factor (R), the over-strength factor (Ω_o), and the deflection amplification factor (C_d) are 8, 2.5, and 5, respectively. In this thesis, the effects of different R-Factors were investigated. The ELF method was used for the design of archetypes. The deflection amplification factor (C_d) recommended by ASCE7-16 is 5 for BRBFs. This factor is used to calculate the lateral frame drifts which, in turn, are used to calculate the BRB axial deformation demands. Because the lateral forces are reduced by the R factor, the elastic displacements calculated using the ELF method should be amplified by a displacement amplification factor (C_d) to calculate the design story drifts. According to Newmark's equal displacement rule, C_d should be equal to the R factor. This is the type of approach adopted in Eurocodes, where the elastic displacements are amplified by the q factor. On the contrary, ASCE7-16 recommends a C_d factor for each SFRS, which is generally different than the R factor. In the present study, the C_d/R ratio was kept constant (5/8=0.625) for archetypes designed using response factors other than the codified limit of 8. It should be mentioned that the design of members was controlled by strength limit states rather than the lateral drift limits. The redundancy factor was taken as one ($\rho = 1$) for all archetypes for design of structural system archetypes, since larger values of ρ would be unconservative as FEMA P695 methodology suggests.

For each number of stories, 8 different archetypes were designed with response modification factors in the range of 1 to 8. The base shear and distribution of design lateral story loads with respect to the R-factor is given in Table 2.2.

Table 2.2 Lateral load distribution in terms of R-Factor

Lateral Load Distribution (kN)			
Story No:	**3 Story**	**6 Story**	**9 Story**
9th	-	-	3826.4/R
8th	-	-	3242.6/R
7th	-	-	2689.6/R
6th	-	4523.6/R	2169.4/R
5th	-	3624.4/R	1685.2/R
4th	-	2770.2/R	1240.5/R
3rd	5915.5/R	1968.4/R	840.3/R
2nd	3985.5/R	1231.0/R	492.1/R
1st	2113.2/R	579.1/R	208.4/R
Base Shear	12014.3/R	14697.0/R	16394.9/R

A dead load of 5 kN/m^2 and a live load of 2 kN/m^{2,} which are typical for steel office buildings, were considered as the gravitational loads. Considered load combinations, that were taken from ASCE 7-16, are 1.4D, 1.2D+1.6L, 1.4D+L+E, 1.4D+L-E, 0.7D+L+E, 0.7D+L-E. The E represents lateral earthquake loads, and D and L represent dead and live loads. No wind or snow load effect was considered.

2.4 Computation of Demands and Design of BRBs

In the first step, the axial loads on the BRBs were determined using SAP2000 analysis software. The dead, live, and lateral loads were inputted to the braced frame. Every beam to column connection nodes and base nodes in frames were taken as a pin connection. This design approach was selected to investigate the behavior of BRBF without the influence of moment frame actions. The braces were modeled as truss elements with stiffness equal to equivalent stiffness of non-yield and yielding parts. The yield strength of braces was taken as 235 MPa, and columns and beams were taken as 345 MPa. For all members, the modulus of elasticity was taken as 200 GPa. In the calculation of minimum required design BRB axial strength for both

tension and compression, a resistance factor of 0.9 was applied as recommended by AISC 341-16 provision for LRFD design. As a critical axial load, the maximum value between compression and tension loads was considered. Minimum required BRB core area was calculated using the following equation:

$$A_{sc,min} = \frac{P_{sc}}{0.9 * F_{ysc}} \qquad (1)$$

In the relationship, $A_{sc,min}$ is the minimum require an area of BRB steel core, P_{sc} is the critical axial load from analysis and F_{ysc} is the yield strength of the BRB core. After minimum required cross-sectional areas were determined, the values were rounded up to the next integer for simplicity and safety.

The maximum observed design interstory drift ratios (IDR) between stories per archetype are given in Table 2.3. The allowable story drift ratio was considered as 0.02 in accordance with ASCE7-16. Consequently, none of the archetypes showed excessive story drifts, and, in all cases, the design of BRBFs was governed by the strength limit states.

In the Table 2.4, the designed cross-sectional areas for BRB cores for all archetypes are given in terms of mm^2. As a result of the increased response modification factor, BRB sizes decrease in a nonlinear fashion due to the existence of gravity loads. It must be noted that, in the determination of sizes, the architectural requirements were neglected.

Table 2.3 Deflection amplification factor and max design IDR values

		Max Design IDR %		
R:	**C_d:**	**3 Story**	**6 Story**	**9 Story**
1	0.63	0.34	0.57	1.16
2	1.25	0.64	0.69	1.27
3	1.88	0.54	0.81	1.39
4	2.50	0.64	0.92	1.49
5	3.13	0.73	1.02	1.60
6	3.75	0.82	1.13	1.68
7	4.38	0.91	1.20	1.76
8	5.00	0.97	1.26	1.82

Table 2.4 Determined BRB core areas

		Brace Area (mm^2)							
NS:	**Story:**	**R=1**	**R=2**	**R=3**	**R=4**	**R=5**	**R=6**	**R=7**	**R=8**
3	**3**	9650	5275	3825	3075	2650	2350	2150	1975
	2	15275	8100	5700	4475	3775	3300	2950	2700
	1	20050	10450	7225	5625	4650	4025	3550	3225
6	**6**	7550	4225	3125	2550	2225	2000	1825	1700
	5	12850	6875	4875	3875	3275	2875	2575	2375
	4	16900	8900	6250	4900	4100	3550	3175	2875
	3	19725	10325	7175	5600	4675	4025	3600	3250
	2	21450	11200	7775	6050	5025	4325	3850	3475
	1	24425	12650	8700	6725	5550	4750	4200	3775
9	**9**	6550	3725	2775	2300	2025	1825	1675	1575
	8	11250	6075	4350	3500	2975	2625	2375	2175
	7	15275	8100	5725	4525	3800	3300	2975	2725
	6	18275	9600	6700	5250	4375	3825	3400	3075
	5	20900	10925	7600	5925	4925	4250	3775	3425
	4	22600	11775	8150	6325	5250	4525	4000	3600
	3	23850	12375	8575	6650	5500	4750	4200	3775
	2	24450	12700	8775	6800	5625	4850	4275	3850
	1	27250	14050	9650	7450	6125	5250	4600	4125

2.5 Capacity Design of Columns and Beams

According to AISC 341-16, beam and column sizes of BRBFs should be determined using capacity-limited seismic load effects. These loads are determined using the forces using adjusted brace strengths at expected deformations. The expected deformation is defined as a story drift of at least 2% of the story height or two times the design story drift, whichever is larger. BRBFs are designed with regarding the principle that inelastic deformations under design-based earthquake will occur primarily as brace yielding in tension and compression. For the design process, the steps which were given in the AISC Seismic Design Manual (American Institute of Steel Construction, 2012), was followed.

To estimate the design brace axial strains, from design story drifts, the beam and columns of a story were assumed to be rigid, no moment resistance at the connections, and the braces were assumed to be only members that deform. For simplicity, Eq. 2 is used for the conversion of elastic story drifts to brace axial strains in comparison to the trigonometric approach. The expected design brace axial strain, ε_{br} is given as a function of elastic interstory drift angle θ_s (interstory drift divided by the story height), the brace angle measured with respect to a horizontal axis θ, and the ratio of the yielding length to the total length of a BRB α. Alternatively, it is allowed that brace deformations can be determined from the nonlinear analysis in the provision.

$$\varepsilon_{br} = \frac{C_d * \theta_s}{\alpha} * \sin\theta * \cos\theta \qquad (2)$$

As mentioned, expected deformations are the brace deformation from the largest of 2% drift or two times the design story drift. In order to obtain the forces on columns and beams, the strength of BRBs at expected deformations must be acquired. Due to compression over-strength and strain-hardening effects on the BRBs, adjustment to initial strength must be applied. Compression over-strength adjustment factor, β, and strain-hardening adjustment factor, ω, were used to calculate the strength of BRB at the expected deformation level. The Fig. 2.5 shows the bilinear force-displacement relationship.

To acquire adjustment factors for BRBs, a generic backbone curve, which is presented by Lopez and Sabelli (2004) was used. The compression and tension strength adjustment factors were obtained with respect to design axial strains for expected deformations. Two times the design brace strains, expected brace deformation in terms of BRB core strain, adjustment factors, and adjusted strengths for the first story of each archetype are given in Table 2.5.

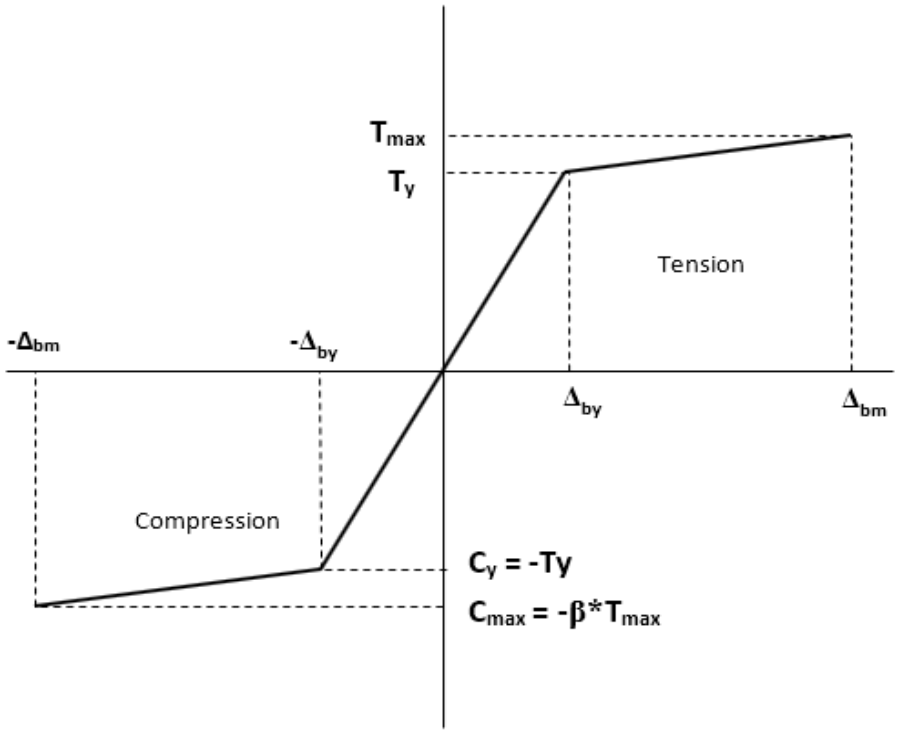

Figure 2.5. BRB strength adjustment

where;

$$T_y = F_{ysc} * A_{sc} \quad (3)$$

$$C_{max} = -\beta * \omega * T_y \quad (4)$$

$$T_{max} = \omega * T_y \quad (5)$$

After adjusted BRB strengths were obtained, the forces applied on columns and beams were computed using load combinations. It must be noted that in the load combinations where no earthquake load applied, it was assumed that the BRBs provide no support for dead and live loads. The details of selected columns and beams are given in Table 2.6 and 2.7. In each archetype, beam sections were kept constant between floors for simplicity. For columns, the sections were kept constant for 3 stories to represent real design procedures. The LRFD design manual (American Institute of Steel Construction, 1994) was used as a supportive source to choose column and beam sizes in order to obtain minimum weight and cost.

Table 2.5 BRB adjustment factors and design capacity in tension and compression for 1st story of each archetype

Archetype	Expected Brace Strain (%)	Brace Yield Strength (kN)	ω	wβ	β	Tmax (kN)	Cmax (kN)
R1-3S	1.51	4711.8	1.38	1.49	1.07	6512.2	7000.0
R2-3S	1.51	2455.8	1.38	1.49	1.07	3394.1	3648.4
R3-3S	1.51	1697.9	1.38	1.49	1.07	2346.7	2522.4
R4-3S	1.51	1321.9	1.38	1.49	1.07	1827.0	1963.8
R5-3S	1.51	1092.8	1.38	1.49	1.07	1510.3	1623.4
R6-3S	1.51	945.9	1.38	1.49	1.07	1307.3	1405.2
R7-3S	1.51	834.3	1.38	1.49	1.07	1153.0	1239.4
R8-3S	1.51	757.9	1.38	1.49	1.07	1047.5	1125.9
R1-6S	1.51	5739.9	1.38	1.49	1.07	7933.2	8527.4
R2-6S	1.51	2972.8	1.38	1.49	1.07	4108.7	4416.5
R3-6S	1.51	2044.5	1.38	1.49	1.07	2825.7	3037.4
R4-6S	1.51	1580.4	1.38	1.49	1.07	2184.3	2347.9
R5-6S	1.51	1304.3	1.38	1.49	1.07	1802.6	1937.7
R6-6S	1.51	1116.3	1.38	1.49	1.07	1542.8	1658.4
R7-6S	1.51	987.0	1.38	1.49	1.07	1364.2	1466.3
R8-6S	1.60	887.1	1.41	1.51	1.08	1246.8	1342.9
R1-9S	1.51	6403.8	1.38	1.49	1.07	8850.8	9513.7
R2-9S	1.51	3301.8	1.38	1.49	1.07	4563.4	4905.2
R3-9S	1.51	2267.8	1.38	1.49	1.07	3134.3	3369.1
R4-9S	1.51	1750.8	1.38	1.49	1.07	2419.7	2601.0
R5-9S	1.51	1439.4	1.38	1.49	1.07	1989.4	2138.4
R6-9S	1.51	1233.8	1.38	1.49	1.07	1705.2	1832.9
R7-9S	1.56	1081.0	1.40	1.50	1.08	1509.2	1624.2
R8-9S	1.68	969.4	1.42	1.54	1.08	1381.2	1490.0

Table 2.6 Column and beam sizes of Archetypes (R1 through R4)

SC:			R1	R2	R3	R4
3	**Columns**	**1-3**	W14x132	W10x100	W10x77	W10x68
	Beams		W21x147	W16x89	W16x57	W16x57
6	**Columns**	**4-6**	W10x112	W10x77	W10x60	W10x60
	Columns	**1-3**	W14x370	W14x211	W14x176	W14x145
	Beams		W21x182	W16x100	W16x67	W16x57
9	**Columns**	**9-7**	W12x106	W14x74	W10x60	W10x60
	Columns	**4-6**	W14x342	W14x211	W14x159	W14x145
	Columns	**1-3**	W14x665	W14x398	W14x311	W14x257
	Beams		W21x201	W21x101	W16x77	W16x57

Table 2.7 Column and beam sizes of Archetypes (R5 through R8)

SC:			R5	R6	R7	R8
3	Columns	1-3	W10x60	W10x60	W10x60	W12x53
	Beams		W16x57	W16x57	W16x57	W16x57
6	Columns	4-6	W10x60	W10x60	W14x53	W14x53
	Columns	1-3	W14x132	W14x132	W12x120	W12x120
	Beams		W16x57	W16x57	W16x57	W16x57
9	Columns	9-7	W10x60	W10x60	W10x60	W14x53
	Columns	4-6	W14x132	W14x132	W12x120	W12x120
	Columns	1-3	W14x233	W14x211	W14x211	W14x193
	Beams		W16x57	W16x57	W16x57	W16x57

2.6 Initial Cost Estimation of Seismic Force Resisting System

In order to interpret the repair costs between various design response factors, initial costs of archetypes were estimated. In the estimation, only the cost of 4 BRBFs was taken into account, since the difference in response factor does not affect the size and cost of gravity frame parts. As the symmetric and square floor plan was adopted with four exactly same BRBF, only one BRBF cost was estimated and multiplied by four. The estimation of the cost was divided into three-part; the cost of the BRB members, costs of beams, columns and connections, and the cost of foundation.

As a first step, the BRB costs were computed. Since BRBs consist of many parts, the generic steel per kg approach is not sufficient. Furthermore, commercially available BRBs are commonly patented, which consequently increases the costs. As a result, estimating the cost of BRBs is difficult, and the help from a manufacturer was needed. In the consultancy of an BRB manufacturer, a series of cost data for different BRBs were obtained and BRB cost function (Eq. 6) which has two parameters; BRB required strength “F” in terms of kilonewton and the length “L_B” in terms of meters, was developed. The function is plotted in Fig. 2.6.

$$C = \left(\frac{7 * F^2}{10^5} + 0.39 * F + 185.2\right) * L_B \qquad (6)$$

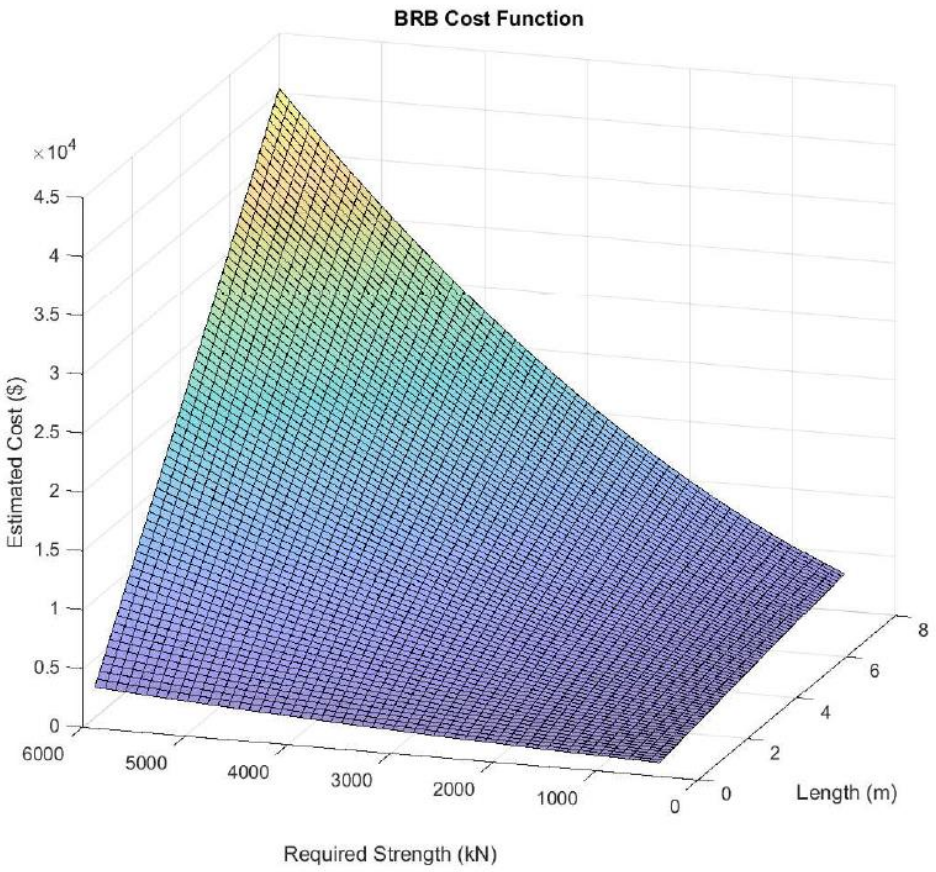

Figure 2.6. Graphical representation of BRB initial cost estimation function

In the second step, the cost of beams and columns were computed with respect to steel weight. The cost was estimated using a cost for steel of $3 per kg (Guerrero *et al.*, 2017). In addition, 5% of beam and column cost was taken into account for connections. The change in the total mass of beams and columns of a single BRBF is indicated in Fig. 2.7 where the mass of the framing was normalized by the mass of the BRBF bay designed with *R*=8. It is clear from this figure that there is a gradual increase in the mass of the members as the *R* is reduced. The mass increases in average by 16 percent when *R* is reduced from 8 to 4.

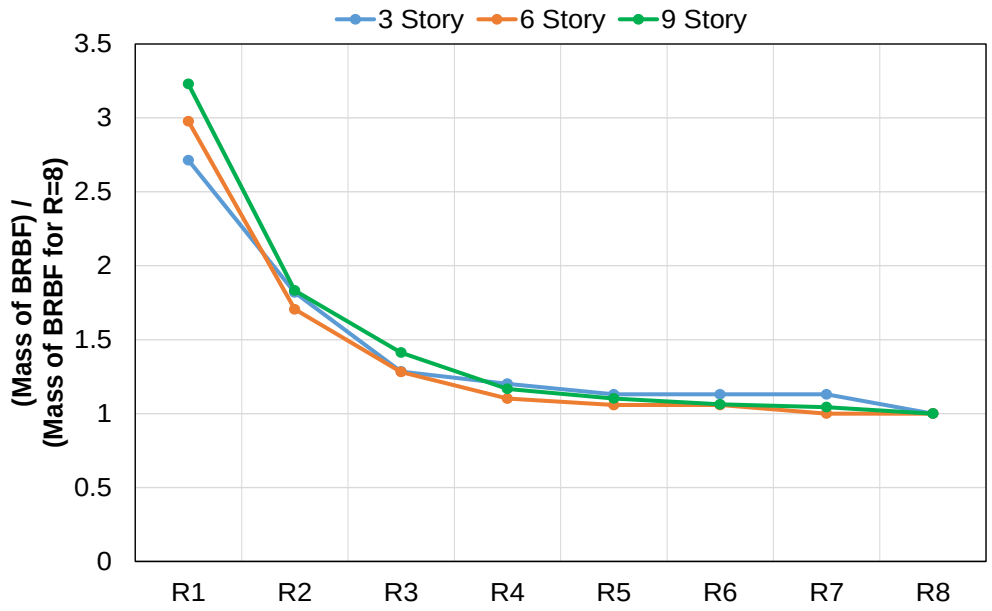

Figure 2.7. Mass of a Single BRBF Bay Excluding BRBs

In the last step, the foundation cost was taken as 50% of the total cost. This percentage was taken from the report of Star Seismic (Star Seismic Europe Ltd., 2010). As different foundation costs are possible with different soil types and conditions, the high foundation cost was selected for more critical difference and to stay on the safe side. In the end, all costs were computed and multiplied by four, and the total SFRS cost was obtained. The Table 2.8 shows the cost distribution and total SFRS costs for each archetype.

Table 2.8 Estimated construction costs for SFRSs of archetypes

NS:	Archetype:	BRB Cost	Column and Beam Cost	Connection Cost	Foundation Cost	Total BRBF Cost
3	R1-3S	$356,732	$177,266	$8,863	$542,862	$1,085,724
	R2-3S	$167,203	$123,586	$6,179	$296,968	$593,936
	R3-3S	$117,255	$89,916	$4,496	$211,667	$423,334
	R4-3S	$94,631	$82,322	$4,116	$181,069	$362,138
	R5-3S	$82,103	$75,814	$3,791	$161,708	$323,415
	R6-3S	$74,111	$75,814	$3,791	$153,715	$307,431
	R7-3S	$68,408	$75,814	$3,791	$148,012	$296,024
	R8-3S	$64,348	$70,390	$3,519	$138,257	$276,514
6	R1-6S	$845,000	$559,286	$27,964	$1,432,251	$2,864,502
	R2-6S	$379,911	$324,826	$16,241	$720,978	$1,441,956
	R3-6S	$260,311	$251,765	$12,588	$524,664	$1,049,329
	R4-6S	$206,891	$217,094	$10,855	$434,840	$869,680
	R5-6S	$177,415	$206,246	$10,312	$393,974	$787,947
	R6-6S	$158,130	$206,246	$10,312	$374,688	$749,377
	R7-6S	$145,251	$191,986	$9,599	$346,835	$693,671
	R8-6S	$135,537	$191,986	$9,599	$337,122	$674,243
9	R1-9S	$1,445,074	$1,164,744	$58,237	$2,668,055	$5,336,110
	R2-9S	$631,242	$680,597	$34,030	$1,345,868	$2,691,736
	R3-9S	$425,647	$526,243	$26,312	$978,203	$1,956,405
	R4-9S	$334,753	$443,537	$22,177	$800,467	$1,600,933
	R5-9S	$284,319	$414,473	$20,724	$719,515	$1,439,031
	R6-9S	$252,466	$396,574	$19,829	$668,868	$1,337,736
	R7-9S	$230,110	$388,006	$19,400	$637,516	$1,275,031
	R8-9S	$213,773	$368,321	$18,416	$600,509	$1,201,019

*NS: Number of Stories

Additionally, Fig 2.8 shows the initial cost of different R-Factors in terms of R=8 archetypes for visualizing the increase in initial cost when different R-Factors used. The Fig. 2.8 shows that the increase in the cost of SFRS is between 29% to 33% when R is reduced from 8 to 4. Lowering beyond R=2 caused 200% or more increase in the initial cost.

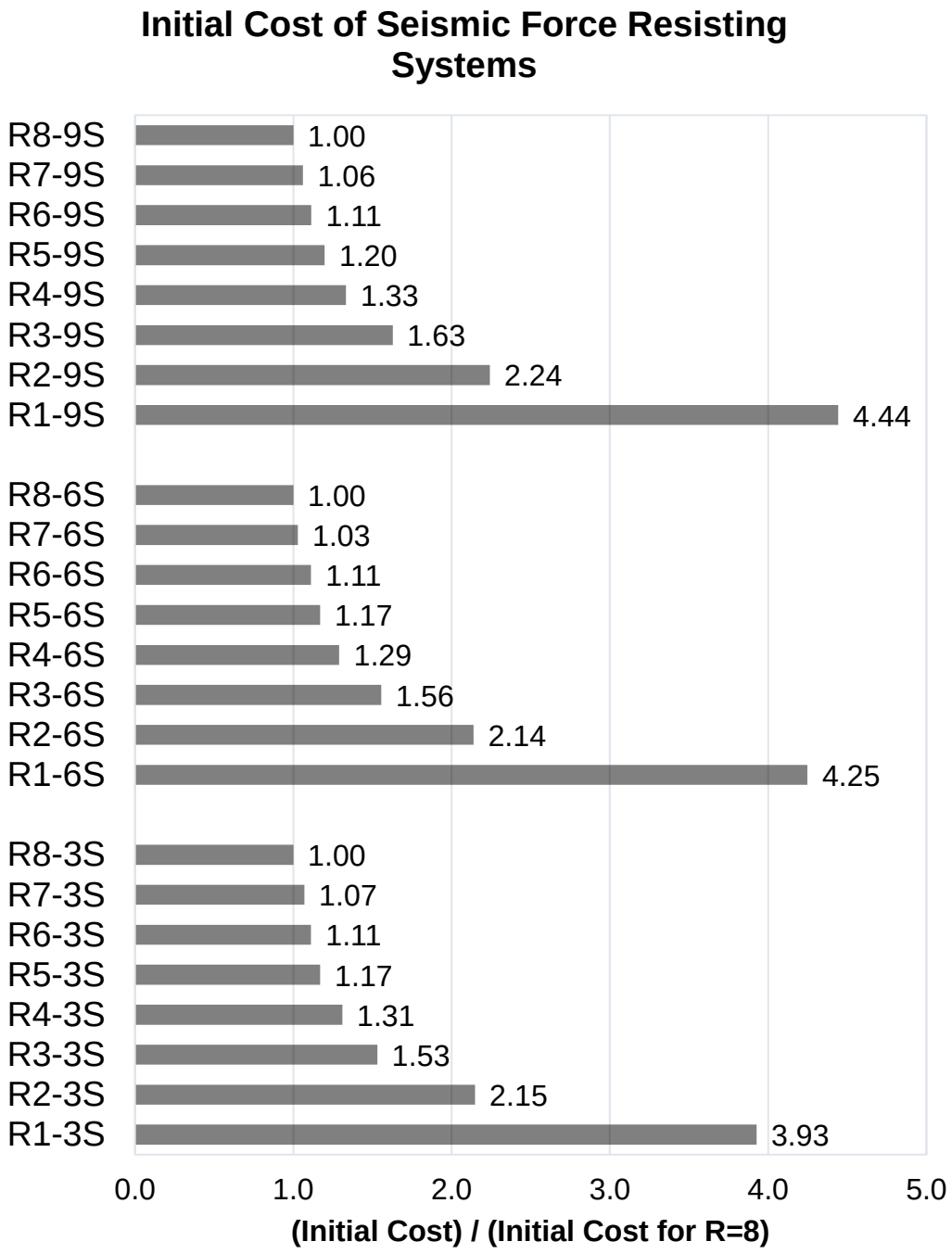

Figure 2.8. Initial cost of SFRSs in terms of initial cost of R=8 archetypes

CHAPTER 3

MODELING AND ANALYSIS OF ARCHETYPES FOR SEISMIC ASSESSMENT

As a part of the performance assessment procedure, time-history analysis results are necessary. FEMA P-58 allows simple analyzing procedures to predict post-earthquake performance of structure systems. However, in this study in order to obtain more realistic and detailed seismic behavior and to assess the performance of archetypes more accurately, non-simulated collapse models analyzed using nonlinear dynamic analysis methods. The open-source software framework OpenSees (Mazzoni *et al.*, 2006) was used for numerical modeling and computational simulation. One of the important advantages of OpenSees software, besides being open-source and free, is that it includes a variety of material models, elements, and analysis options. Each archetype was analyzed under two-dimensional workspace with 3 degrees of freedom per node for efficiency since no irregularities exist.

3.1 Ground Motion Description

The ground motions were taken from the FEMA P695 Far-Field (FF) record set and scaled according to the requirements of the FEMA P695 methodology. The FF record set consists of twenty-two pairs of horizontal ground motion records from sites located greater than 10 km from fault rupture. The properties of ground motions are given in Table 3.1. The acceleration spectrum for individual components of the normalized record set is given in Fig 3.1 with the median of the normalized set. Each BRBF was subjected to all 44-ground motion records, and then results were divided to two according to directions of records since both directions have the same BRBF. In this study, both maximum considered earthquake (MCE) and design-based earthquake (DBE) seismic hazard levels were utilized. These hazard levels correspond to %2 in 50 years and %10 in 50 years, respectively.

Table 3.1 Properties of ground motions in FEMA P695 FF Record Set

ID No.	Earthquake			Recording Station	
	M	Year	Name	Name	Owner
1	6.7	1994	Northridge	Beverly Hills - Mulhol	USC
2	6.7	1994	Northridge	Canyon Country-WLC	USC
3	7.1	1999	Duzce, Turkey	Bolu	ERD
4	7.1	1999	Hector Mine	Hector	SCSN
5	6.5	1979	Imperial Valley	Delta	UNAMUCSD
6	6.5	1979	Imperial Valley	El Centro Array #11	USGS
7	6.9	1995	Kobe, Japan	Nishi-Akashi	CUE
8	6.9	1995	Kobe, Japan	Shin-Osaka	CUE
9	7.5	1999	Kocaeli, Turkey	Duzce	ERD
10	7.5	1999	Kocaeli, Turkey	Arcelik	KOERI
11	7.3	1992	Landers	Yermo Fire Station	CDMG
12	7.3	1992	Landers	Coolwater	SCE
13	6.9	1989	Loma Prieta	Capitola	CDMG
14	6.9	1989	Loma Prieta	Gilroy Array #3	CDMG
15	7.4	1990	Manjil, Iran	Abbar	BHRC
16	6.5	1987	Superstition Hills	El Centro Imp. Co.	CDMG
17	6.5	1987	Superstition Hills	Poe Road (temp)	USGS
18	7.0	1992	Cape Mendocino	Rio Dell Overpass	CDMG
19	7.6	1999	Chi-Chi, Taiwan	CHY101	CWB
20	7.6	1999	Chi-Chi, Taiwan	TCU045	CWB
21	6.6	1971	San Fernando	LA - Hollywood Stor	CDMG
22	6.5	1976	Friuli, Italy	Tolmezzo	--

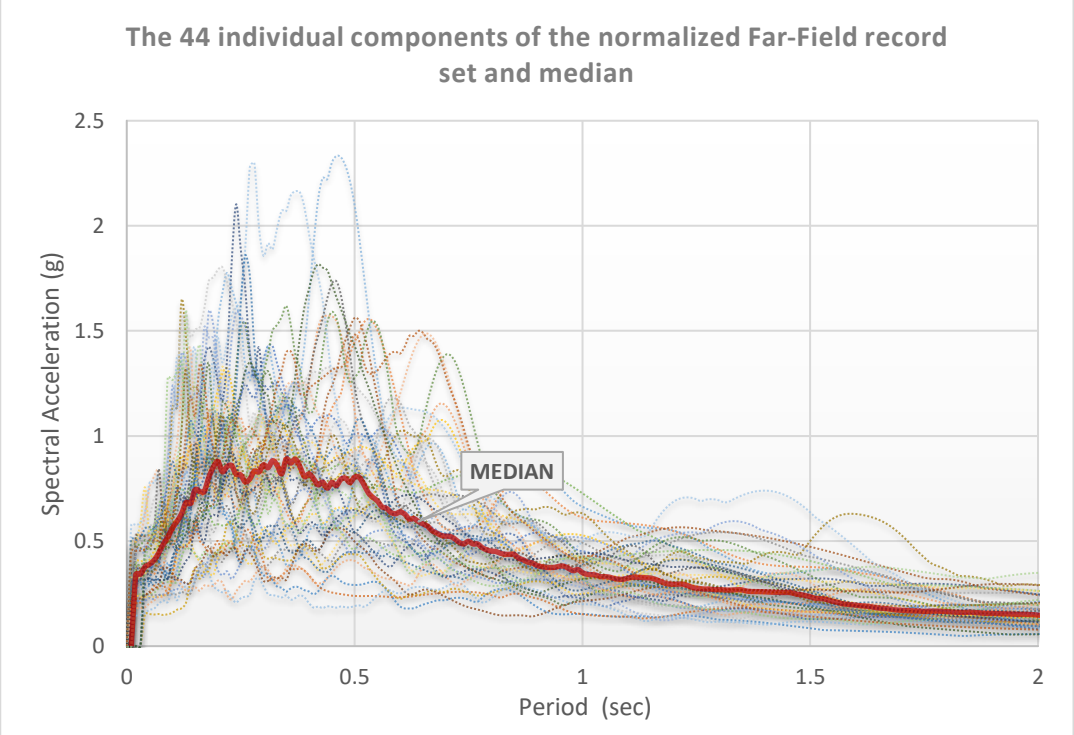

Figure 3.1. FEMA P695 FF Record Set Spectrum

Far field record set was subjected to a two-step scaling defined by FEMA P695 for the MCE level. For the first step, individual records were normalized by their respective peak ground velocities. The normalization factors are supplied by the methodology. In the second step, normalized ground motions were scaled up to a specific ground motion intensity such that the normalized far-field record set anchored to MCE spectral demand at the fundamental period, T, of the archetype that was being analyzed. $T=C_u \times T_a$ is the code-defined period, and not the period computed using an eigenvalue analysis of the structural model. Since the code-defined period depends on the structural height, system, and response acceleration, the periods were constant for different R-Factors.

According to the scaling of the FEMA P695, median value of the scaled record set need only to match the MCE demand at the fundamental period, rather than over the range of periods, as ASCE 7 requires. As a result, some deviations of the ground motion histories from the design spectra is expected. The methodology also indicates this situation and categorize as unavoidable due to the approximate shape of code-defined spectra.

After MCE level scaling, ground motions downscaled to DBE seismic hazard level in order to assess their performance and to determine the consequences under a lower level of seismic input. According to ASCE7-16, the design earthquake basis ground motions are defined as two-thirds of the corresponding MCE ground motions. Therefore, the DBE spectral demands were considered as 2/3 of the MCE spectral demands. The median curves of all scaled ground motion records are compared with DBE and MCE spectra in Fig. 3.2 for 9 Story archetypes. As expected, due to the scaling only at the “anchor” period, unavoidable deviations observed.

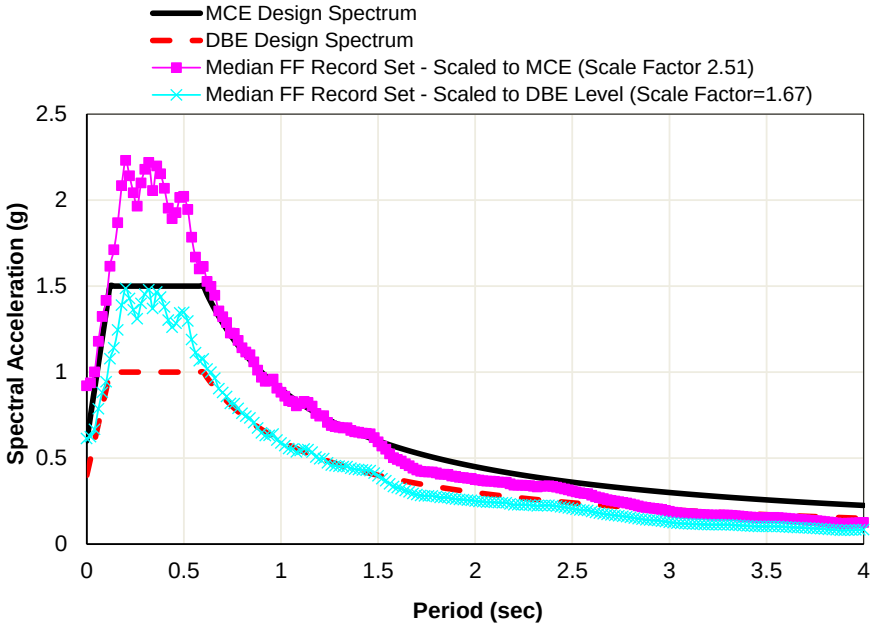

Figure 3.2. Scaling of the Far-Field Record Set for 9-story Archetypes

In order to acquire residual interstory drift ratios (R-IDR), each archetype was subjected to 5-second zero-g excitation after the ground motion history. In other words, after ground motion history was completed, analyses were continued for 5 seconds with no excitation to obtain R-IDRs with minimal vibration of the structure.

3.2 Material Modeling

For steel material, the uniaxial Giuffre-Menegotto-Pinto steel material model (Steel02) was used for all members of the archetypes except the leaning frame. For column and beam material model, strain hardening ratio was taken as 0.02, and all other coefficients were used as recommended values. No isotropic hardening was applied for beam and column material models. The material model of BRB was calibrated using the experimental results of Bozkurt and Topkaya (2016). The results of Bozkurt and Topkaya presented that isotropic hardening is necessary to model BRBs properly. Additionally, Zona and Dall'Asta (2012) proved the significant role of isotropic hardening in modeling BRB behavior; consequently, isotropic hardening was introduced to the model. As a result, the hysteretic behavior of BRBs was

simulated with coefficients that are given in Table 3.2. A comparison of the numerical response of defined material and the experimental response for Specimen 7, which has been reported by Bozkurt and Topkaya (2016), is given in Fig 3.3. The comparison of backbone curve proposed by Lopez and Sabelli (2004) and numerical model is also given in Figure 3.4. The comparisons show that the adjustment factors used at the design stage are accurately represented in the BRB numerical model.

Table 3.2 OpenSees Steel02 Material Properties for BRB Core

BRB Steel02 Material Properties			
Fy (MPa):	235	**cR2:**	0.6
E (GPa):	200	**a1:**	0.053
B:	0.013	**a2:**	1
R0:	23	**a3:**	0.02
cR1:	0.955	**a4:**	1

The parameters are explained below (Mazzoni *et al.*, 2006):

- Fy: yield strength.
- E: initial elastic tangent.
- B: strain-hardening ratio.
- R0 cR1, cR2: parameters to control the transition from elastic to plastic branches.
- a1: isotropic hardening parameter, increase of compression yield envelope as proportion of yield strength after a plastic strain of a2*(Fy/E).
- a2: isotropic hardening parameter.
- a3: isotropic hardening parameter, increase of tension yield envelope as proportion of yield strength after a plastic strain of a4*(Fy/E).
- a4 isotropic hardening parameter.

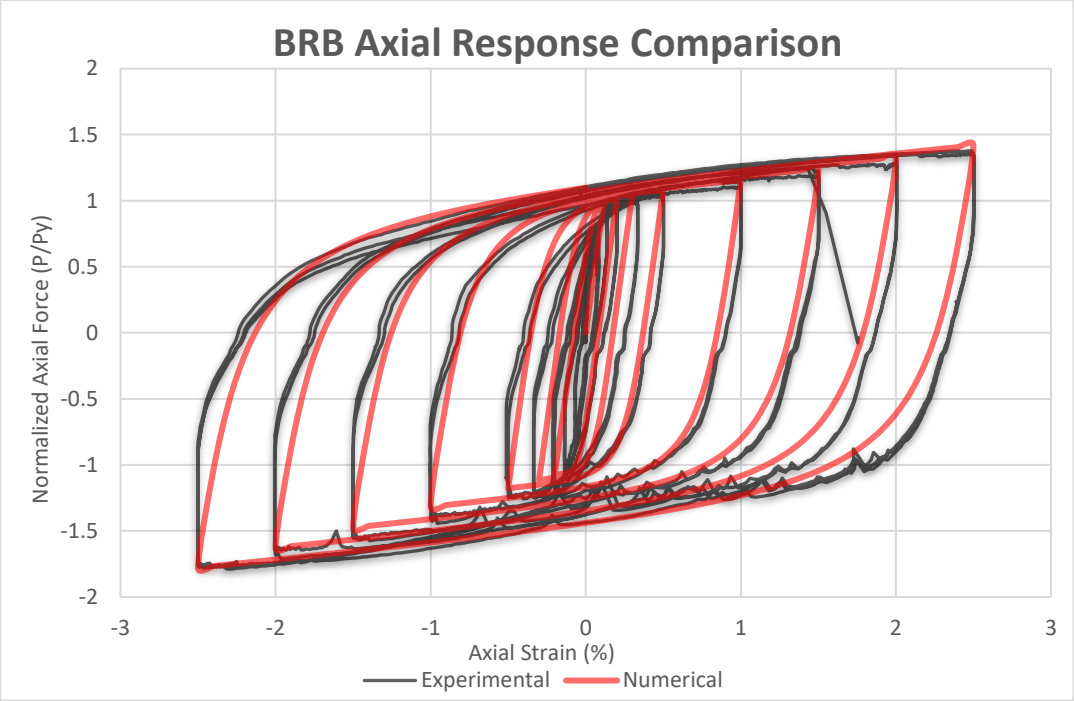

Figure 3.3. Comparison of BRB numerical model and experimental model

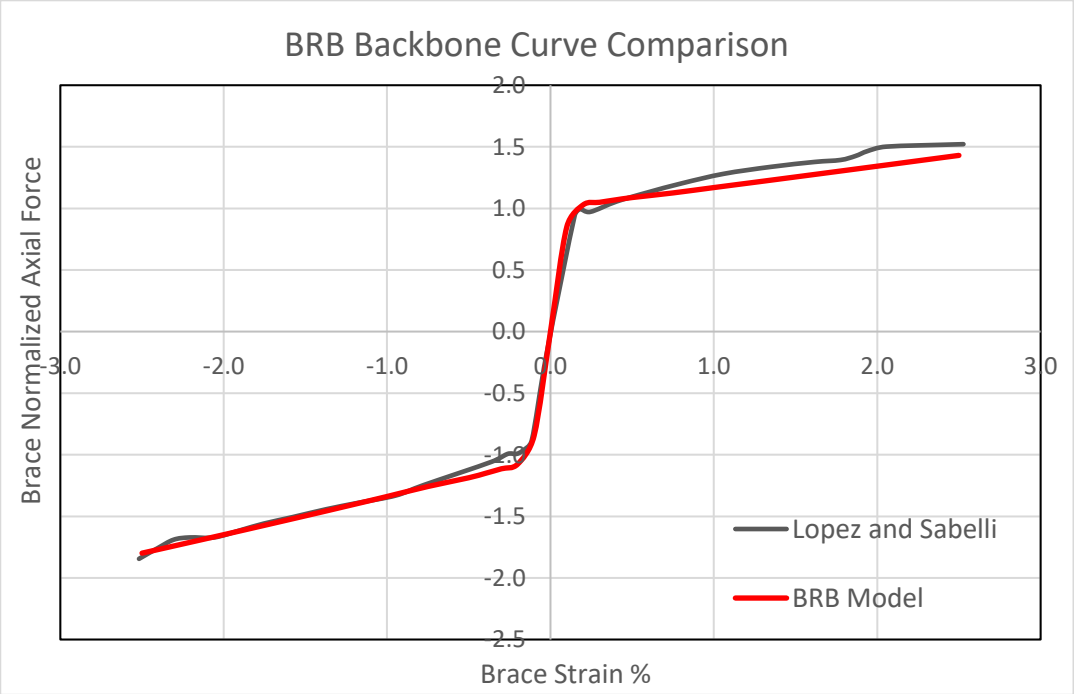

Figure 3.4. Backbone Curve Comparison of BRB numerical model and Lopez and Sabelli (2004) model

3.3 Modeling of Archetypes

The fundamental periods of archetypes were calculated by eigenvalue analysis of OpenSees software. Obtained periods are given in Fig. 3.5. The T=Cu× Tα values are 0.64 sec, 1.04 sec and 1.39 sec for 3-, 6-, and 9-story archetypes, respectively. The fundamental periods were normalized by the fundamental period of the archetype designed with R=8 and the ratios are given in Figure 3.6(a). In general, the trend is similar for 3-, 6, and 9-story archetypes. The fundamental period reduces by about 18% as the R value reduces from 8 to 4. The impact of using different fundamental periods on design can be examined from Figure 3.6(b). In this figure, the fundamental period from eigenvalue analysis (T) is normalized with the fundamental period used in design ($C_u \times T_a$). Two bounds are also displayed as solid black lines. The first bound $T/(C_u \times T_a)=1$ is used to compare the fundamental period with the one used in design. The lower bound $(T/T_a)=1/1.4=0.71$ is used to compare the fundamental period with the approximate fundamental period (T_a). Data points mostly fall within the two bounds indicating that the fundamental periods range between T_a and $C_u \times T_a$. For 9-story archetypes with R≥4 and for 6-story archetypes with R≥6, the ratios are above unity, indicating that the upper bound on the period governs the design and the member sizes do not change even if the fundamental period from eigenvalue analysis is adopted. Although the ratios for 3-story archetypes are less than unity, the member sizes are not influenced by the fundamental period because the fundamental periods are less than 0.6 sec for R≤6, indicating that the fundamental periods fall into the constant acceleration region. The base shear increases by only 5% if the 3-story archetype with R=7 is designed with T=0.61 sec instead of T=0.64 sec. For 6-story archetypes designed with R=4 and R=5, the increase in the base shear is only 10% and 4%, respectively, if the fundamental period from eigenvalue analysis is adopted.

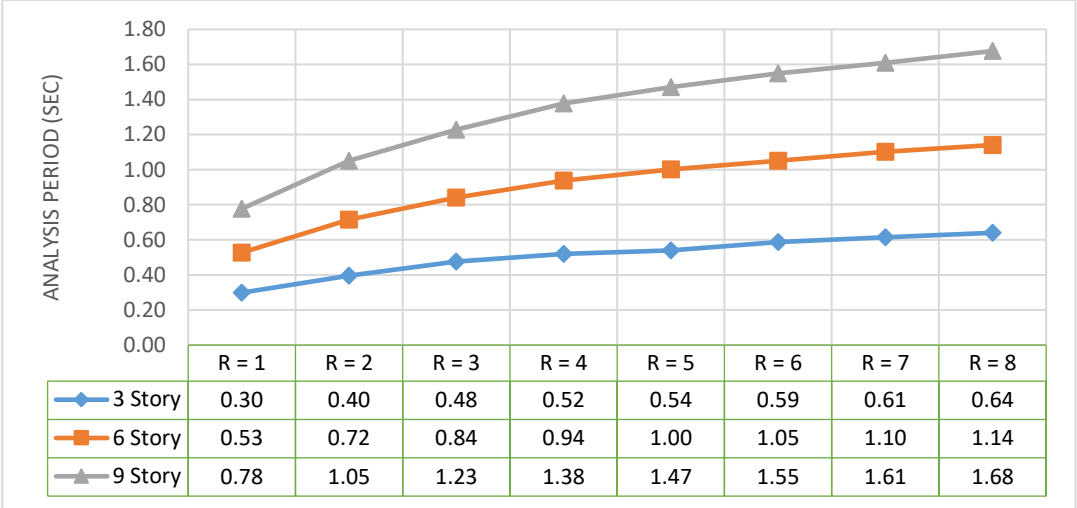

	R = 1	R = 2	R = 3	R = 4	R = 5	R = 6	R = 7	R = 8
3 Story	0.30	0.40	0.48	0.52	0.54	0.59	0.61	0.64
6 Story	0.53	0.72	0.84	0.94	1.00	1.05	1.10	1.14
9 Story	0.78	1.05	1.23	1.38	1.47	1.55	1.61	1.68

Figure 3.5. Fundamental periods of archetypes

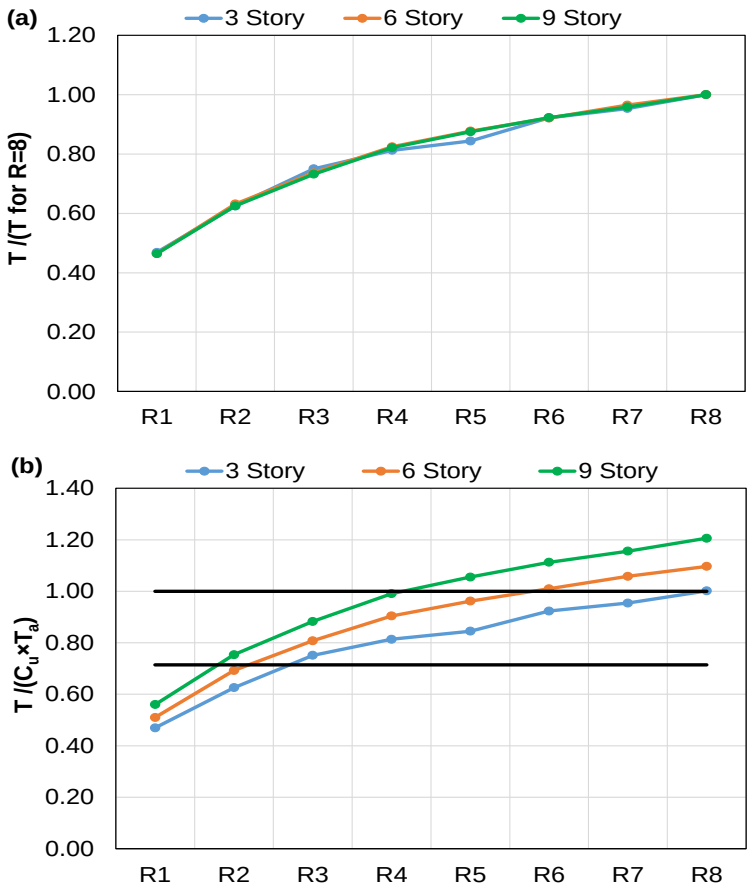

Figure 3.6. Normalized Fundamental Natural Periods of Archetypes

The models were assigned a 2% mass and stiffness proportional damping, which was applied to elements committed stiffness matrix. Damping was assigned to all members in the numerical model, including the BRBs. In order to account for second-order P-Δ effects, the leaning column approach was used. Correlatively, PDelta geometric transformation was applied to members of BRBF. The leaning columns were connected to the BRBF by trusses. In order to avoid the effect of moment resistance from connections, beam to column connection and column base nodes were modeled as a pin.

As only one BRBF bay was modeled in each direction, the tributary mass was divided into two and applied to leaning column nodes for simplicity. It was verified that the distributing masses among the two nodes of BRBF gives the exact same results. Similarly, gravity loads were also applied to leaning column nodes. The beam and column element sections were modeled as a fiber section to obtain a precise result. Representation of fiber section with the number of fiber elements of a typical column section is given in Fig. 3.7. In order to model BRBs, yielding, and nonyielding parts were modeled separately and connected with nodes. The yielding part of the braces was modeled with nonlinear truss elements, whereas non-yielding parts were modeled using elastic beam-column elements. The non-yielding parts of the BRBs were rigidly connected to the columns and pin-connected to the yielding part of the BRBs. Leaning columns carrying gravity loads were modeled as continuous from the base to the roof of the structure and were linked to the BRBF to simulate P- Δ effects.

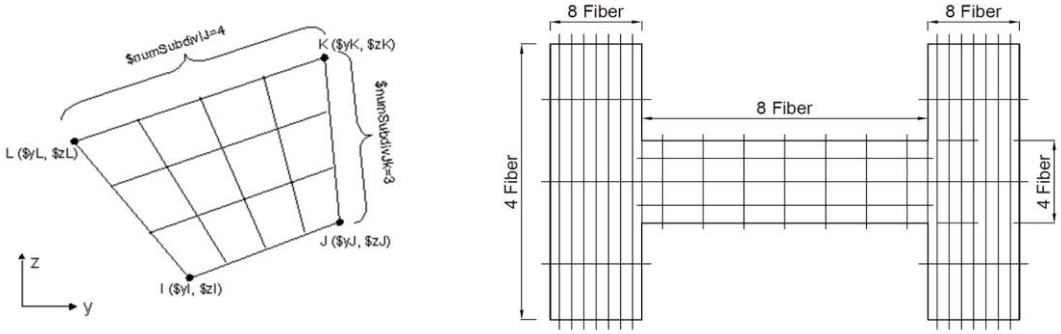

Figure 3.7. Fiber section definition and column section fiber representation

In order to understand the analyses results of the archetypes, the contributions of modes to the response should be determined. The modal participation masses for first 3 mode was computed using OpenSees software. The results are given in Table 3.3. It has been observed that as R-Factor increase, the mass participation of the first mode is increases. This increase is equal to 4.0%, 5.2% and 5.8% for 3-, 6-, and 9-story archetypes, respectively. For R=8 archetypes, at 1st mode, mass participation ratio of 3 story archetype is 89% which goes down to 78.1% in 9 story. From these results it can be said that 1st mode is the dominant mode for all archetypes.

Table 3.3 Modal Mass Participation Ratios (%)

3 Story								
MODE	**R=1**	**R=2**	**R=3**	**R=4**	**R=5**	**R=6**	**R=7**	**R=8**
1	85.5	86.8	87.5	87.8	87.9	88.0	89.0	89.0
2	12.6	11.4	10.9	10.6	10.5	10.5	9.6	9.7
3	1.9	1.8	1.6	1.6	1.5	1.6	1.4	1.4
6 Story								
MODE	**R=1**	**R=2**	**R=3**	**R=4**	**R=5**	**R=6**	**R=7**	**R=8**
1	78.0	78.8	79.9	80.4	80.8	81.4	81.5	82.0
2	15.6	15.2	14.3	14.1	13.9	13.4	13.5	13.1
3	4.2	3.9	3.7	3.6	3.5	3.4	3.3	3.2
9 Story								
MODE	**R=1**	**R=2**	**R=3**	**R=4**	**R=5**	**R=6**	**R=7**	**R=8**
1	73.9	75.2	75.8	76.7	77.0	77.4	77.9	78.1
2	17.5	16.8	16.4	15.8	15.7	15.4	15.1	15.0
3	4.6	4.3	4.2	4.0	4.0	3.9	3.8	3.8

3.4 Analysis Properties

The nonlinear dynamic analysis was conducted in two steps. In the first step, before dynamic analysis, to calculate P-Delta effects and to simulate gravity loads, 10 step gravity analysis is conducted. To minimize bandwidth, RCM optimization was used. For the time-history analyzing part, the ground motions were applied with scaling factors and an additional zero-g excitation part.

3.5 Analysis Results

In total, 24 archetypes with 8 different R-Factor and 3 different height were analyzed. Each archetype was subjected to both MCE and DBE level scaled ground motion set. The results are presented and commented in terms of median results of 44 ground motions for maximum observed value at each archetype.

3.5.1 Interstory Drift Ratio Demands

Representative variations of interstory drifts along the height of buildings are given in Figs 3.8 and 3.9 for the 9-story archetypes. In these figures, median results with one standard variations (+) for the cases with R=1, 4, and 8 are indicated. The maximum IDR is non-uniform along the height for the archetypes designed with the codified R=8. The non-uniformity in response is more pronounced under MCE level ground motions when compared with DBE level ground motions. The maximum IDRs tend to reduce and become more uniform along the height as the R factor is reduced. When the variation is investigated it was observed that R=8 archetype shows significantly high variation specifically at below levels. This high variation is also visible at DBE level. For all archetypes both median story drift ratios and variations at upper stories are approximately same.

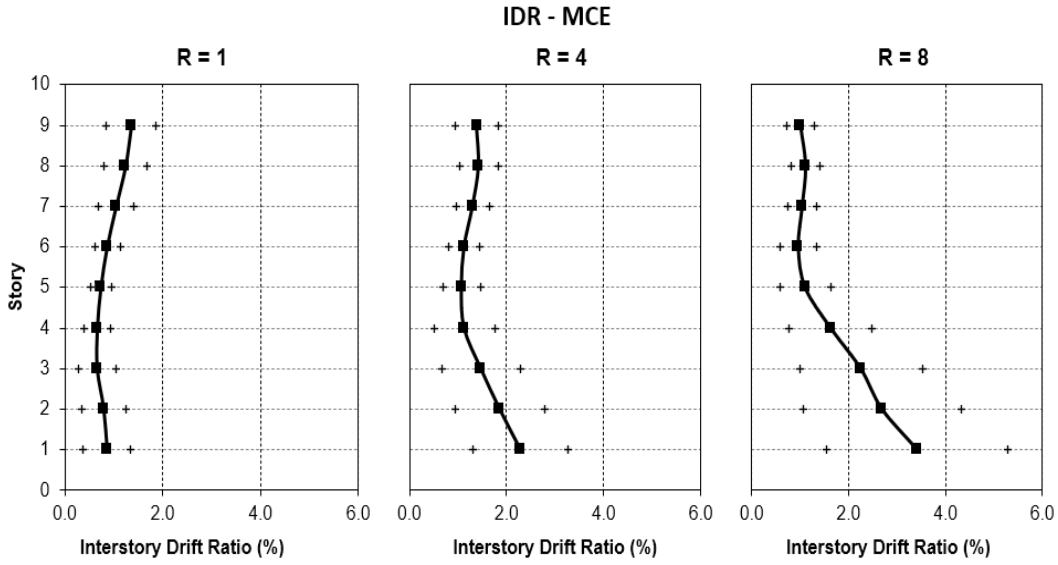

Figure 3.8. IDR Response of 9 Story Archetypes - MCE

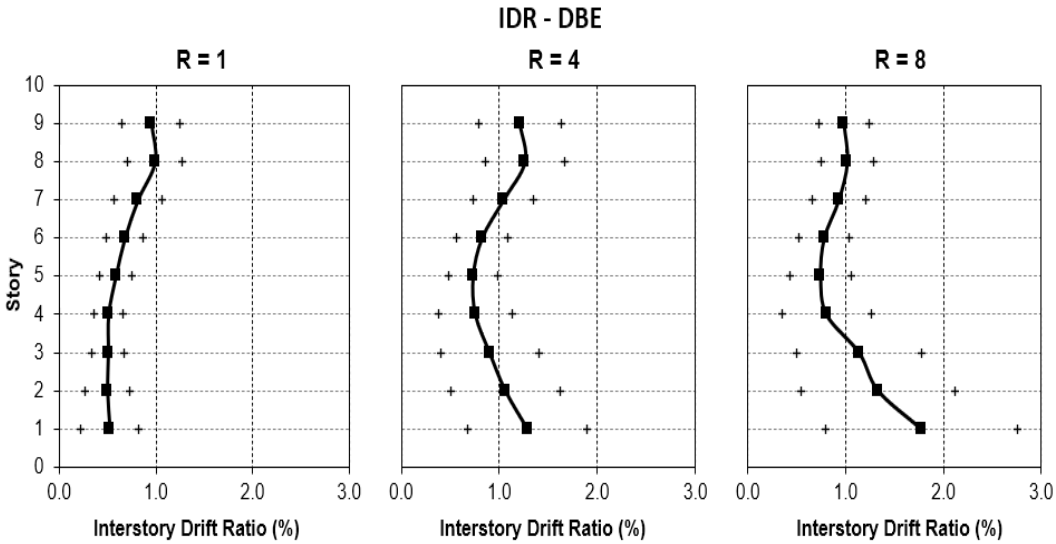

Figure 3.9. IDR Response of 9 Story Archetypes - DBE

The maximum observed median IDRs in each archetype for MCE and DBE are presented in Figs. 3.10-3.12. The IDRs for each story were computed from the lateral displacement of story and a median of 44 time-history analysis was obtained. The maximum IDR among all stories decreases significantly as the R factor is reduced. For example, the maximum IDR reduces from 3.42% to 1.35% as the R factor decreases from 8 to 1 in the 9-story archetype subjected to MCE level ground motions. The amount of reduction in IDR is presented in Figure 3.13 where the ratio of the IDR to IDR for *R*=8 is considered. Both the maximum and the average of IDR among the stories were taken into account. When responses given in Figures 13a and 13b are compared, it is evident that the reduction in maximum IDR is more pronounced when compared with the reduction in average IDR.

According to Figs. 3.10-3.12, IDRs tend to increase as the number of stories increases, for archetypes designed with the same R factor. This observation does not hold for 9-story BRBFs designed with R≥4 where the IDRs are less than their counterparts calculated for 6-story archetypes. The difference can be attributable to the amount of scaling applied to the BRBFs. According to Figure 3.2, the median spectral acceleration of scaled ground motions tends to be less than the design spectral acceleration for fundamental periods greater than about 1.5 seconds. The 9-

story archetypes with R≥4 have fundamental periods that mostly fall into this domain. If the ground motion scaling was conducted according to the fundamental period obtained from eigenvalue analysis, the IDRs for these archetypes could be greater than has been reported in Figure 3.12.

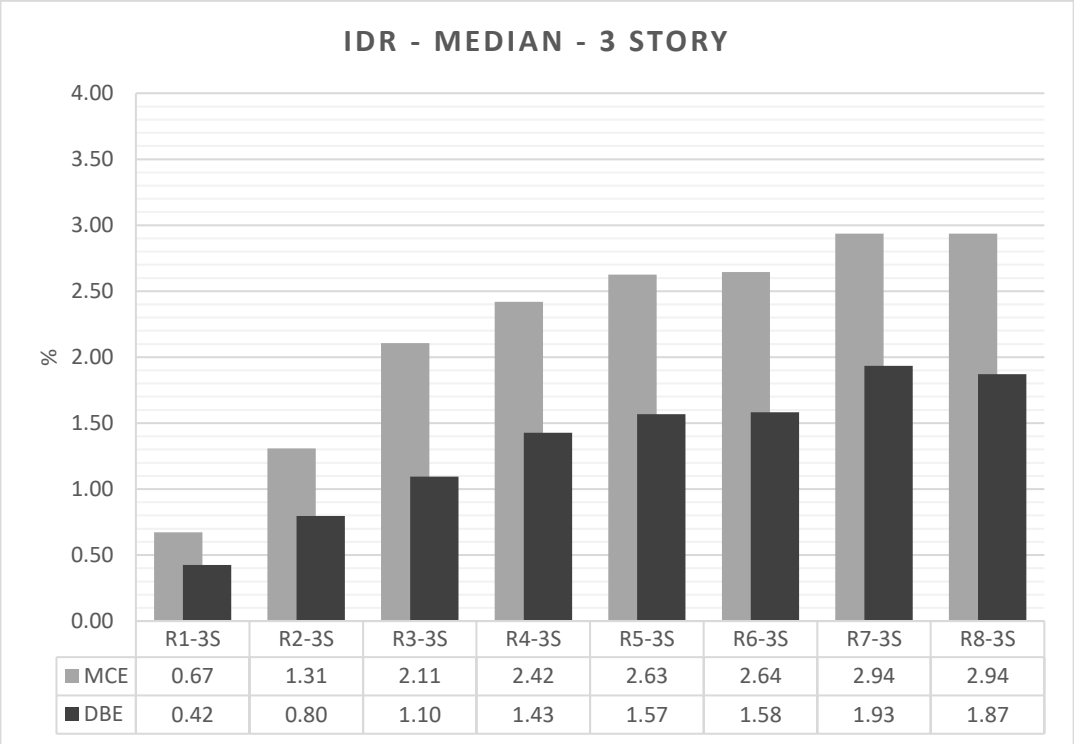

	R1-3S	R2-3S	R3-3S	R4-3S	R5-3S	R6-3S	R7-3S	R8-3S
MCE	0.67	1.31	2.11	2.42	2.63	2.64	2.94	2.94
DBE	0.42	0.80	1.10	1.43	1.57	1.58	1.93	1.87

Figure 3.10. IDR demands for 3 Story archetypes (Median)

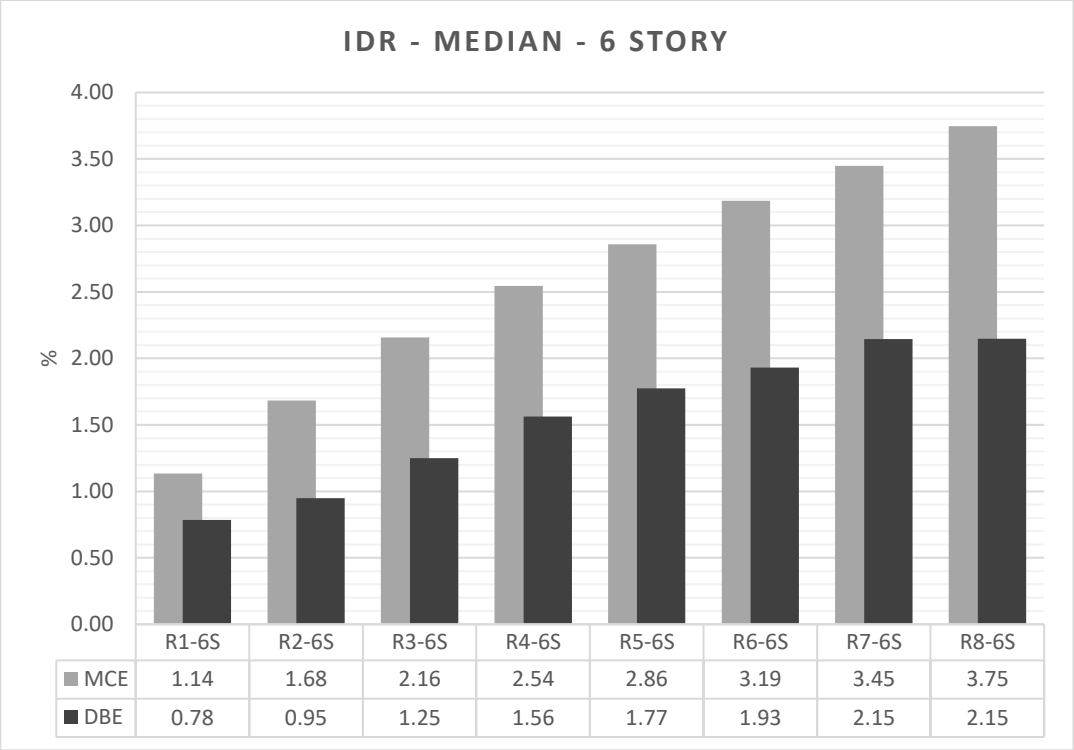

Figure 3.11. IDR demands for 6 Story archetypes (Median)

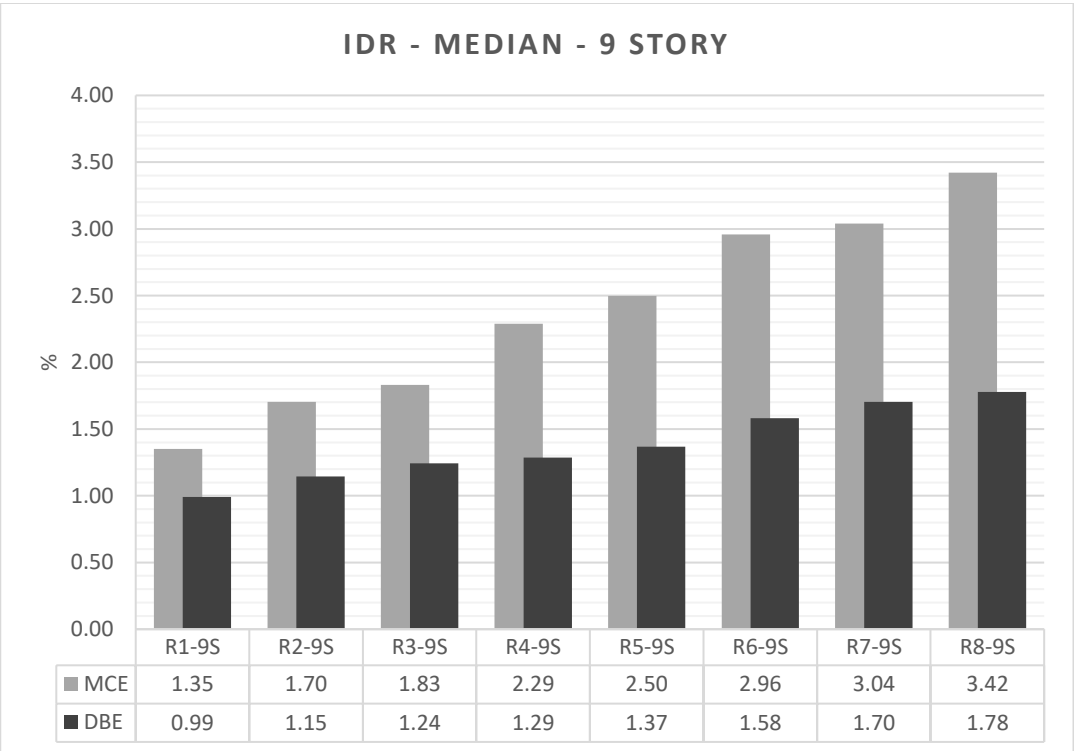

Figure 3.12. IDR demands for 9 Story archetypes (Median)

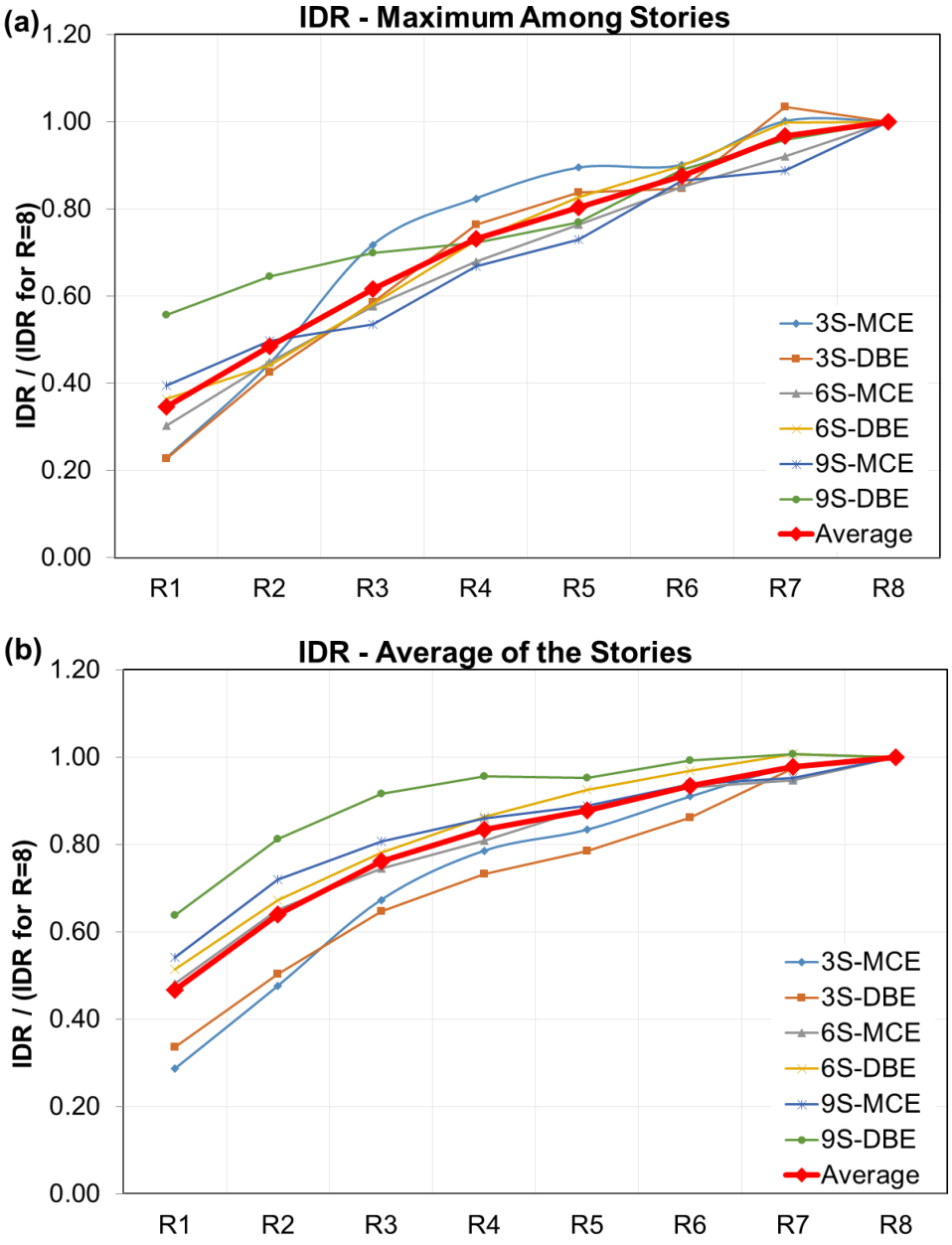

Figure 3.13. Variation of Normalized IDRs

3.5.2 Residual Interstory Drift Ratio Demands

As given, residual drift values are one of the important indicators of post-earthquake performance. A structure which designed according to code provisions can give high residual deformations which could potentially cause the demolishment of building, even if all structure behaves as expected. In order to determine the reasons of the residual deformations, many studies were conducted. The one important parameter is determined as the shape of the hysteretic behavior of the load carrying member. In compare to maximum drifts, the residual drifts were found out to be more sensitive to the hysteretic modeling parameters (Christopoulos et al., 2004; Dazio, 2004; Jorge Ruiz-Garcia and E. Miranda, 2005; Yazgan, 2010). As a result, in the consideration of residual deformations, it must be noted that these results majorly depend on the hysteretic model used for BRBFs. For other hysteretic models, different results could be achieved. However, as mentioned by Christopoulos et al. (2004), members with "fatter" hysteretic behaviors are most likely to produce the highest residual deformations and the high residual drifts that presented in here were expected due to the hysteretic shape of the BRB members.

The variations of median RIDR for 9-story archetypes are indicated in Figs 3.14 and 3.15. Similar to the IDR, the RIDR values reduce and become more uniform along the height of the building as the *R* factor is reduced. The maximum observed median R-IDRs in each archetype for both sets of ground motions are presented in Figs. 3.16 - 3.18. Values were taken as the IDR at the end of ground motion excitation. Under MCE level ground motions, the 6- and 9-story BRBFs were found to experience very high residual drifts, especially for R=6, 7, and 8 cases. BRBF structures tend to exhibit excessive residual drifts, which confirm the results of Erochko et al. (2011). According to the work of McCormick et al. (2008) the R-IDRs larger than 0.5% are generally perceivable by occupants, and they concluded that in Japan, it was less expensive to rebuild a structure rather than repair it when R-IDRs greater than 0.5%. Similarly, FEMA P-58 gives a probabilistic distribution of irreparable residual drift, which starts replacement change at 0.5% and reaches the

median at 1%. As a result, R-IDRs greater than 0.5% could be classified as a possible replacement zone. When the MCE analysis results were investigated, it has been seen that almost all archetypes with R-Factor greater than 4 were in the possible replacement zone, which shows that residual displacement is a problem for BRBF structures. Moreover, it was confirmed that BRBF buildings designed according to ASCE 7-16 have a high chance of irreparable damage after MCE level earthquake. As a consequence, the total economic loss of structure is highly possible. When DBE analysis results investigated, almost none of the archetypes were shown replacement possibility by R-IDR staying under 0.5%. The ratios of RIDR to RIDR for R=8 are given in Fig. 3.19 for maximum RIDR and average RIDR among the stories, respectively.

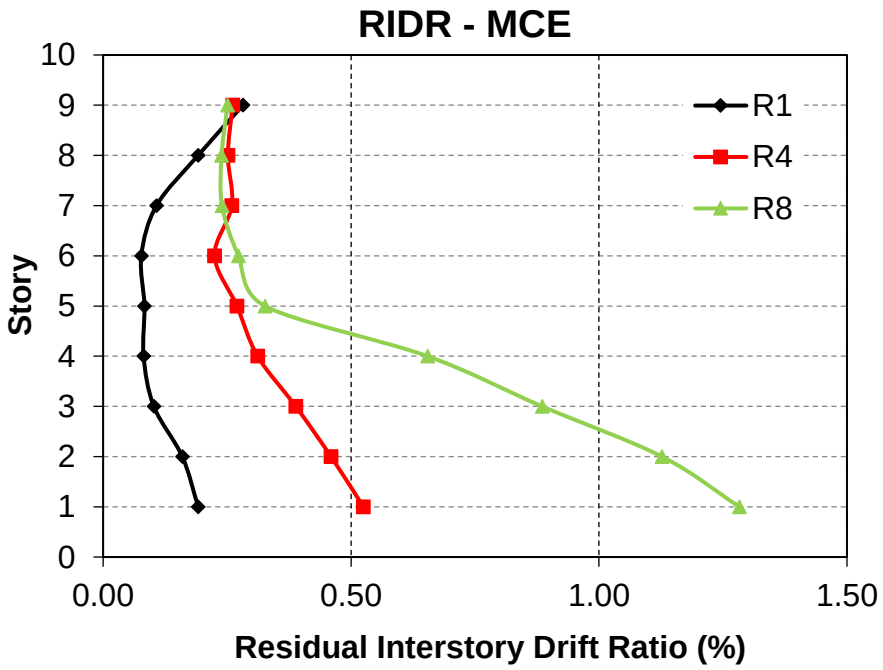

Figure 3.14. RIDR response of 9-story Archetypes - MCE

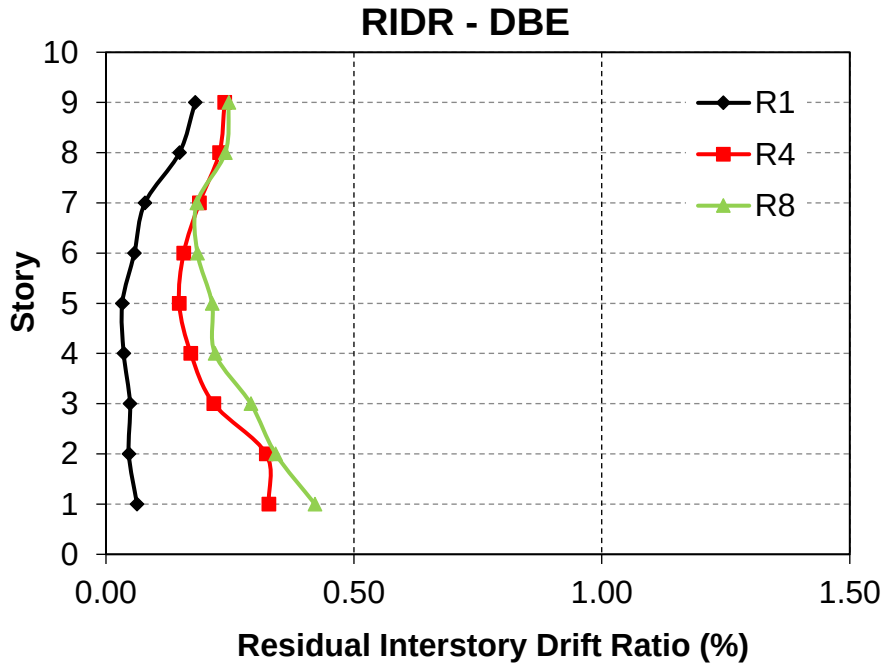

Figure 3.15. RIDR response of 9-story Archetypes - DBE

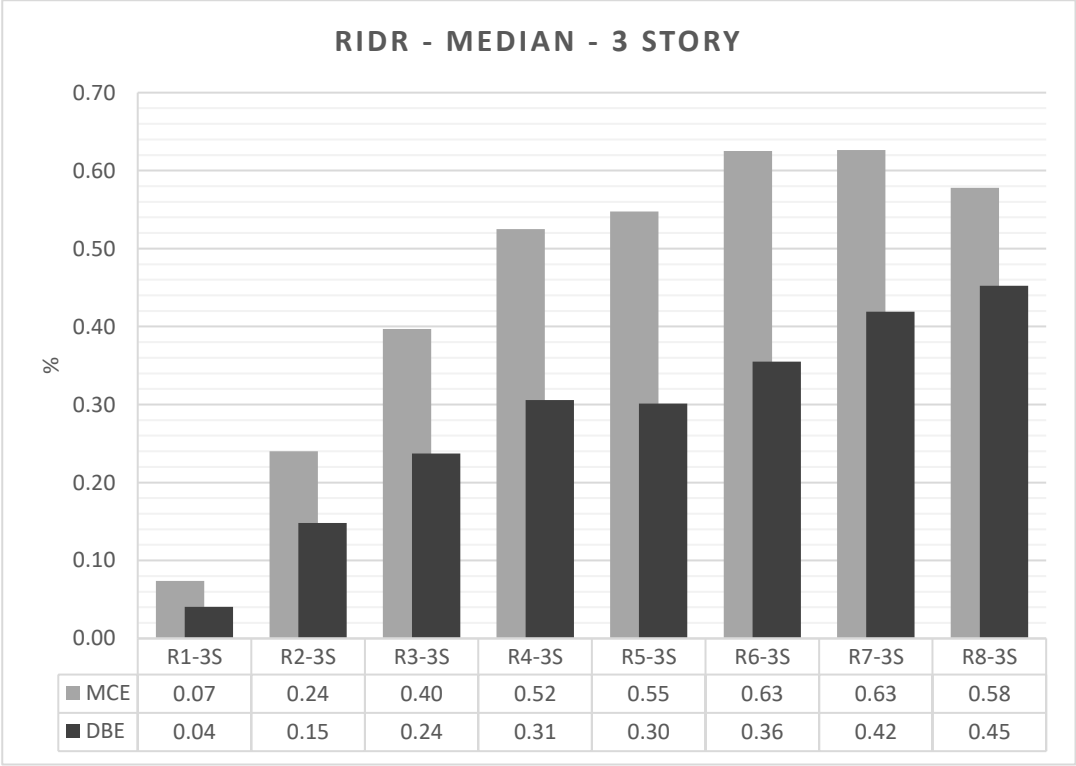

Figure 3.16. R-IDR demands for 3 Story archetypes (Median)

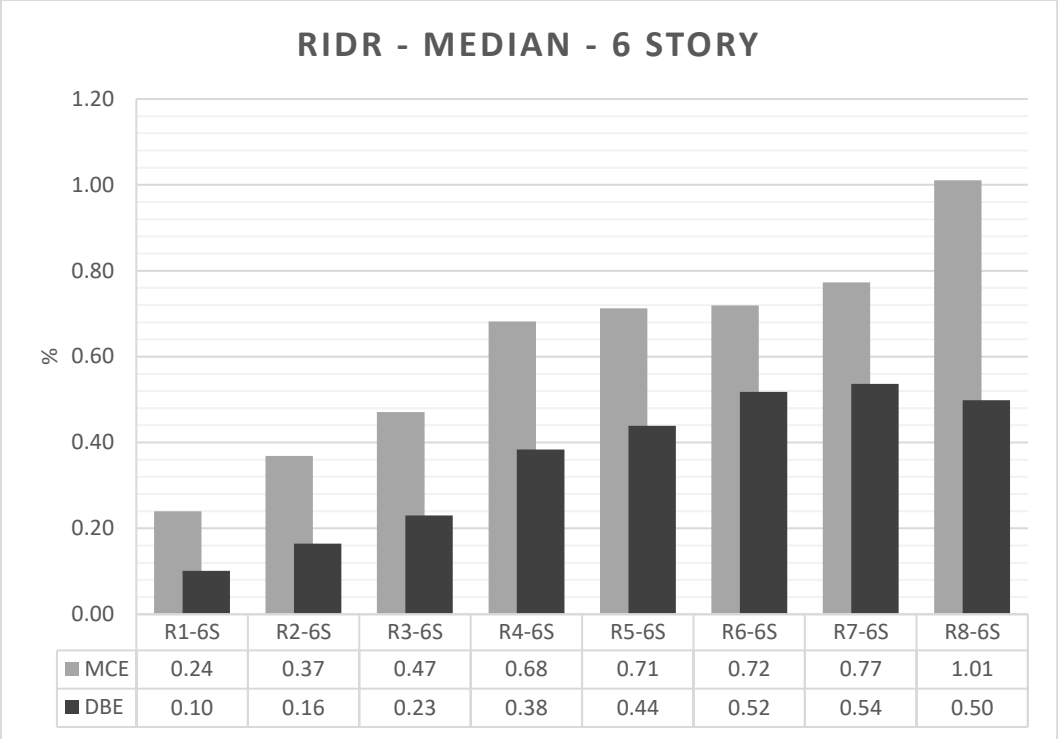

Figure 3.17. R-IDR demands for 6 Story archetypes (Median)

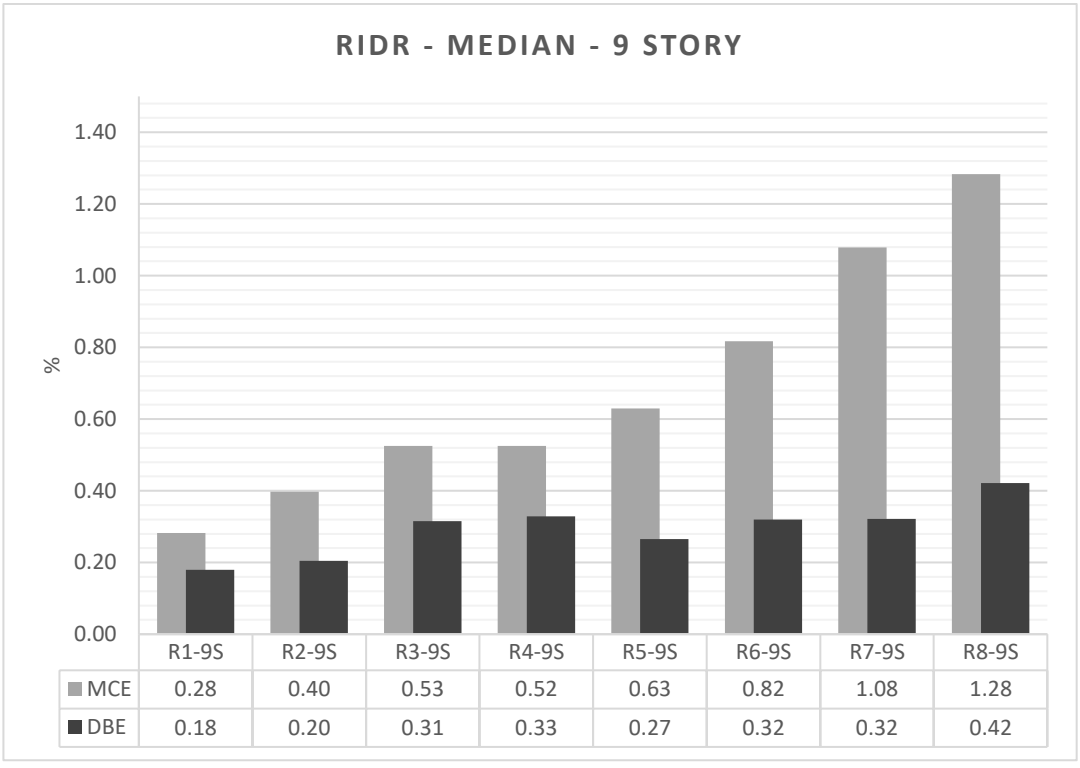

Figure 3.18. R-IDR demands for 9 Story archetypes (Median)

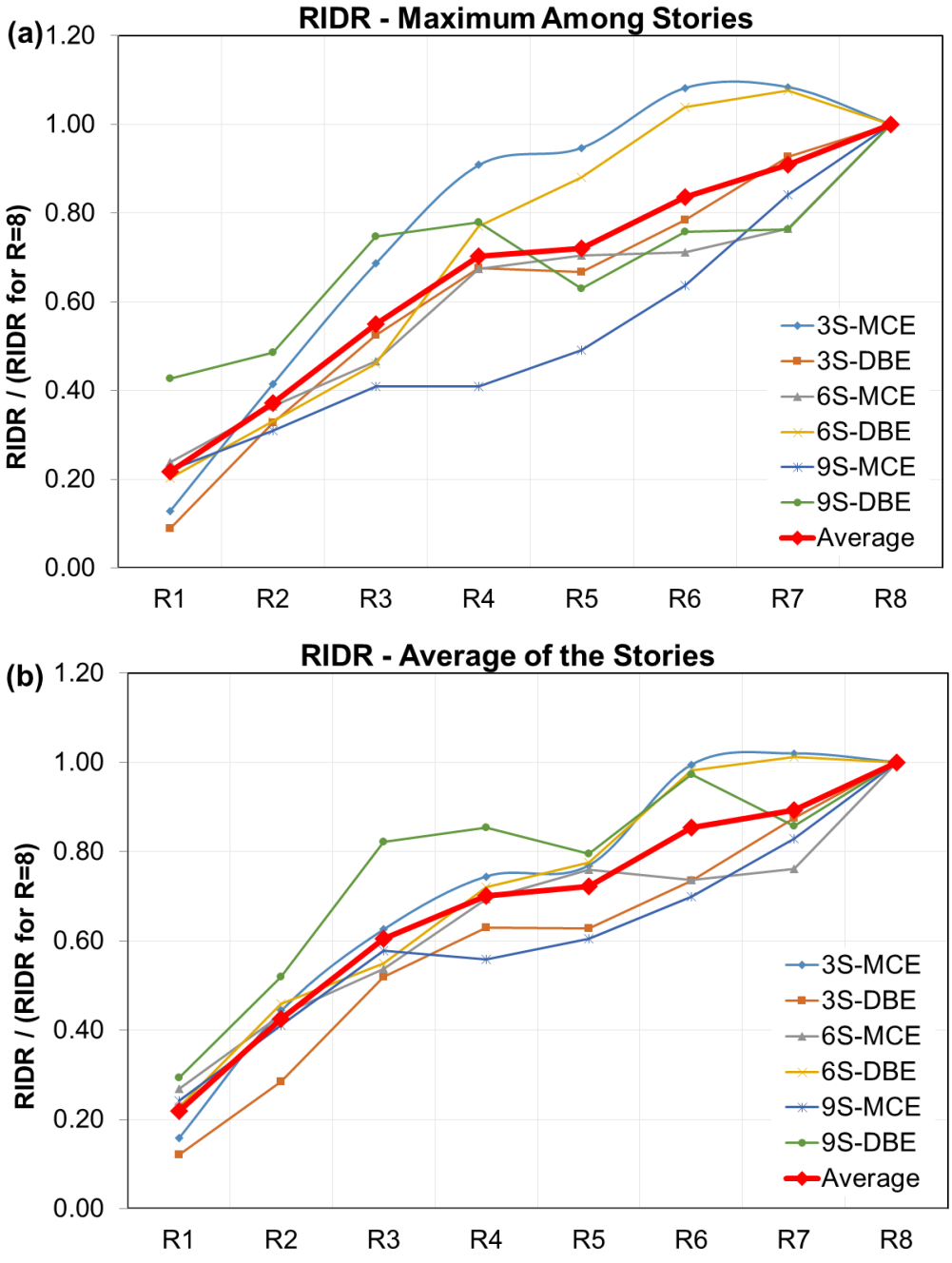

Figure 3.19. Variation of Normalized RIDRs

In order to determine the effect of interstorey drift ratios on the residual drifts, the ratio of max observed median IDR at each archetype to max observed median R-

IDR is determined and presented. In overall, the results seems to be inside the 0.15 to 0.25 band. However, 9 story R=8 archetype showed a significantly higher value of 0.38 and, 3 Story R=1 archetype showed a lowest value of 0.10. When the ratios investigated, it was observed that as the story count and R-Factor increase, slight increase in this ratio is observed however, this change is not significant or clear enough.

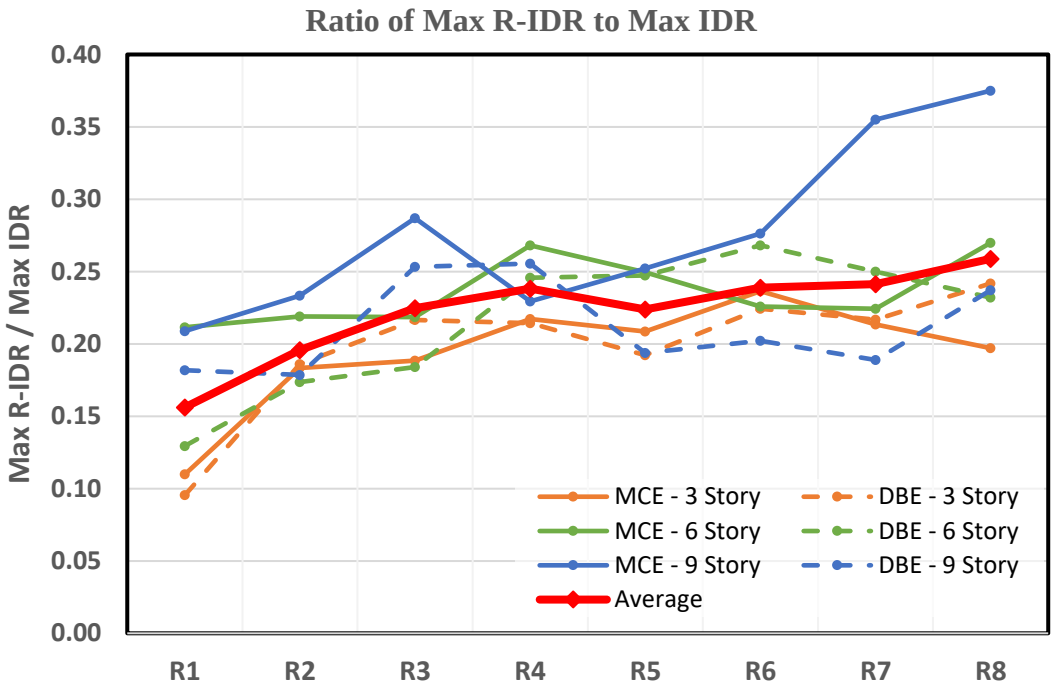

Figure 3.20. Max R-IDR to Max IDR Ratio (Median)

3.5.3 Story Acceleration and Velocity Demands

In performance evaluation, observed story accelerations (SA) and velocities under seismic activity are very important for acceleration sensitive fragilities. As a result, story velocities and story accelerations values were taken from nodes in which masses were defined by using recorders. Representative variations of SA along the height are presented in Figs 3.21 and 3.22 for 9-story archetypes. Unlike IDR and RIDR, the SA has an inverse relationship with R factor. In other words, as the R

factor is reduced the SA increases. In addition, the variation of SA along the height become non-uniform as the R factor is reduced. Story acceleration median values are given in Figs. 3.23 - 3.25. Story acceleration results showed that increasing R-Factor effects accelerations significantly. For many nonstructural components, acceleration values larger than 1g could cause significant damage. In accordance with that, MCE level seismic motions have a very high potential to cause nonstructural damage, irrespective from R-Factor. Only the level of damage depends on the R-Factor. However, under DBE excitations, only R-Factor smaller than 4 shows nonstructural damage. The ratios of SA to SA for *R*=8 are given in Fig. 3.26. The SA increases in average 10% when *R* is reduced from 8 to 4. On the other hand, the ratios can reach to 2.0 as the *R* factor is reduced from 8 to 1. Maximum observed story velocity demands are given in Fig. 3.27. For 3 story archetypes, it was observed that changing R-Factor did not change the story velocities. In contrast, 6- and 9- story archetypes showed increased velocities as the R-Factor decrease.

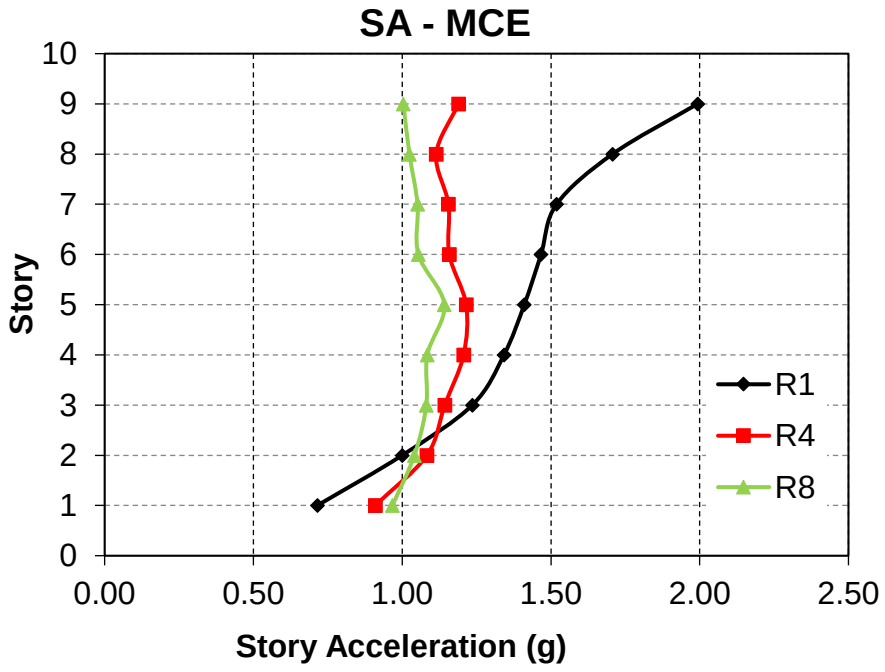

Figure 3.21. Story Acceleration response of 9-story Archetypes - MCE

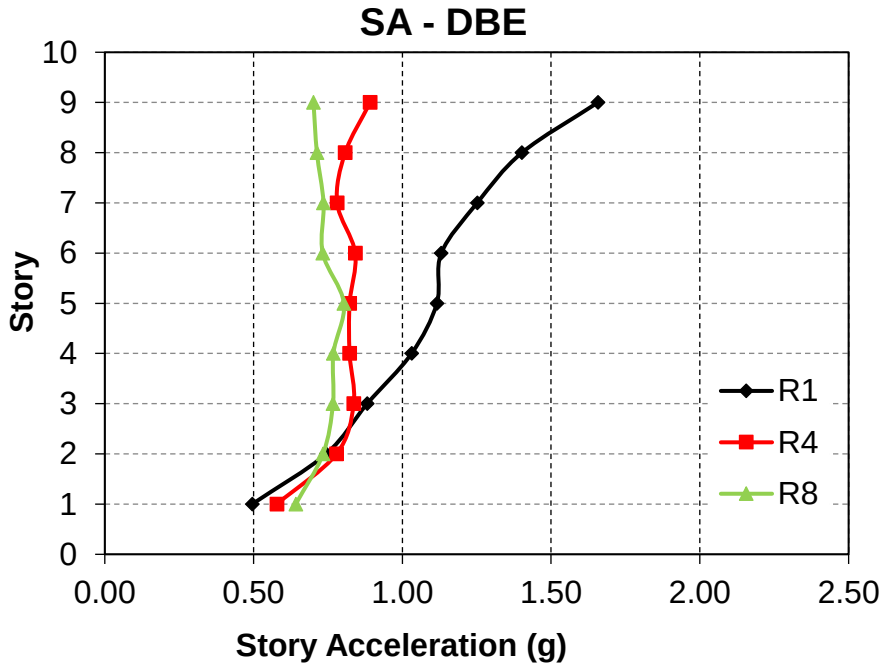

Figure 3.22. Story Acceleration response of 9-story Archetypes - DBE

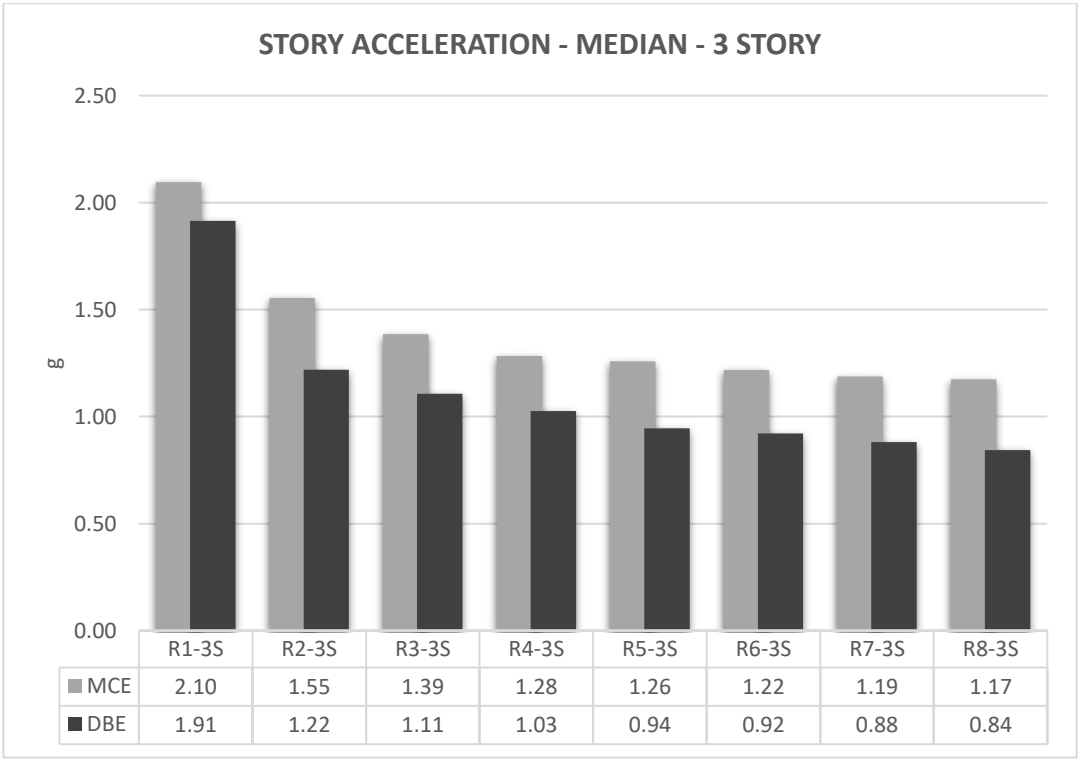

	R1-3S	R2-3S	R3-3S	R4-3S	R5-3S	R6-3S	R7-3S	R8-3S
MCE	2.10	1.55	1.39	1.28	1.26	1.22	1.19	1.17
DBE	1.91	1.22	1.11	1.03	0.94	0.92	0.88	0.84

Figure 3.23. Peak story acceleration demands for 3 Story archetypes (Median)

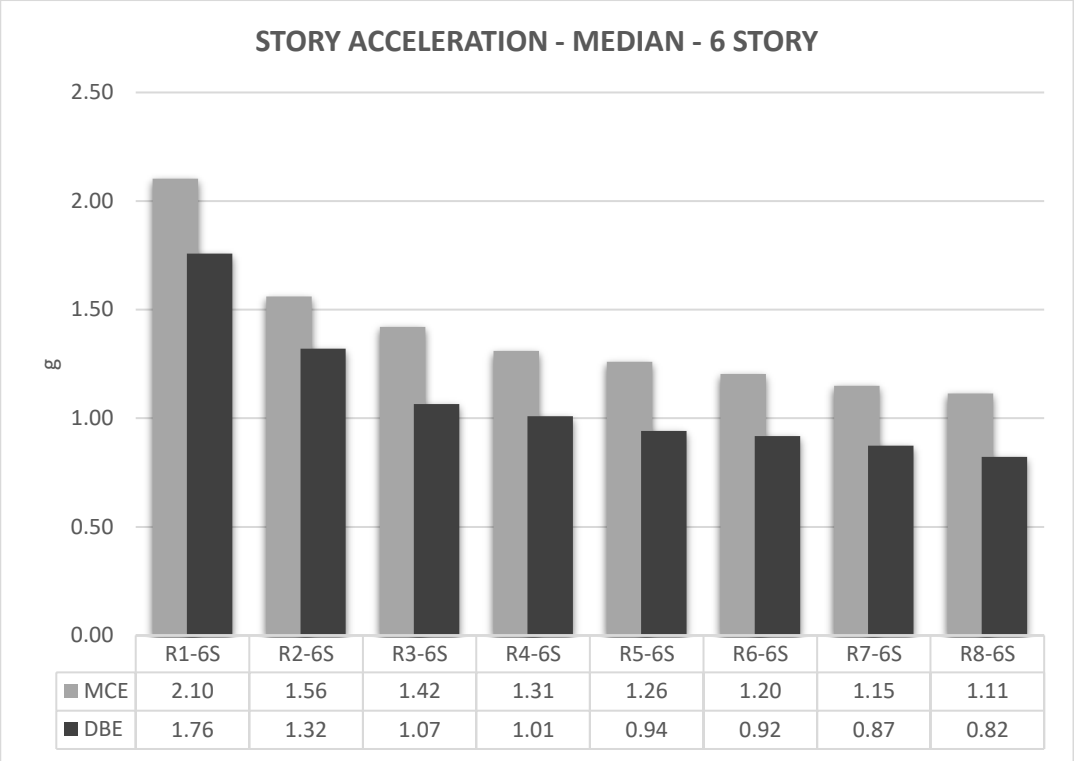

Figure 3.24. Peak story acceleration demands for 6 Story archetypes (Median)

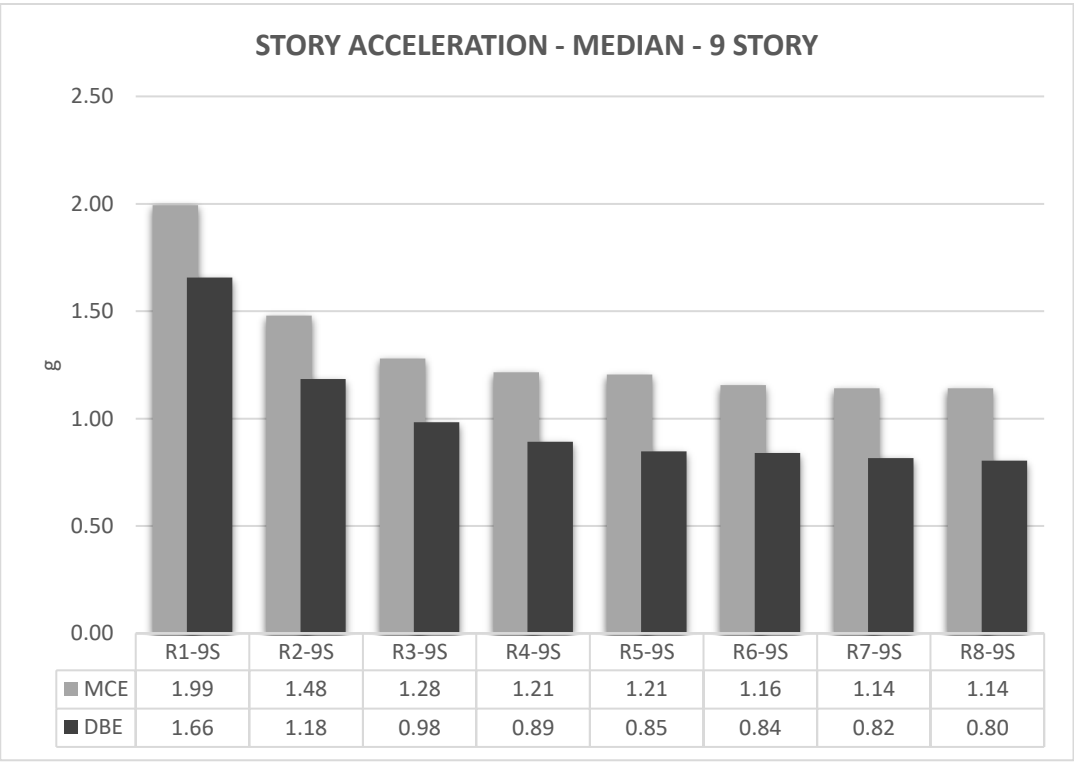

Figure 3.25. Peak story acceleration demands for 9 Story archetypes (Median)

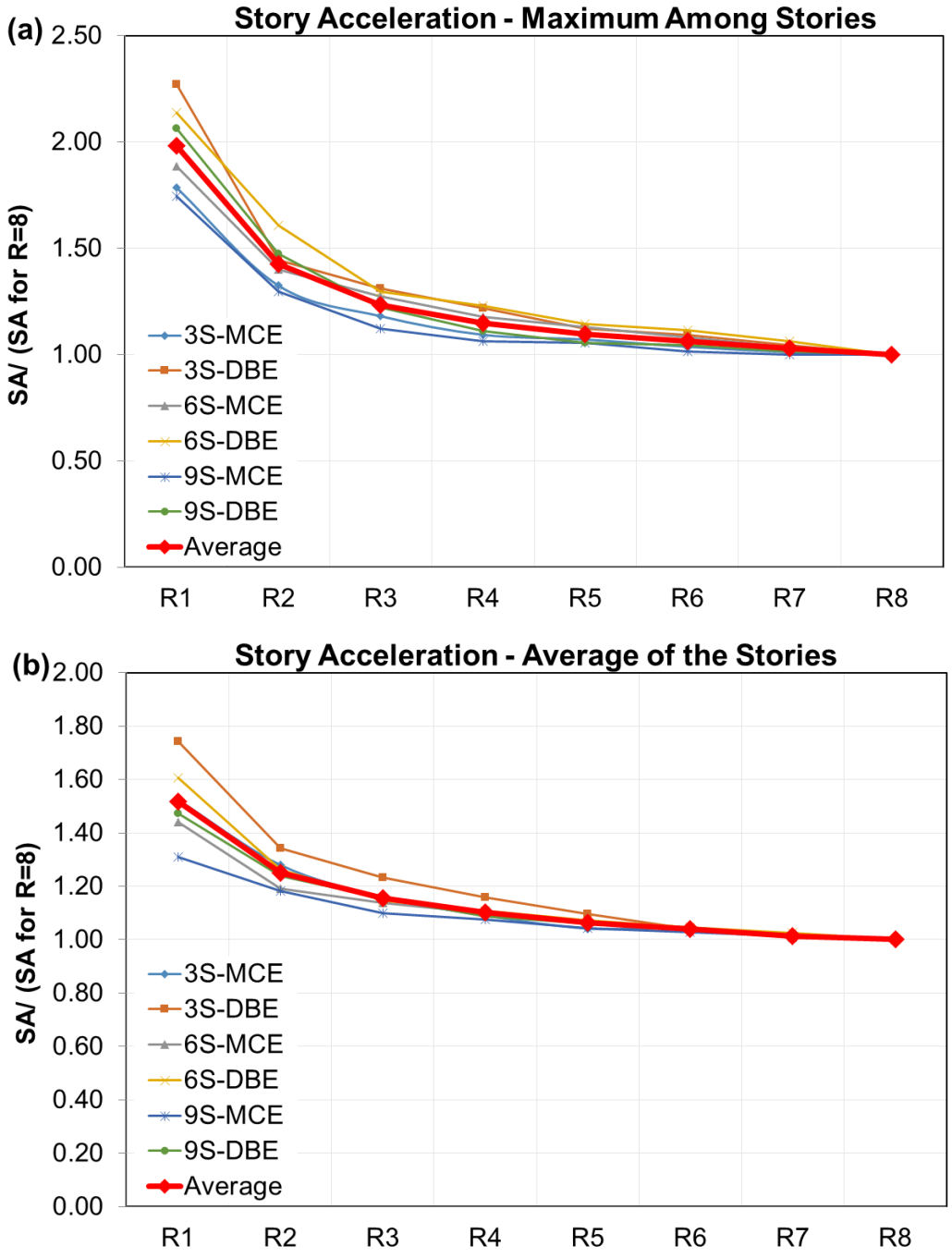

Figure 3.26. Variation of Normalized Story Accelerations

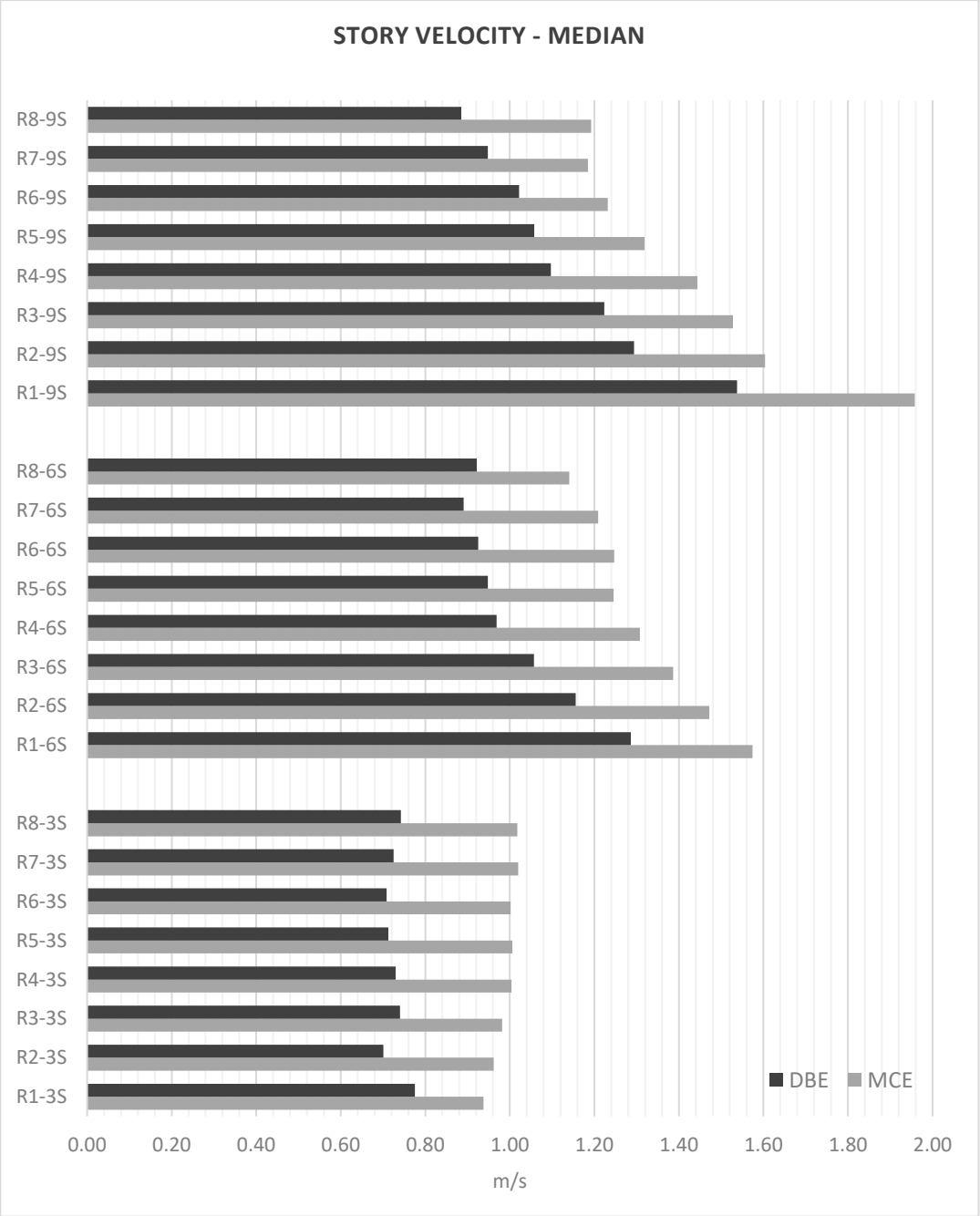

Figure 3.27. Peak story velocity demands (Median)

3.5.4 BRB Axial Strains and Ductility

The seismic performance assessment tool used in this study uses IDR, RIDR and SA as an input. On the other hand, BRB axial strains and associated ductility demands should also be taken into account such that the systems do not exhibit collapse behavior. As mentioned in the introduction section, the archetypes used in the beta testing of FEMA P695 Methodology were found to have adequate performance when designed with R=8 (Federal Emergency Management Agency, 2009). This essentially means that designs based on the US specifications with R=8 should provide acceptable performance. The maximum BRB axial strain and associated ductility for the archetypes were monitored and the median values from 44 ground motions were recorded. Representative variations of maximum brace axial strain and brace ductility for 9-story archetypes subjected to MCE level ground motions are given in Figures 3.28(a) and 3.28(b), respectively. The maximum BRB axial strains are usually reported for the first story of each archetype. The maximum value tends to decrease with a decrease in the R factor. Archetypes with R=8 experience the largest amount of axial strains which are 2.11%, 2.71% and 2.47% for 3-, 6-, and 9-story archetypes, respectively. These axial strains correspond to brace ductilities that range between 18 and 23. Brace axial strains of the order of 4% can be easily accommodated by BRBs manufactured with present-day technology. Therefore, collapse triggered by brace fracture is not expected for the archetypes considered in this study.

In addition to maximum axial strains, the cumulative axial strains were also investigated. Due to low cycle fatigue, a BRB core which experience many cycles of high amplitude axial strains, can fracture. For this purpose, the axial strain histories of BRB cores under 44 ground motions were obtained and the cumulative amount of axial strains were calculated using the rainflow counting procedure. The medians of cumulative axial strain demands were computed and normalized by the codified demand of 200. The normalized axial strain demands per story for 3-, 6- and 9- Story R=8 archetypes are reported in Fig. 3.29. Fahnestock et al. (2007b) and Sabelli et al.

(2003) reported mean cumulative axial strains as 179 (179/200 = 0.895) and 139 (139/200 = 0.695) times the yield strains for MCE level events, respectively. As a result, the findings are similar with the available studies.

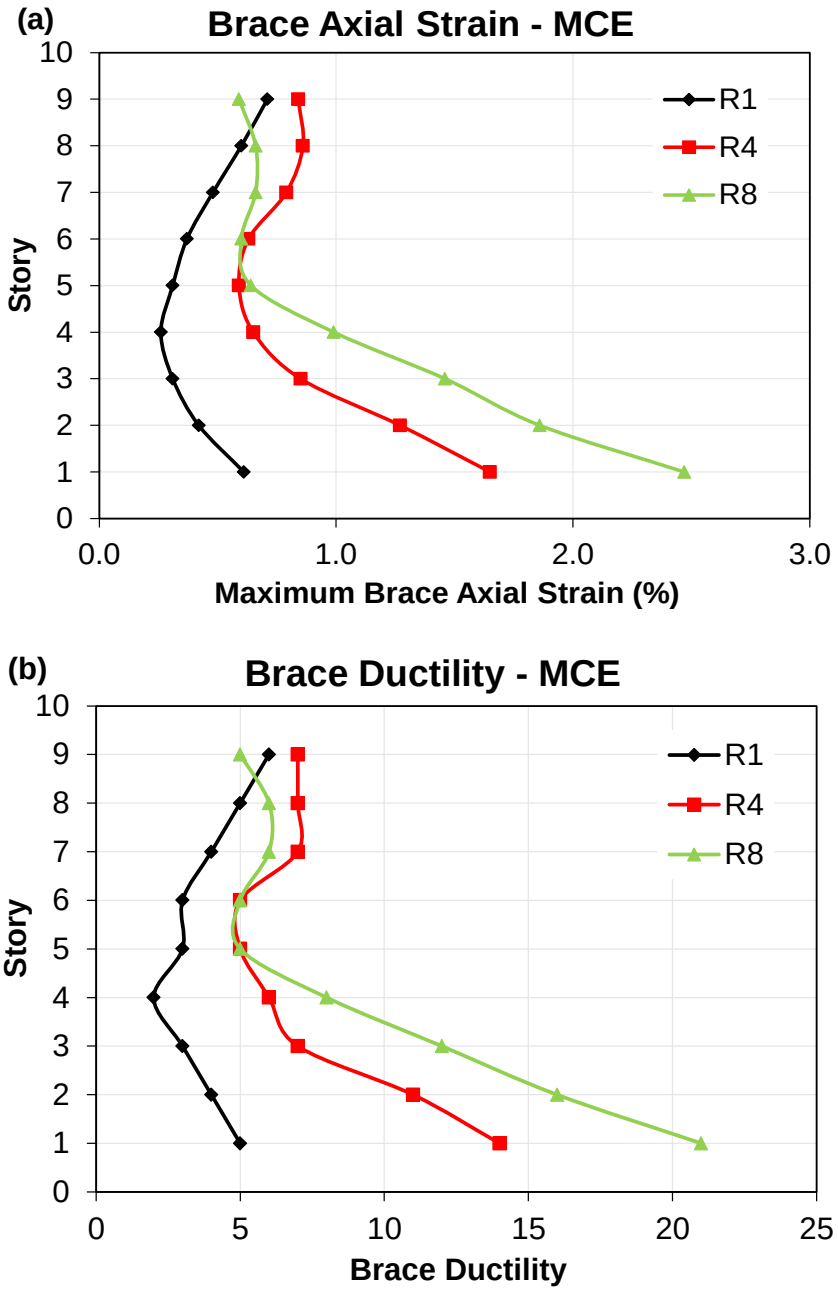

Figure 3.28. Maximum Brace Axial Strain and Ductility for 9-story Archetypes

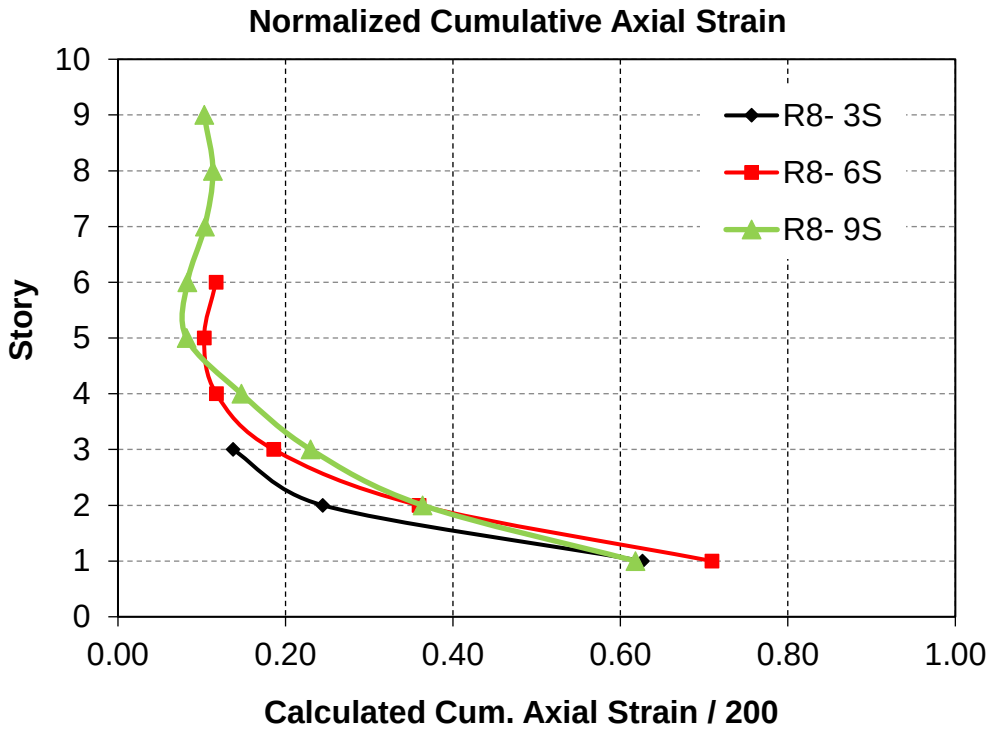

Figure 3.29. Normalized cumulative brace axial strain demands

CHAPTER 4

SEISMIC PERFORMANCE ASSESSMENT

The main aim of this study is to show the advantages of using alternative design response factors in the seismic design of BRBFs in terms of the performance of the building. In this manner, the archetypes were evaluated through repair time, down-time, unsafe placard, and replacement probability performance criteria. In the end, the optimal response modification factor in order to obtain optimal performance was determined. PACT (Performance Assessment Calculation Tool), a companion program for the methodology, is used to assist in the evaluation of performance.

4.1 Description of FEMA P-58 Methodology

Building codes establish minimum safety requirements through the specification of prescriptive criteria. Although these prescriptive criteria are intended to result in buildings capable of providing certain levels of performance, the actual performance of individual building designs is not assessed directly in traditional code. Therefore, performance-based seismic design evaluates how a building performs under a given potential hazard it is likely to experience (Federal Emergency Management Agency, 2006). In past earthquakes, it has been seen that the costs associated with the loss of usability can exceed the value of the building itself. As a result, the general need for predicting post-earthquake performance of the structure has increased significantly. In the first generation, the performance of the structure is expressed in terms of a series of discrete performance levels. However, as the knowledge and necessity after earthquake performance increase, a more detailed evaluation and assessment become necessary. In this manner, FEMA P-58 second-generation seismic performance assessment of the buildings guide has been developed and published by FEMA in 2018.

In this thesis, in order to assess performance, FEMA P-58 procedure was utilized. In summary, FEMA P-58 is a methodology to quantifies the performance measures of a structure in terms of repair cost, down-time, unsafe placard probability, casualties, injuries, etc. This information enables a detailed analysis of the consequences of earthquakes for new and existing buildings. As a result, decision-makers can evaluate the risk and make decisions about the design of structure (Federal Emergency Management Agency, 2018a).

4.2 Performance Assessment Calculation Tool (PACT)

The PACT tool is provided in the 3rd Volume of FEMA P-58 Methodology to provide a user-friendly platform for performance assessment procedures. It accepts results obtained from nonlinear time history analyses or results from simplified analyses. It can be used for scenario-based, intensity-based and time-based loss calculations. The tool provides 3 basic functions; input for building information, fragility functions, and demand parameters, computing performance measures and providing overall and performance group specific loss information

In general, the tool has 3 sections; modeling of the building, evaluate performance and examine results. In addition to these sections, tool also supplies 2 helpful functions; fragility specification manager and building population modeler.

The modeling section is the section where the performance model is created and analyses results entered. This section can be divided in 6 parts. The first part is related with information about the project and building. This information includes number of stories, total replacement cost and time, core and shell replacement cost, floor area, story heights, total loss threshold and some related factors. The second part consist of population model. PACT tool supplies several typical population models. The 3rd part simply used to select fragilities which determined to include in model. The 4th part includes inputs to model structural collapse, if necessary. The 5th part is used for structural analysis results. According to demand parameters of

fragilities, necessary demands were asked from user automatically. In this part, the assessment type, analysis type, number of demand vectors (number of ground motion) and number of realizations can be changed. Apart from the demand parameters, PACT also asks for maximum observed residual drift at each archetype and all stories, if available. In order to analyze these values, tool also gives editable probabilistic relation for irreparable residual story drift probability and residual drift. The last part is used for hazard curve if hazard analysis necessary.

After performance model is created, the tool evaluates the model and gives performance results. The tool gives various results including, repair cost, repair time, injuries, fatalities, embodied energy, carbon emission, unsafe placard probabilities and irreparable residual drift probabilities.

4.3 PACT Building Performance Models

The first step is to create a building performance model that was developed in PACT. Both structural and non-structural elements were considered in the model. The necessary information to evaluate the performance of the structure consists of the components of structural system, nonstructural members, occupancy information, number of stories, story heights, floor areas, total replacement cost, and replacement time. The PACT tool has default components that are at risk during an earthquake. Each of these components are associated with fragility and repair cost function. Peak structural response parameters from ground motion analyses were used in combination with fragility data to determine probable damage states for building components, which were then converted to repair costs (Del Gobbo, Williams and Blakeborough, 2018).

4.3.1 Replacement Cost and Time

As mentioned, the estimations of total building replacement costs are necessary for PACT. Total replacement cost includes the cost of essential building

structure components, cladding, and all nonstructural components. The RSMeans square foot cost estimator (*RSMeans Online Square foot estimator*) was used to determine building replacement costs, including material costs, architectural fees, and contractor fees. US National average and office building were selected in the computations. The cost data in PACT are based on 2011 averages, so 2011 data was selected in RSMeans estimator. In trial analyses, it has been seen that replacement due to residual drift always governs before high repair cost which causes replacement. As a result, it is concluded that no need for precise estimation of replacement cost is necessary for archetypes with different response modification factors. For a generic approximation between 3-, 6- and 9- Story buildings, the replacement cost was taken as constant $1900 per square meter. For replacement time, the estimations, which were given by Jarrett et al. (2015) was considered, and they were interpreted for 3-, 6- and 9- Story buildings. The final replacement values and times are given in Table 4.1. In addition, the PACT tool needs core and shell replacement cost, which was taken as 20% of total replacement cost, as suggested by Guerrero et al. (2017). The total loss threshold, which is the ratio of the total replacement cost to irreparable cost, was taken as 1. This value is given default in PACT and in examples provided with FEMA P-58 documentation (Federal Emergency Management Agency, 2018d). In practice, this value is closer to 0.4 (Federal Emergency Management Agency, 2018c); however, in order to compare results over 0.4, these value is kept constant as 1.

Table 4.1 Replacement cost and time values used in PACT models

	Total Replacement Cost ($)	**Replacement Time (days)**
3 Story	$4,670,000	360
6 Story	$9,350,000	420
9 Story	$14,000,000	480

4.3.2 Population

In order to assess casualties and injuries, the population model, i.e., the distribution of occupants among various times of day and year, should be specified. In the PACT tool, 8 different population models are provided, which are typical commercial office, education K-12 (elementary, middle, high school), healthcare, hospitality, multi-unit residential, research, retail, and warehouse occupancies. In this study, a typical commercial office occupancy model supplied by PACT was used directly without any modification. The weekday and yearly population distributions are given in Fig. 4.1 and Fig 4.2

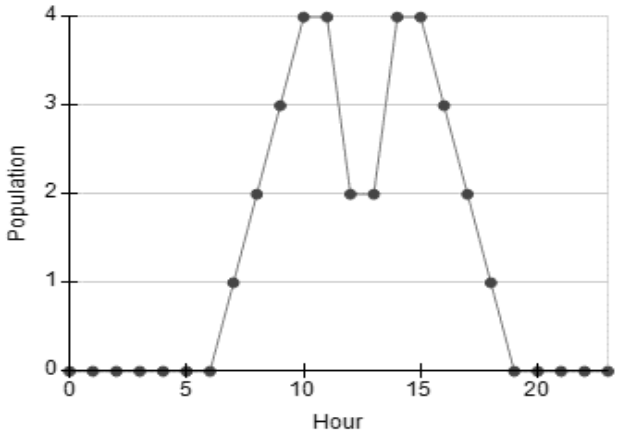

Figure 4.1. Weekday population distribution model (FEMA, 2018c)

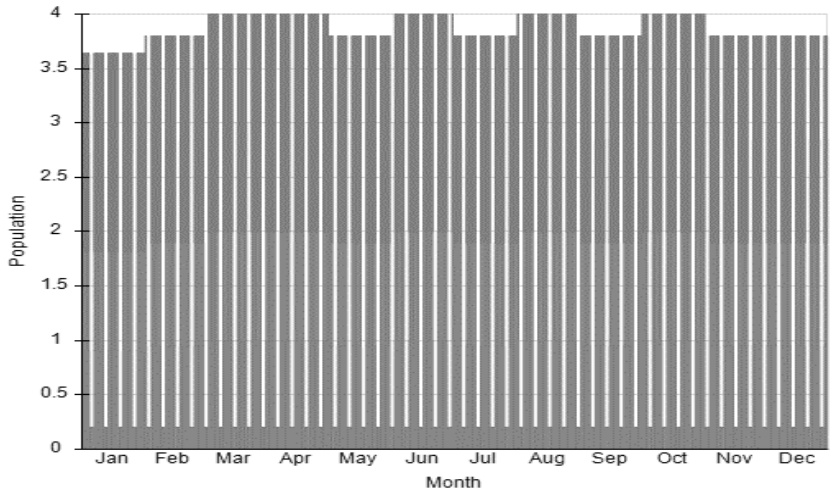

Figure 4.2. The yearly population distribution model (FEMA, 2018c)s

4.3.3 Component Fragilities and Performance Groups

In order to estimate performance, it is necessary to define the quantity and distribution of damageable components. PACT uses fragilities to describe these components. Each fragility has fragility function and consequence function. The fragility function specifies damage state probability for a single demand parameter. The fragilities divide into two by their directionality of demand parameter as directional or non-directional. Three types of demand parameters are commonly used; the peak story drift ratio, peak floor acceleration, and peak floor velocities. Consequence functions represent the consequence of damage states by predefined repair cost, repair time, and other consequences if applicable.

The non-structural fragility quantities were computed with the help of the Normative Quantity Spreadsheet, which is a supplemental file provided by FEMA P-58. This spreadsheet estimates the type and number of non-structural components in a building based on square area and occupancy type. Table 4.2. shows the fragilities per story used in the models. Furthermore, for first and top stories, additional fragilities were inputted to model. These are also mentioned in Table 4.2. For fragility estimations, the buildings were assumed to be in the occupancy type of commercial office building.

4.3.4 Analysis Inputs and Residual Drift

In the structural analysis results part, 22 demand vectors for each direction were specified. In the nonlinear analysis, each BRBF archetype was subjected to 44 ground motion. However, these ground motions were paired, and each pair consisting of two different directions. As a result, the results were divided into two different directions and inputted to PACT, respectively. For 24 archetypes, 22 pairs of IDR and story accelerations were defined. As none of the fragilities have story velocity as a demand parameter, no story velocity result was supplied. Two hundred Monte Carlo realizations were used, as suggested by FEMA P-58.

Table 4.2 Structural and Non-structural fragilities used in PACT models

Stories	No.	Component Name	Quantity	Directional	Demand Parameter
All	B1031.001	Bolted shear tab gravity connections	4	Yes	Story Drift
All	B1033.101b	Steel Buckling Restrained Brace (BRB)	4	Yes	Story Drift
All	B2022.001	Curtain Walls	93	Yes	Story Drift
All	C1011.001a	Wall Partition, Type: Gypsum with metal studs	9.26	Yes	Story Drift
All	C2011.001b	Prefabricated steel stair	2	Yes	Story Drift
All	C3011.001a	Wall Partition, Type: Gypsum + Wallpaper	0.7	Yes	Story Drift
All	B3011.011	Concrete tile roof	25	No	Acceleration
All	C3027.001	Raised Access Floor	70	No	Acceleration
All	C3032.001a	Suspended Ceiling	37	No	Acceleration
All	C3034.001	Independent Pendant Lighting	277.72	No	Acceleration
All	D2021.011a	Cold or Hot Potable	0.39	No	Acceleration
All	D3041.011a	HVAC Galvanized Sheet Metal Ducting	0.69	No	Acceleration
All	D3041.012a	HVAC Galvanized Sheet Metal Ducting	0.19	No	Acceleration
All	D3041.031a	HVAC Drops / Diffusers in suspended ceilings	8.33	No	Acceleration
All	D3041.041a	Variable Air Volume (VAV) box with in-line coil	6.48	No	Acceleration
All	D4011.021a	Fire Sprinkler Water Piping	1.85	No	Acceleration
All	D4011.031a	Fire Sprinkler Drop Standard Threaded Steel	0.83	No	Acceleration
All	D5012.021a	Low Voltage Switchgear	1	No	Acceleration
1st	D1014.011	Traction Elevator	1	No	Acceleration
1st	B1031.011a	Steel Column Base Plates	4	Yes	Story Drift
Roof	D3031.011a	Chiller - Capacity: < 100 Ton	0.35	No	Acceleration
Roof	D3031.021a	Cooling Tower - Capacity: < 100 Ton	0.35	No	Acceleration
Roof	D3041.101a	HVAC Fan - Capacity: all	1	No	Acceleration
Roof	D3052.011a	Air Handling Unit - Capacity: <5000 CFM	1.62	No	Acceleration
Roof	D5011.011a	Transformer/primary service - Capacity: <100 kVA	1	No	Acceleration
Roof	D5012.013a	Motor Control Center - Capacity: all	0.37	No	Acceleration
Roof	D5012.031a	Distribution Panel - Capacity: 100 to <350 Amp	1	No	Acceleration

In the residual drift part, the default values were kept constant. The probabilistic distribution of the irreparable residual story drift ratio graph is given in Fig 4.3. The median value and dispersion are taken as 1% and 0.3, respectively. Maximum R-IDR was inputted to the program. Since archetypes are designed using location-neutral spectra, no hazard curve is available. As a consequence, no time-based assessment is performed.

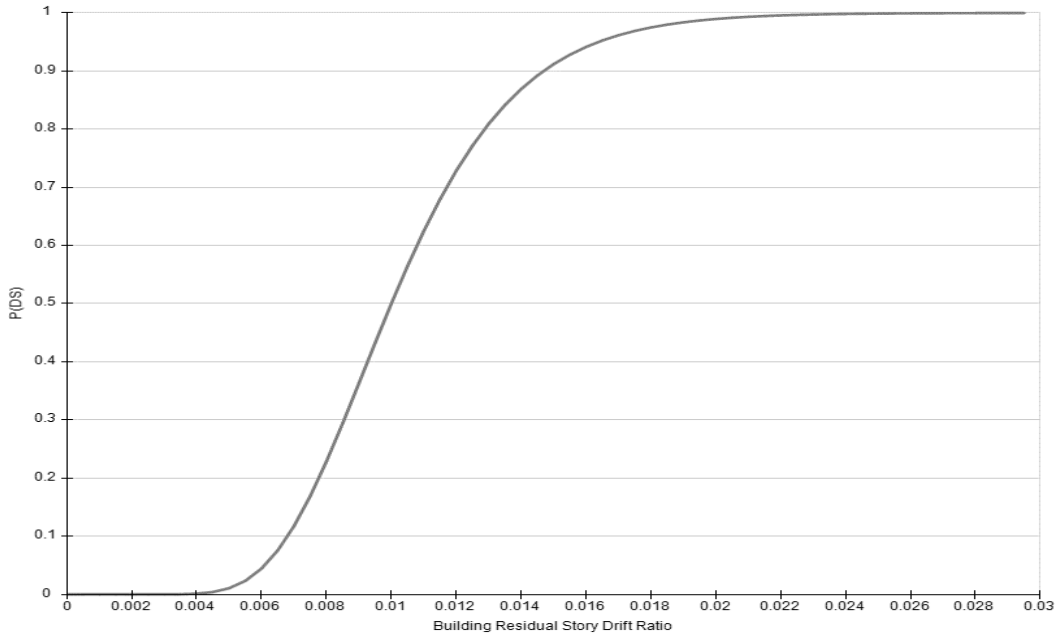

Figure 4.3. Irreparable damage probability distribution depends on R-IDR (FEMA, 2018c)

4.4 Performance Assessment Results

PACT tool supplies result as a probabilistic distribution for repair cost and downtime (repair time). However, due to the necessity to compare many archetypes, the comparison from these distributions is not a basic task. In FEMA P-58, the confidence level was defined as the level that reflects the desired certainty that the performance of a building will be at least as good or better than a target level (Federal Emergency Management Agency, 2018b). Three confidence levels are used commonly. The median confidence level represents the value, which will be exceeded half the time or 50% chance the value will be exceeded. The mean confidence level was defined as an average outcome, and typically there is a 40% chance that mean value is exceeded. The 90^{th} percentile level represents the worst performance in 9 out of 10 buildings. The choice of confidence level depends on the needs of the building and stakeholders. In this study, the median confidence level was selected for the comparison of repair cost and repair time results of archetypes.

The repair cost and repair time consequence functions that were supplied in PACT includes all work associated with the repair of the actual damage as well as collateral work associated with removal and replacement of finishes, relocation of utilities, provision of scaffolding, and similar actions. However, the repair time estimates were not included the time needed to design, permit, and fund the repair project. Furthermore, unsafe placard probabilities and irreparable damage probabilities are also supplied. Apart from these results, average casualties and injuries, average carbon emission, and embodied energy values are presented. The following subsections present performance metrics that were gathered from PACT output.

4.4.1 Repair Cost

The probabilistic distributions of repair costs are indicated in Figs 4.4-4.6 for BRBFs subjected to MCE level ground motions. The vertical axis shows the non-exceedance probability. While the movement of the plot to the left indicates a reduction in repair cost, the upward movement implies the decrease in replacement possibility. The probability distributions do not reach to 100% in all cases and the distributions reach the plateau at lower levels of confidence. This is due to the large amounts of residual drifts that result in total replacement of the building. In other words, residual drifts dominate over the repair costs in cases where the building has to be demolished due to the presence of large residual drifts. For 3-story BRBFs, the plateaus are reached above the median level, indicating that the costs at the median level are not influenced by the presence of residual drifts. For the 6-story BRBFs cases, the plateaus lies slightly below the median line for archetypes designed with R=5 and 6 and below the 35% level for archetypes designed with R=7 and 8. This observation indicates that the buildings designed with R≥5 require total replacement after being subjected to an MCE level seismic event. Similar observations can be made for the 9-story archetypes where the buildings designed with R≥6 require total replacement. For brevity, probability distributions for BRBFs subjected to DBE level ground motions are not presented herein.

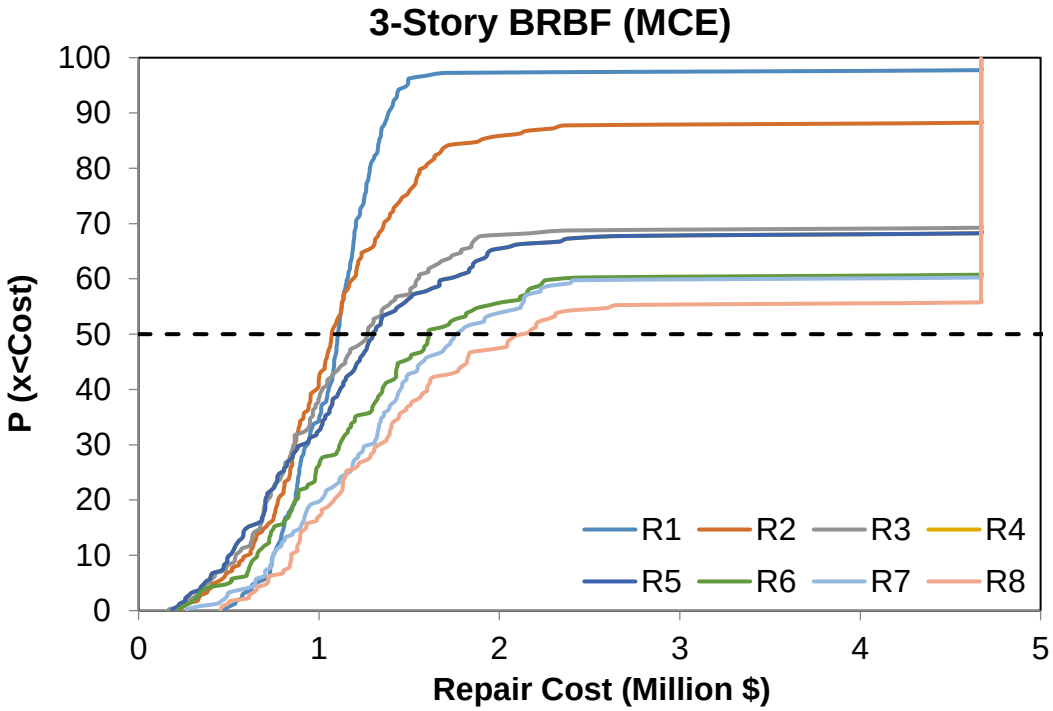

Figure 4.4. The repair cost non-exceedance probabilistic distribution (3-Story)

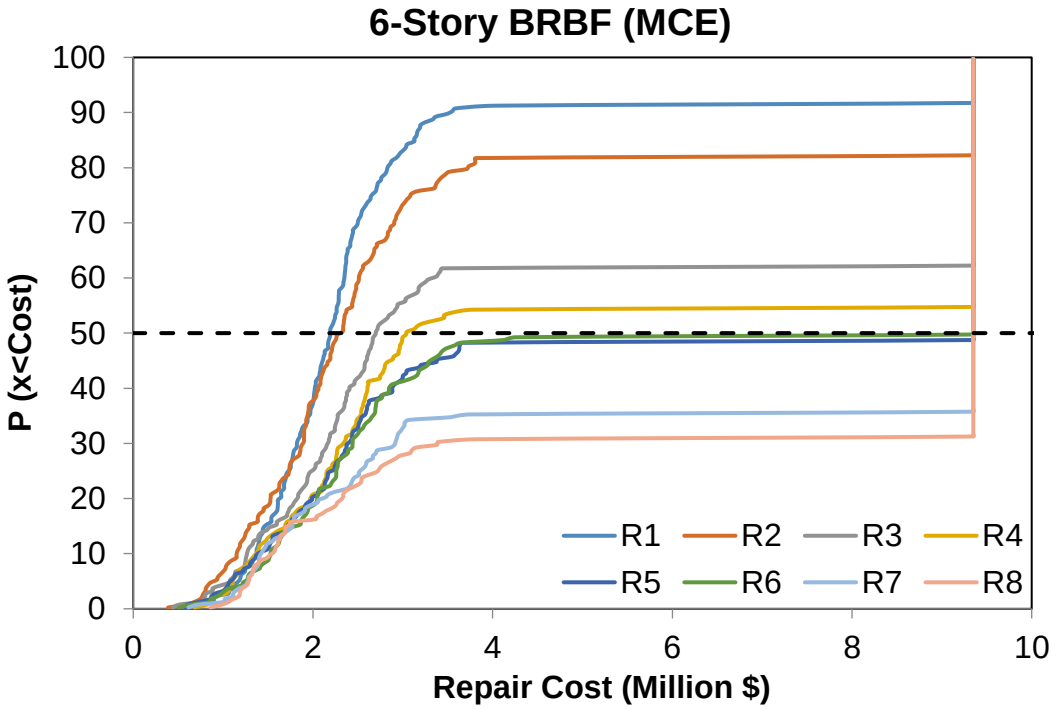

Figure 4.5. The repair cost non-exceedance probabilistic distribution (6-Story)

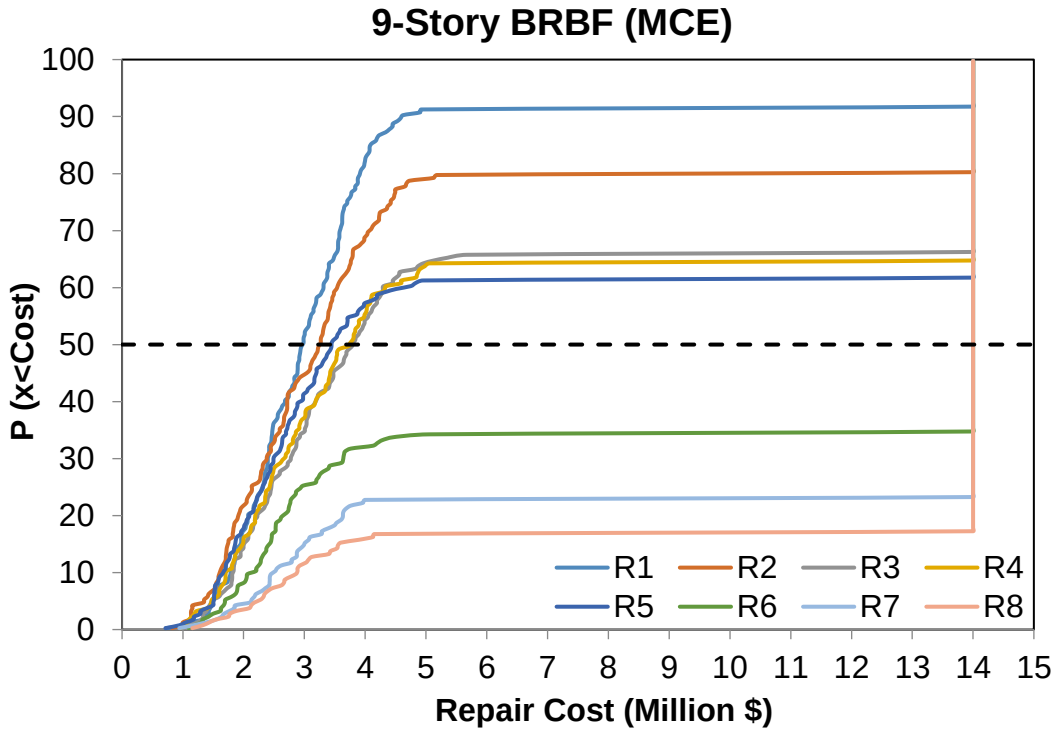

Figure 4.6. The repair cost non-exceedance probabilistic distribution (9-Story)

The median repair costs were normalized by the initial costs and the ratios are presented in Figs 4.7-4.9 for BRBFs subjected to MCE and DBE level ground motions. For 3 story archetypes, in the range of R8-3S to R4-3S for both earthquake levels, the repair costs decrease as the R-Factor reduces. However, at DBE level as the R-Factor reduces beyond four, story accelerations started to govern. An increase in repair costs, which was caused by nonstructural fragilities, overpassed the decrease in the repair cost of structural fragilities, and the total repair cost increased. This situation was more visible under the DBE level because the contribution to cost majorly comes from nonstructural fragilities. The effect of acceleration was seen most actively in the R=1 case under the DBE level. The cost of nonstructural fragilities increased such that the repair cost of R1-3S overpass the repair cost of the R8-3S archetype. Under the MCE level, the most significant change in repair cost was observed between going from R5-3S to R4-3S, where median repair cost decreased by approximately 18%. In contrast, the largest improvement at DBE level has seen between R7-3S to R6-3S with a 17% decrease.

When the results of 6 story archetypes (Fig. 4.8) investigated, it was observed that at MCE level, R>=5 archetypes have more than 50% probability of replacing rather than repair; as a result, the median repair costs of these archetypes were equal to replacement cost. Similar results were also obtained for 9 story archetypes, which are given in Fig. 4.9, with R>=6. Four 6-story and three 9-story archetypes had a repair cost equal to the initial cost of the building, indicating total replacement after an MCE level event. No total replacement was necessary for any of the archetypes subjected to DBE level seismic events. When the non-replacement governed 6 story archetypes compared, for MCE level as the R-Factor reduce, a linear decrease in repair costs was observed. However, 9 story archetypes show a local increase around R4-9S, while the R1-9S archetype showed the minimum median repair cost. At the DBE level, while 6 story results show a similar trend to 3 story results, 9 story archetypes showed a decrease around R6-9S and increased around R4-9S.

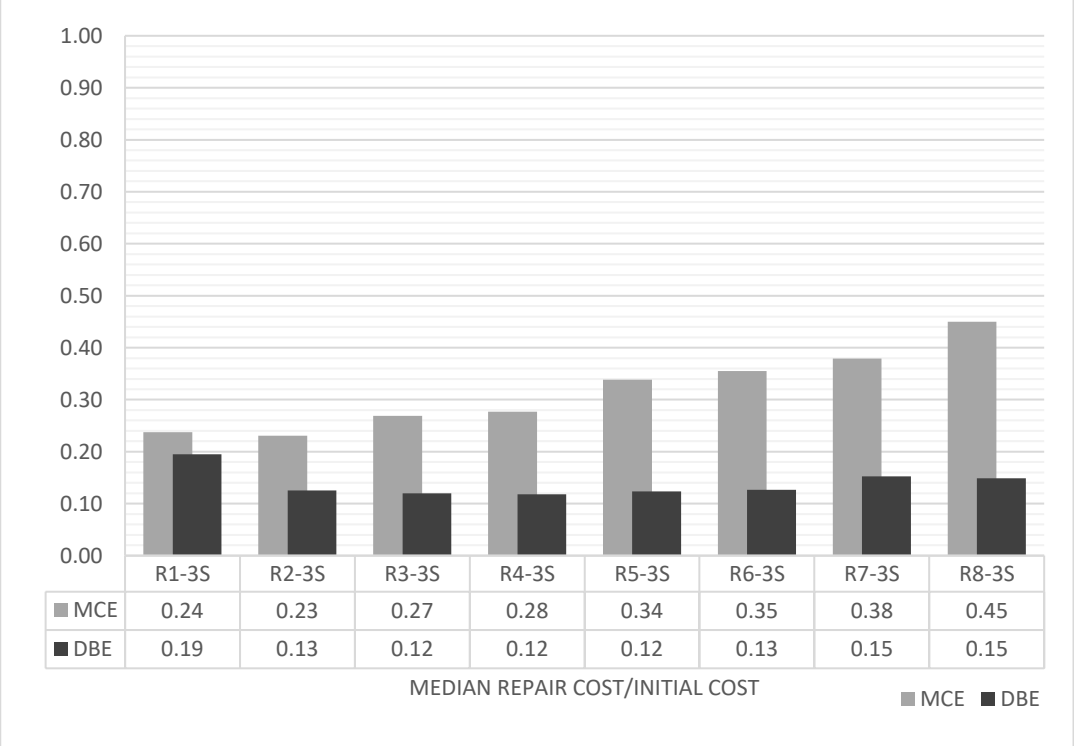

	R1-3S	R2-3S	R3-3S	R4-3S	R5-3S	R6-3S	R7-3S	R8-3S
MCE	0.24	0.23	0.27	0.28	0.34	0.35	0.38	0.45
DBE	0.19	0.13	0.12	0.12	0.12	0.13	0.15	0.15

Figure 4.7. Normalized Median repair cost values for 3-Story archetypes

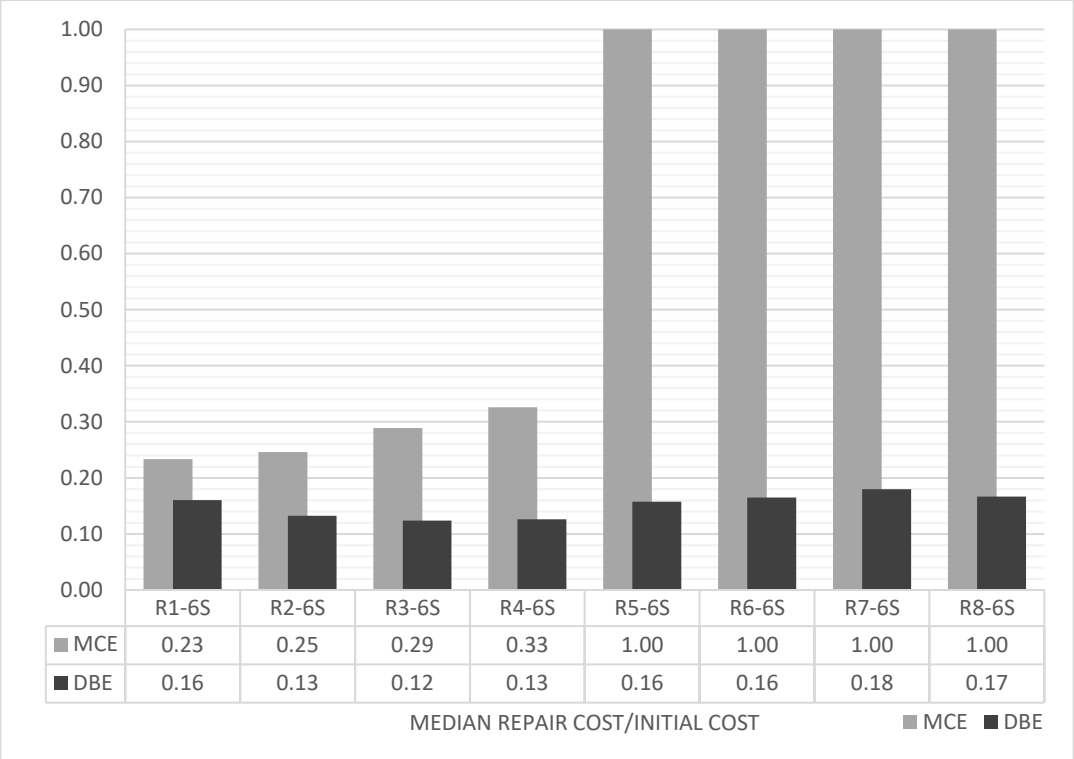

Figure 4.8. Normalized Median repair cost values for 6-Story archetypes

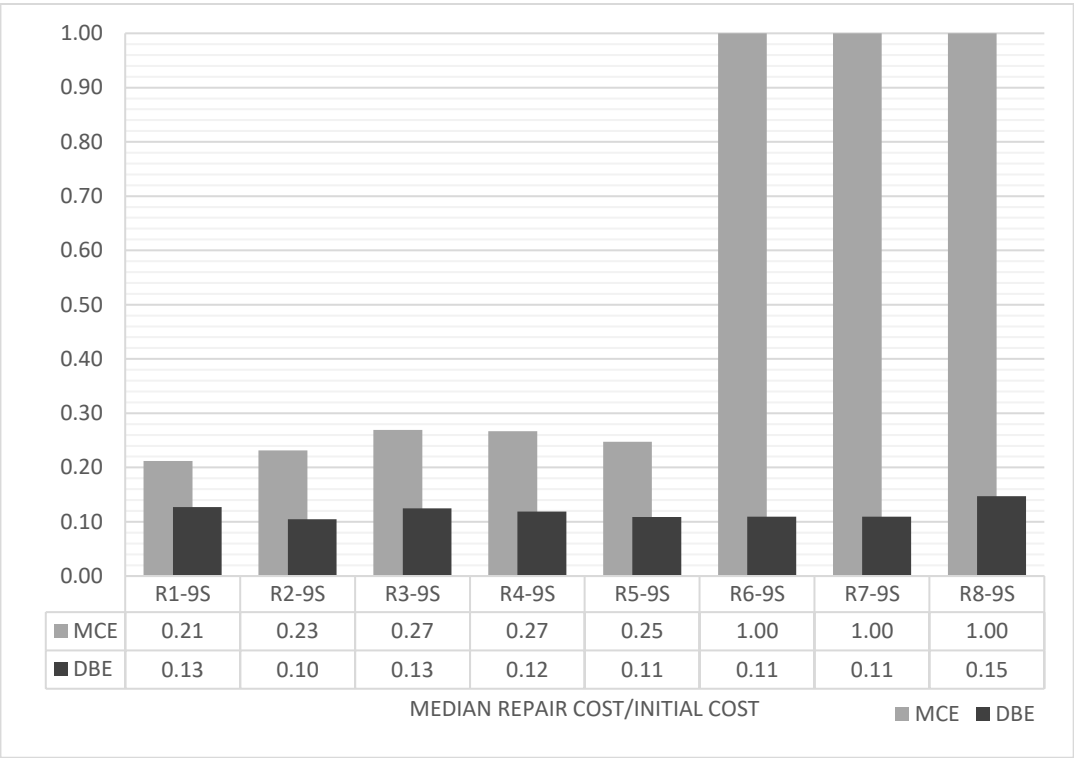

Figure 4.9. Normalized Median repair cost values for 9-Story archetypes

Detailed investigations show that the total repair cost is mostly influenced by the repair cost of the drift sensitive components for archetypes designed with R=8. As the R factor is reduced, the repair cost of the drift sensitive components reduces but the repair cost of acceleration sensitive components increases. This in turn results in an overall increase in the median repair cost for archetypes designed with R=1 or 2. That is why the R=1 design can have a higher median repair cost as compared to the R=4 design for the DBE case. The top four components in terms of the repair cost are indicated in Fig. 4.10 for these cases. While the repair cost of BRBs is the highest among all components for R=8 and R=4 cases, repair cost of suspended ceiling is the highest among all components for R=1 case. In addition, a representative decomposition of the costs for 6-story archetypes designed with R=1, 4, and 8 is presented in Fig. 4.11. In this figure, the total replacement cost is decomposed into the cost of drift sensitive and acceleration sensitive components.

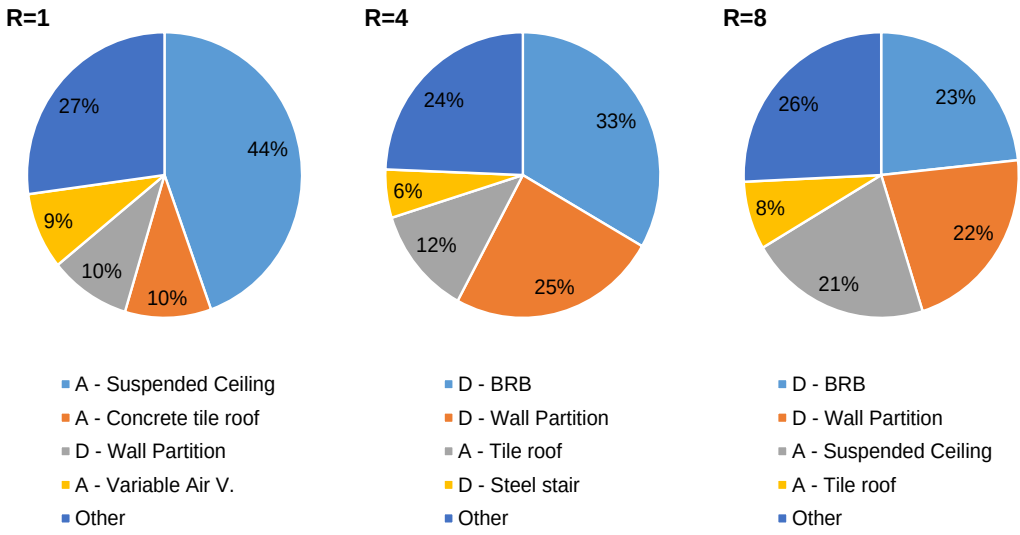

Figure 4.10. Repair Costs of Components for 6-story Archetypes

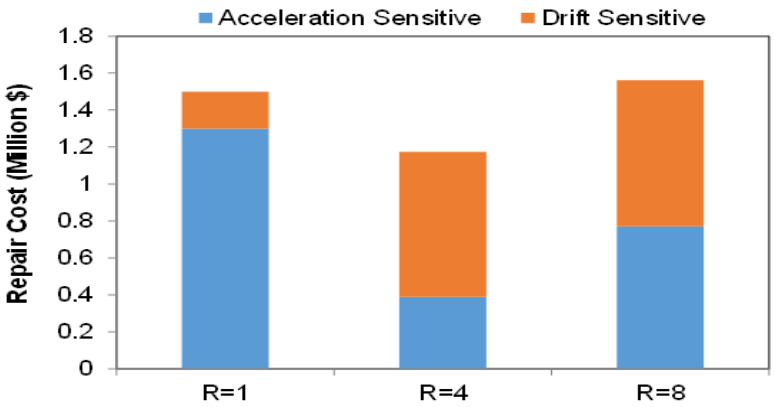

Figure 4.11. Decomposition of Repair Costs for 6-story Archetypes Subjected to DBE Level Ground Motions

4.4.2 Irreparable Residual Drift Probability

Figs. 4.12 - 4.14 shows irreparable residual drift probabilities. The investigation of 3 story archetypes results demonstrated that the R1-3S archetype showed almost no irreparable residual drift. At the MCE level, archetypes with R>=3 have more than 30% of probability that residual drifts cause total replacement and between R3-3S and R2-3S, the largest improvement was seen as 19% drop in replacement chance was determined. At MCE level, R>=5 archetypes have irreparable residual drift probabilities more than 50%, which shows that the replacement for median confidence level caused by residual drifts for these archetypes. The largest improvement was seen between R3-6S to R2-6S as 20%. Under the DBE level, archetypes with R-Factor greater than 4 showed more than 30% of replacement probability, and a major drop of 14% was observed between R5-6S and R4-6S. At the MCE level, the most substantial improvement for 9 story archetypes was observed between R6-9S and R5-9S as a 27% drop while at DBE level, a 23% drop was observed between R8-9S and R7-9S archetypes. At the MCE level, similar to the result of 6 story archetypes, archetypes with high R-factors (R>6) showed more than %50 probability of replacement. Larger residual drifts observed in taller archetypes are in line with the findings of Erochko et al. (2011) ,where similar conclusions were reported. These large residual drifts are mainly due to the large P-Δ effects that develop in taller frames.

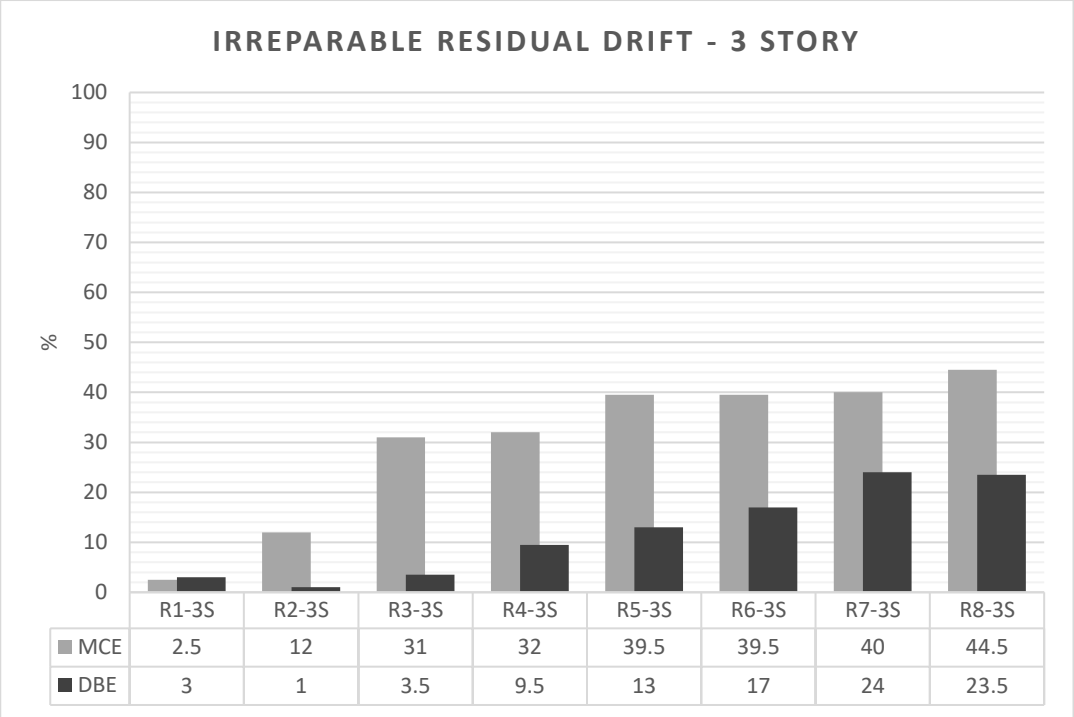

Figure 4.12. Irreparable residual drift probabilities for 3-Story archetypes

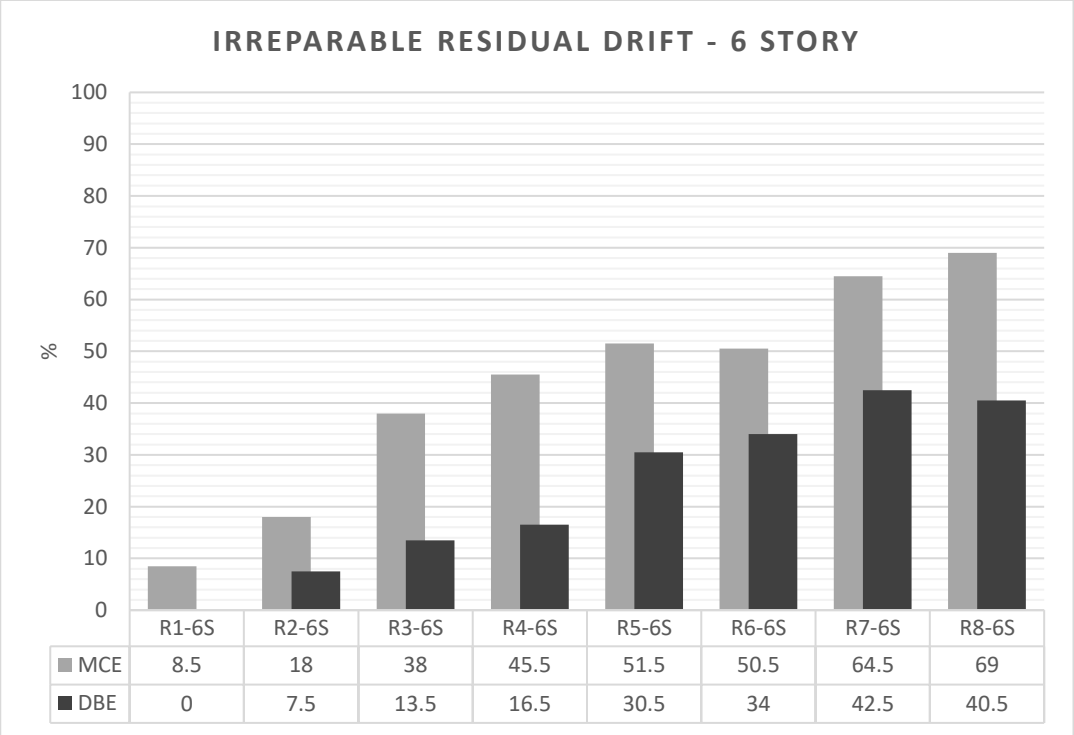

Figure 4.13. Irreparable residual drift probabilities for 6-Story archetypes

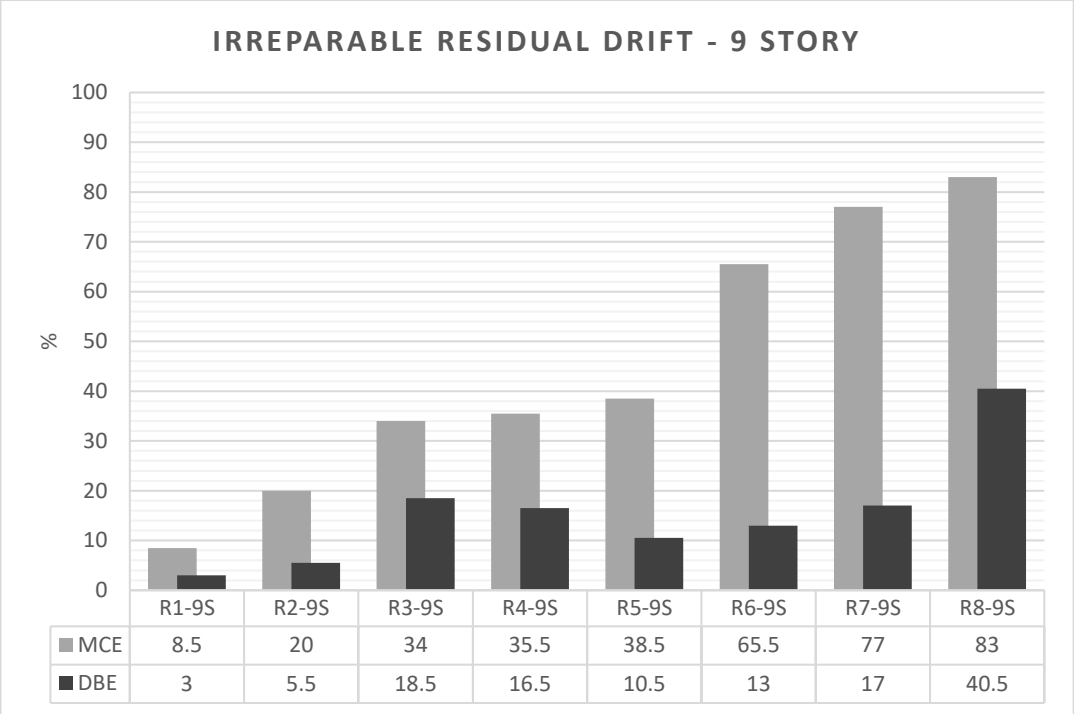

Figure 4.14. Irreparable residual drift probabilities for 9-Story archetypes

4.4.3 Repair Time

The performance analysis results in terms of median repair time are given in Figs. 4.15 – 4.17. In order to improve visibility, a maximum repair time of 50 days is used in Figs. 4.16 and 4.17; although for 6- and 9-story archetypes, where total replacement is necessary, the values reach to 420 days and 480 days, respectively. For all heights, median repair time results show a similar trend to median repair cost results. The same increase and decrease patterns were observed. The repair time after MCE level events tend to reduce with a reduction in the R factor; however, the difference is limited to 5-15 days. The repair time after DBE level events seems to be the lowest for the designs with R=4.

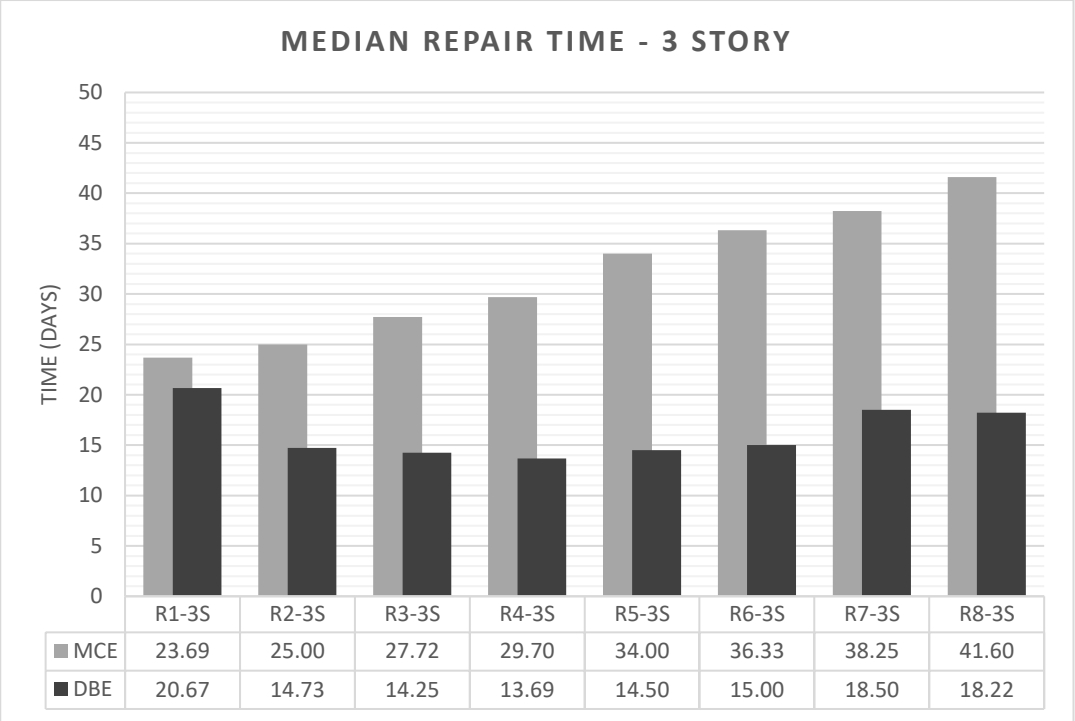

Figure 4.15. Median repair time values for 3-Story archetypes

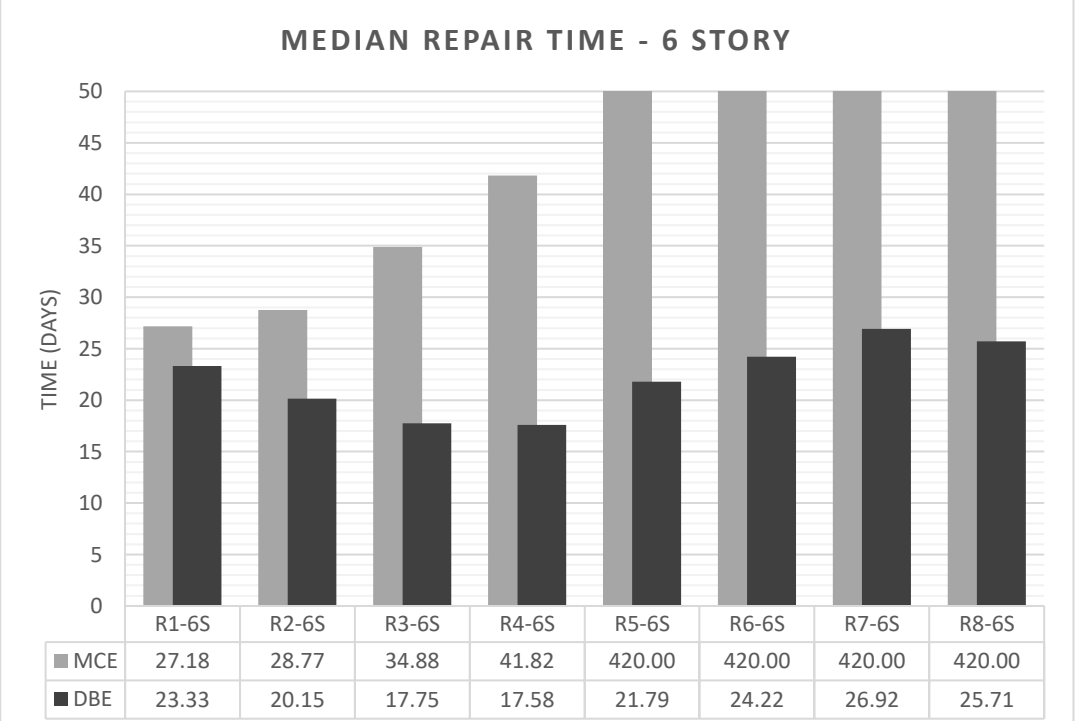

Figure 4.16. Median repair time values for 6-Story archetypes

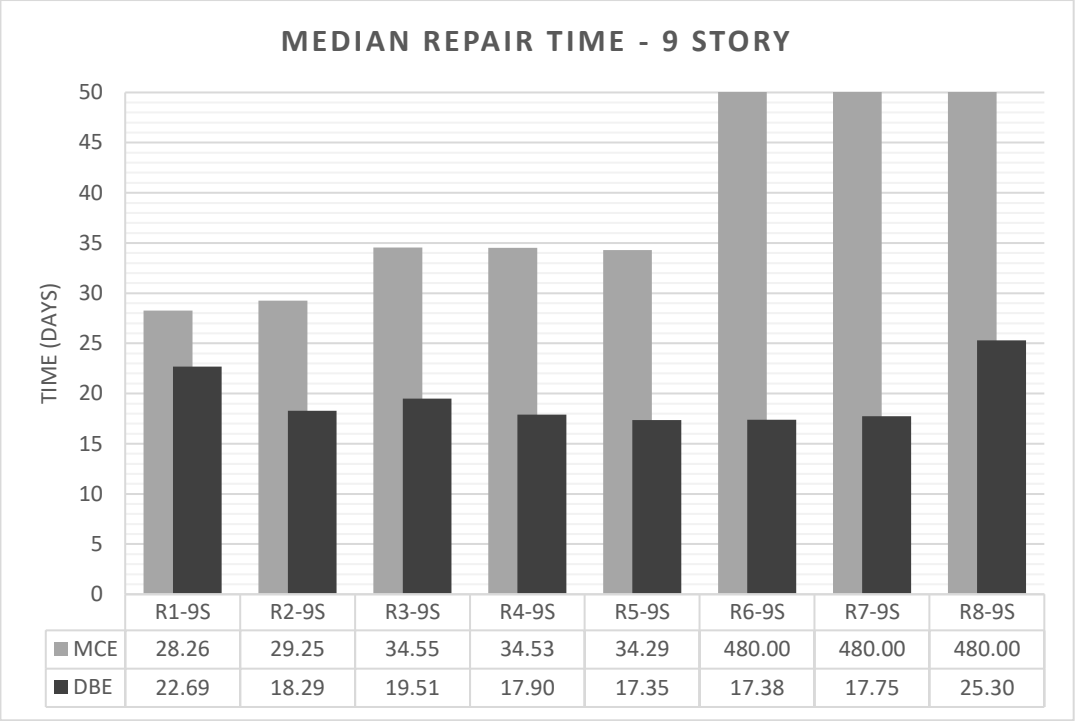

Figure 4.17. Median repair time values for 9-Story archetypes

4.4.4 Unsafe Placard Probability

Unsafe placarding is a post-earthquake inspection rating that deems a building, or portion of a building, damaged to the point that entry, use, or occupancy poses an immediate risk to safety. It is equivalent to the red unsafe placard, according to ATC-20 (Applied Technology Research Council, 1989). The component damage states are converted into unsafe placard consequences using the PACT tool. The methodology has pre-defined placard consequence functions, which are determined using engineering judgment. The default functions are used to analyze placard probabilities. Unsafe placard probabilities are given in Figs. 4.18 – 4.20. Regardless of the R factor and number of stories, all archetypes are expected to have unsafe placards with at least 60 percent probability after the MCE level ground motions. This means that all buildings will need some sort of repair after MCE level events. The probability of unsafe placards reduces for DBE level events where designs with R=4 provide one of the lowest cases for 3-, 6-, 9-story buildings. It was observed that at higher intensity ground motions, unsafe placard probabilities were less

sensitive to R-Factor in design. In contrast, at DBE level, at all heights, R=1 archetypes showed increase unsafe placard probability.

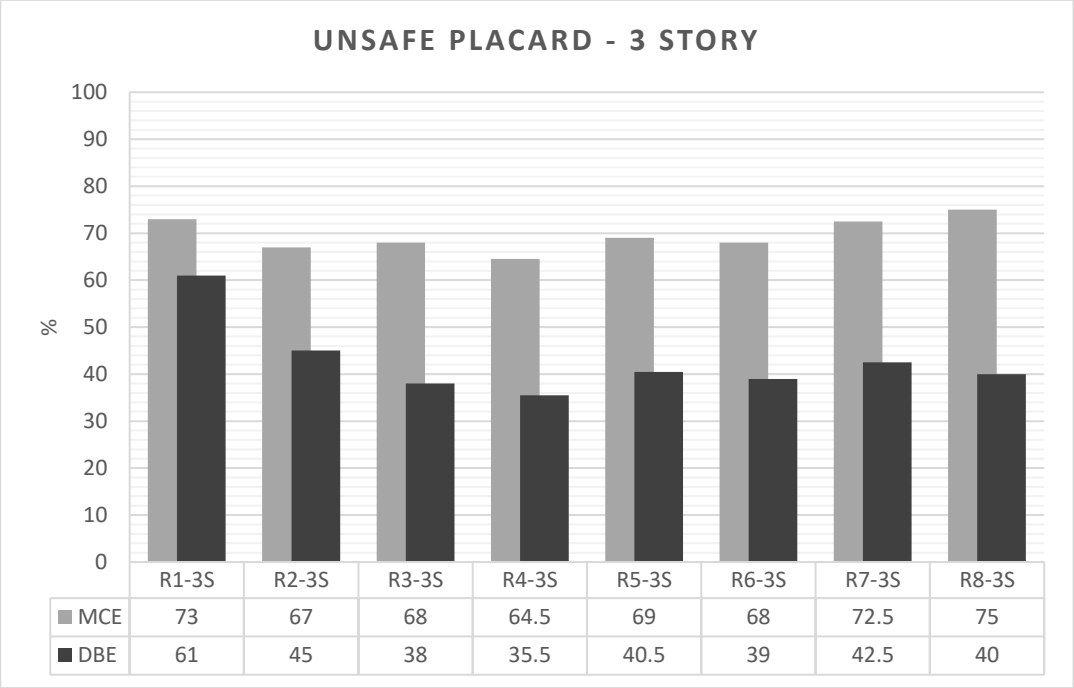

Figure 4.18. Unsafe placard probabilities for 3-Story archetypes

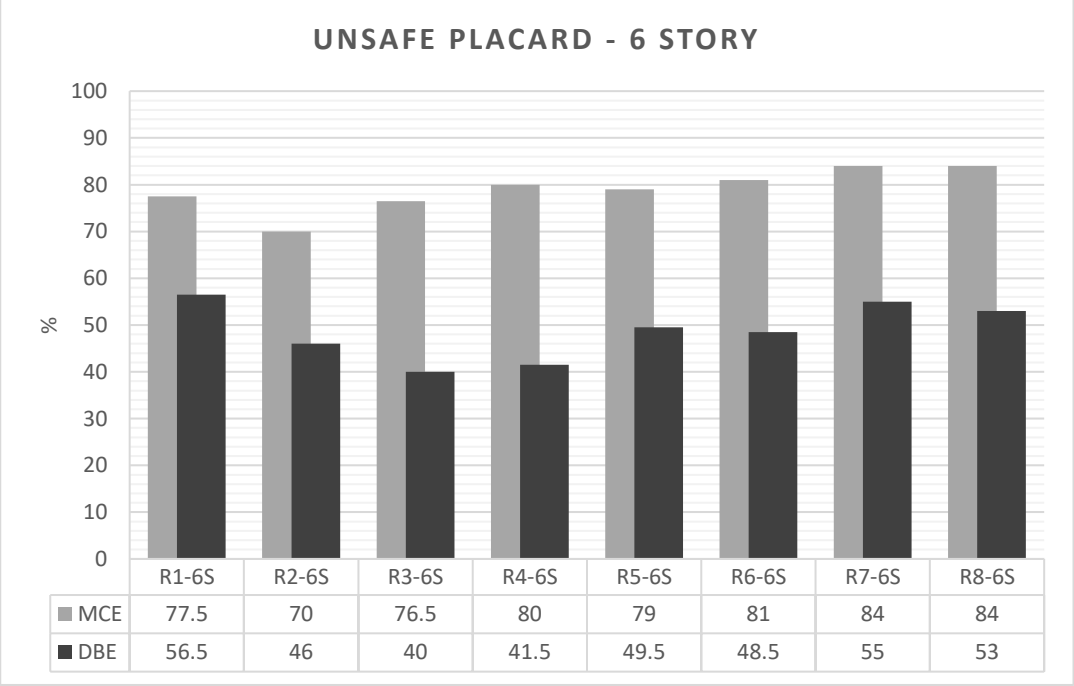

Figure 4.19. Unsafe placard probabilities for 6-Story archetypes

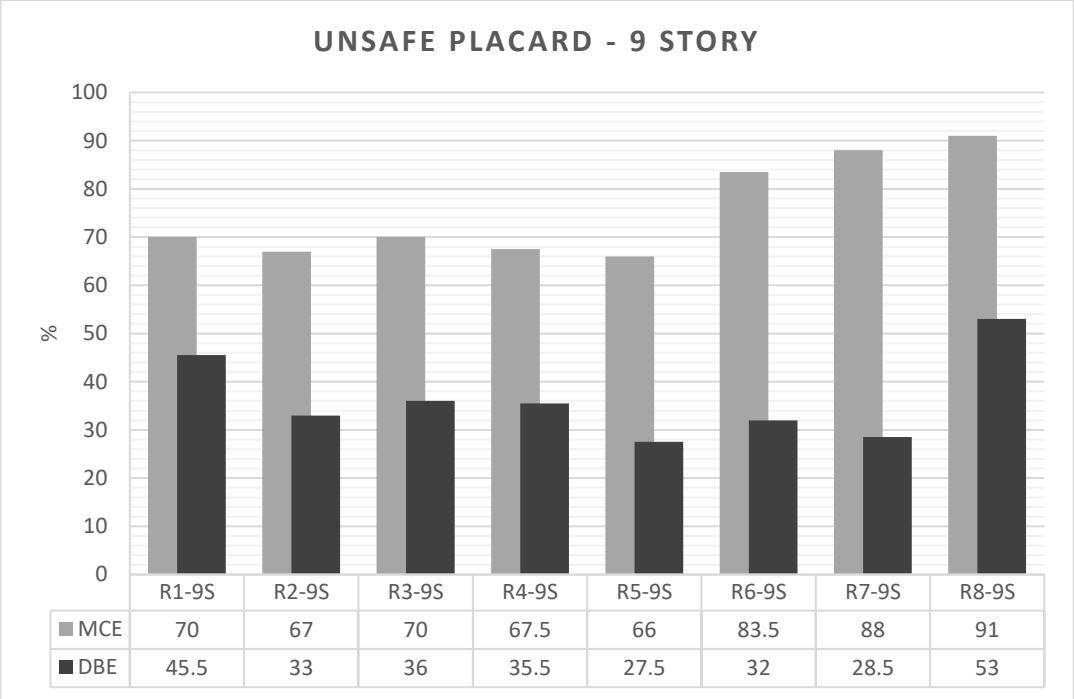

Figure 4.20. Unsafe placard probabilities for 9-Story archetypes

4.4.5 Other Results

In addition to the above-given performance results, the PACT tool also supplies several more data for the usage of contractors or decision-makers. For instance, for each damage state of fragilities, consequence functions include whether loss of life or serious injuries are possible as a result of the damage. These functions determined based on the component's weight and location and judgment. As a result of these values, the PACT tool calculates the possibility of a loss of life or severe injuries in the impacted area. In addition, with the new edition of FEMA P-58, the PACT tool also supplies environmental impact values in terms of carbon emissions and embodied energy, to restore a building to its pre-earthquake condition, or to replace the building with a new structure in the case of a total loss. The Carbon Emissions value represents the total carbon impact of repairing or replacing the building. This is calculated by multiplying the repair cost or replacement cost by the global warming potential (labeled in the dataset as "impact potential/GCC/kg co2

eq") from the United States Environmentally Extended Input-Output (USEEIO) database. The Embodied Energy value signifies the embodied energy impact of replacing or repairing the building. This value is calculated by multiplying the repair or replacement cost by the energy impact (labeled in the dataset as "resource use/enrg/MJ") from the USEEIO dataset.

Average values of fatalities, injuries, carbon emission estimations, and embodied energy values are presented in Figs. 4.21 – 4.24 for MCE seismic level. In terms of fatalities and injuries, it was observed that changing the R-Factor did not affect the results significantly. However, reducing R-Factor causes a substantial change in environmental impacts. For example, using R=2 instead of R=8 decrease the environmental impacts more than 50% in all heights.

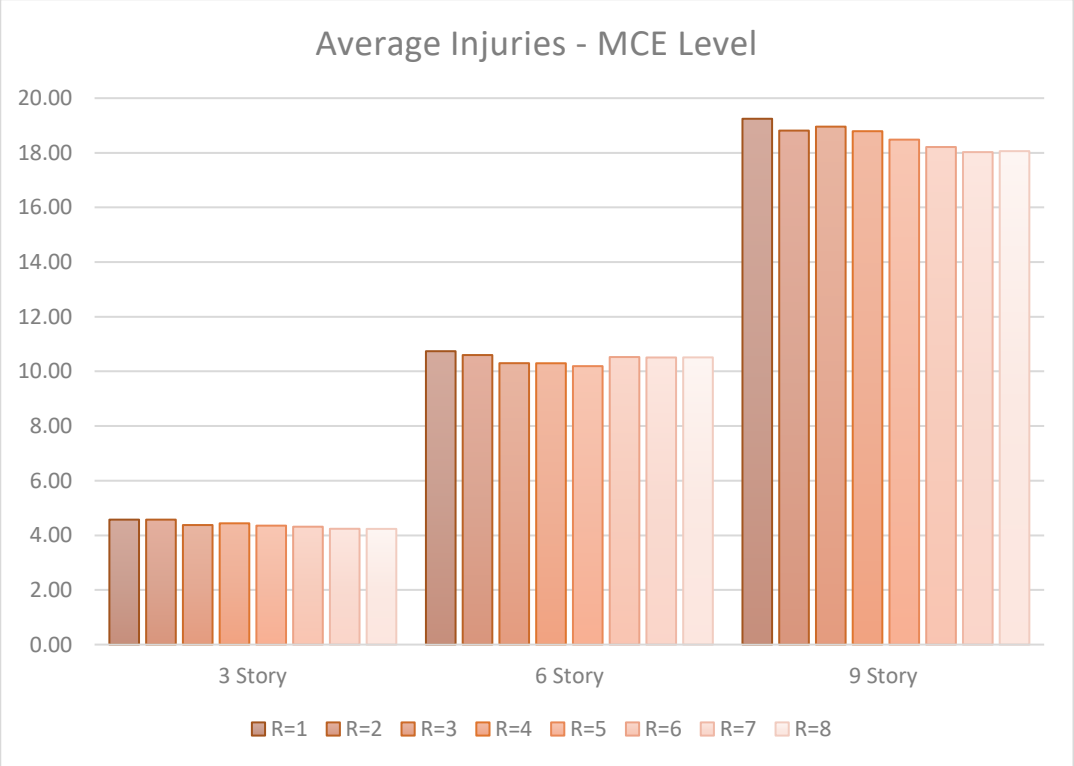

Figure 4.21. Average injury values

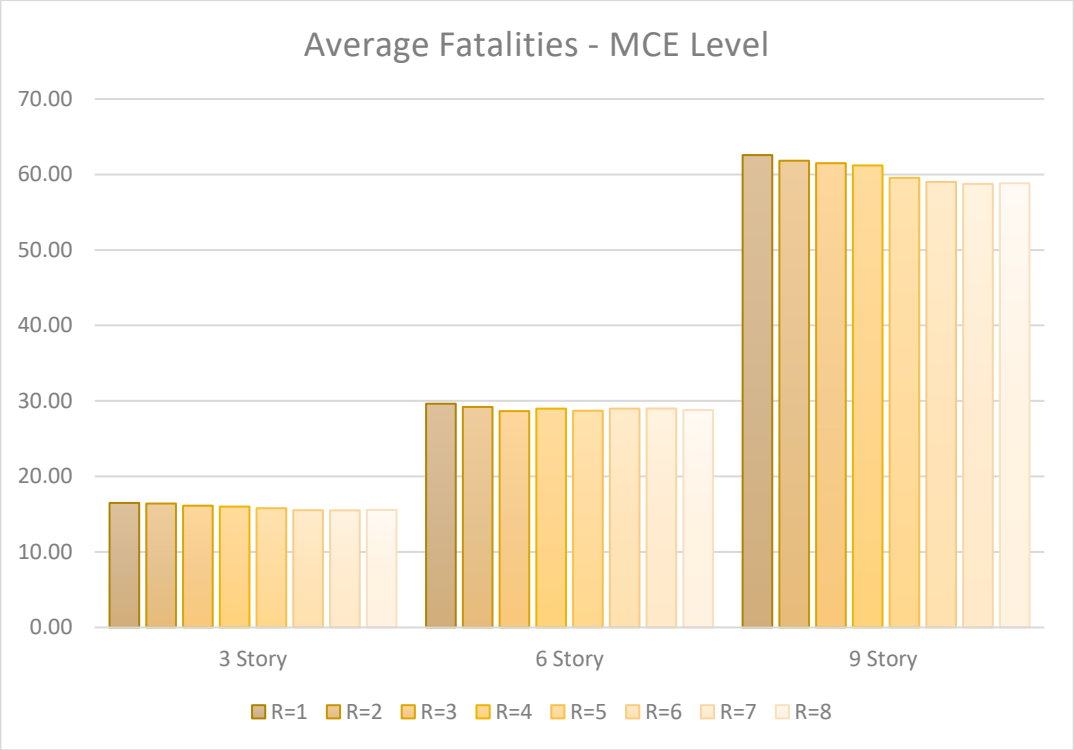

Figure 4.22. Average fatality values

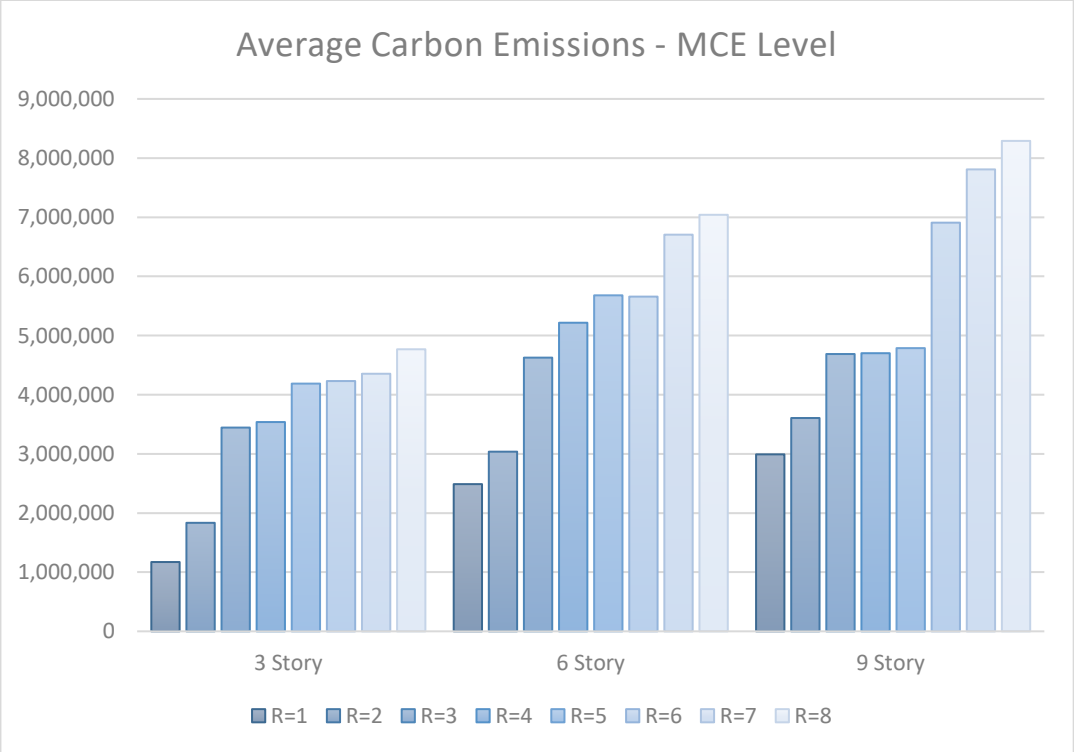

Figure 4.23. Average carbon emission values

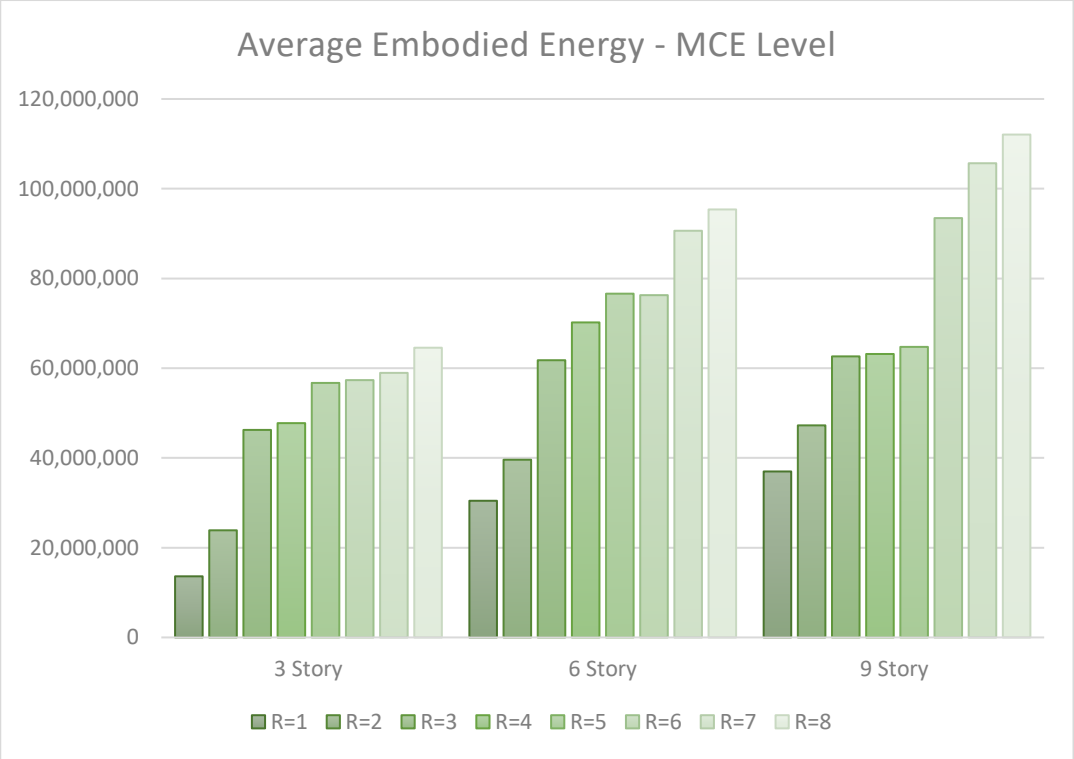

Figure 4.24. Average embodied energy values

CHAPTER 5

EVALUATION OF PERFORMANCE ASSESSMENT RESULTS

The results show that BRBFs designed using different R factors perform differently under the two seismic hazard levels considered herein. It is not possible to recommend a single R factor that will give the most satisfactory performance for all cases because of the nature of probabilistic analysis. In order to compare the performance results, the additional costs of BRBFs were computed. Repair cost after a seismic event and the initial cost of the SFRS were added to calculate the additional cost. In other words, this is the cost required to repair the building and the additional initial investment to be made if an R factor less than 8 is selected at the design stage. The additional investment values are the ones presented in Section 2.6. The additional costs for all BRBFs are presented in Figs. 5.1 – 5.3 for the archetypes subjected to both the DBE and MCE level events.

One of the most critical performance parameters of the structure is the post-earthquake irreparable residual drift. As seen from results, the replacement of BRBFs is not generally governed by high repair costs rather because of high residual drifts. Consequently, when the residual drifts govern, the repair costs stay still at very low levels (in comparison to total construction cost), which creates a major jump in the repair cost. Therefore, for BRBF buildings, avoiding residual drifts is very important. Lowering R-Factor resulted in a decrease in residual drifts in exchange for the increased initial cost.

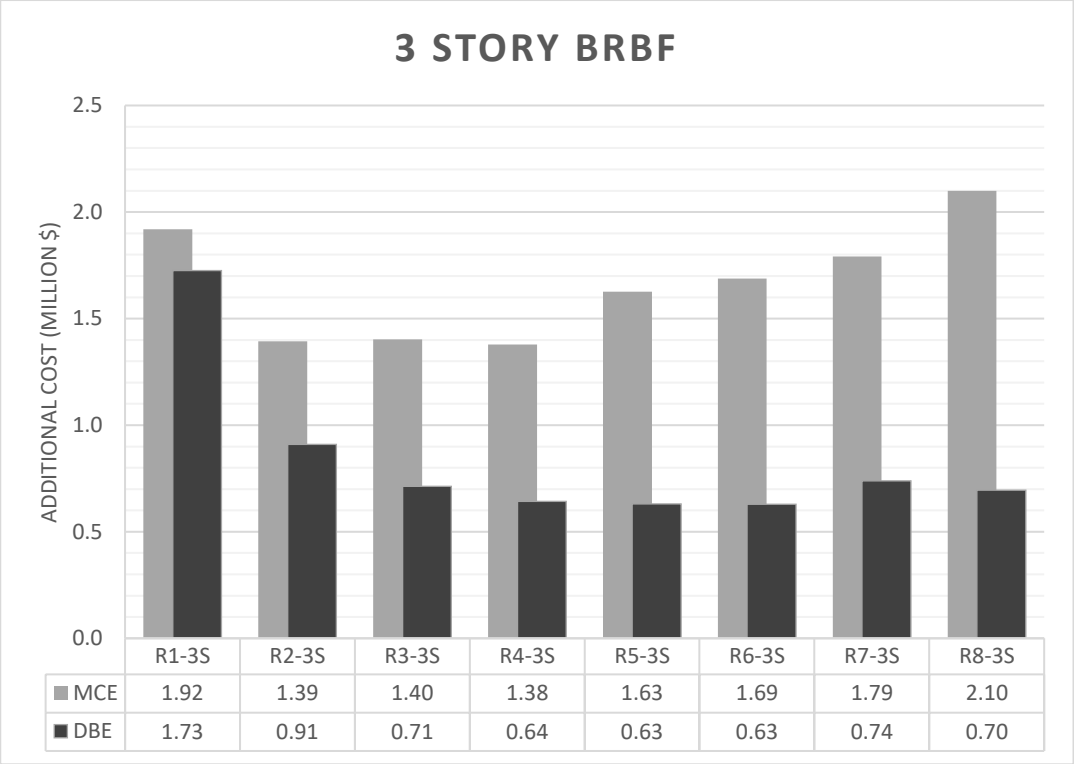

Figure 5.1. Additional Cost Analysis of 3 Story BRBF Archetypes

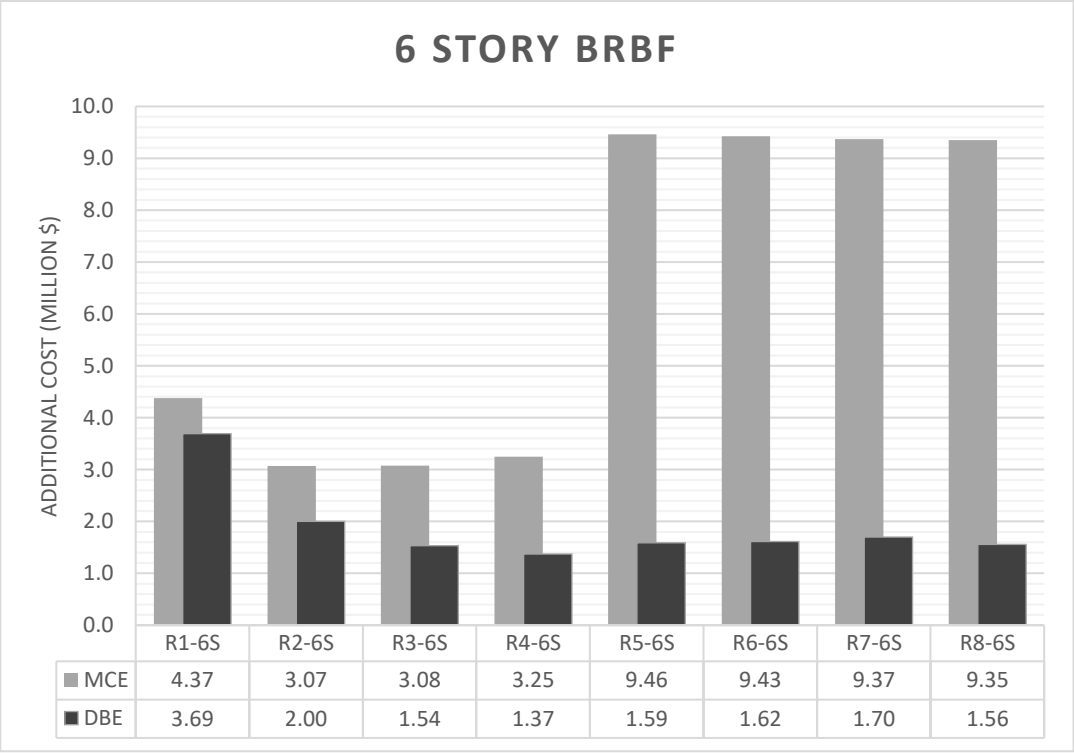

Figure 5.2. Additional Cost Analysis of 6 Story BRBF Archetypes

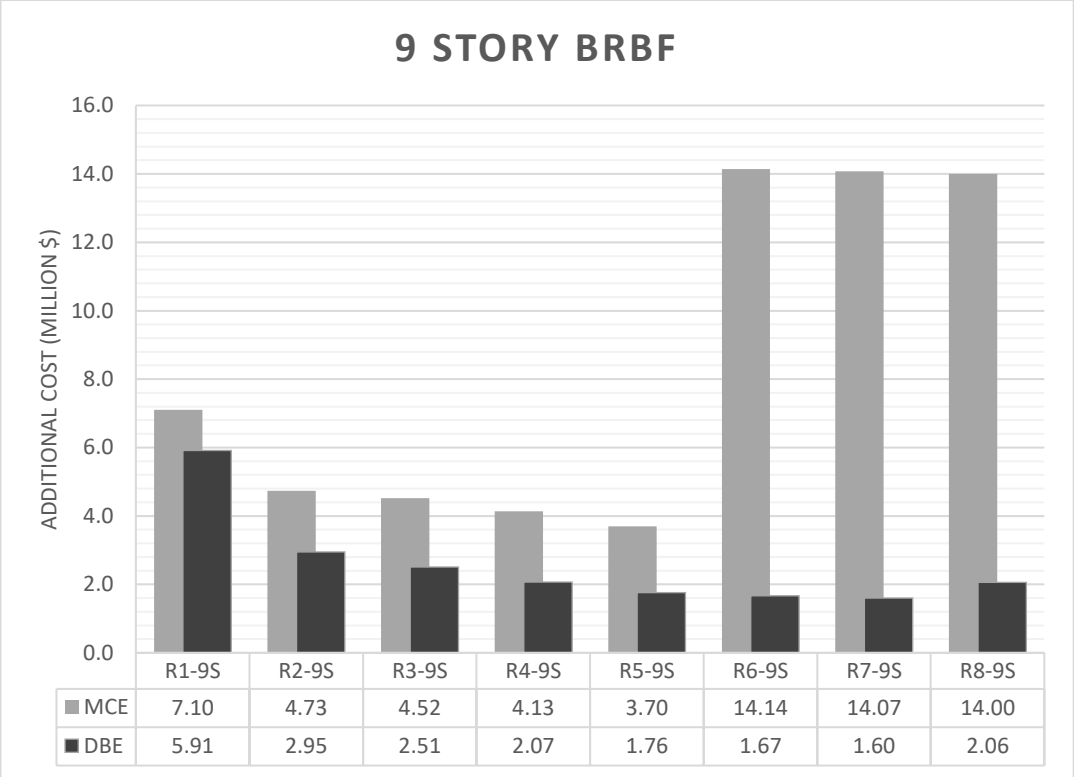

Figure 5.3. Additional Cost Analysis of 9 Story BRBF Archetypes

As mentioned earlier, 6-story BRBFs with R≥5 and 9-story BRBFs with R≥6 are expected to have an additional cost equal to the total cost of the building because these buildings will have to be demolished due to the large amounts of residual drift. Therefore, the highest R factor that can be adopted during the design stage is 4 when the damage after MCE level events is considered. For 3- , 6- and 9-story buildings, selecting an R factor of 4 is reasonable because lower R factors either do not perform better or perform slightly better. For the 3-, 6- and 9- story BRBFs the lowest additional costs are obtained by using R=4, 2 and 5, respectively. Selecting R=4 as opposed to R=2 results in only 5% change in the additional cost for the 6-story BRBF. On the other hand, selecting R=4 instead of R=5 results in 12% increase in the additional cost for the 9-story BRBF. R=4 can be recommended, considering that the R=4 design has a lower initial investment when compared with R<4 designs.

When the additional costs after a DBE level event are considered, the R=6, 4, and 7 cases produced the lowest cost for 3-, 6, and 9-story BRBFs, respectively.

The difference in costs between R=6 and R=4 cases is only 2% for the 3-story archetypes. On the other hand, this difference between R=7 and R=4 cases is 28% for the 9-story archetypes. These observations also strengthen the assertion that R=4 can be a viable option for the design of BRBFs. If an R factor of 4 is used, this will significantly reduce the probability of total replacement of especially tall BRBFs subjected to MCE level events. In addition, R=4 designs present ideal solutions for BRBFs subjected to DBE and MCE level events in terms of keeping the additional costs to a minimum.

A noteworthy observation is that lowering R-Factor too much seems to increase repair costs due to increased accelerations; however, almost no possibility of governing residual drifts was observed. Despite this fact, using such lower response factors were not suggested due to acceleration related damages that were very critical in terms of serviceability of building after an earthquake. When DBE level results for unsafe placards investigated, it was observed that due to nonstructural damages, a significant increase in unsafe placard probability was observed for R=1 archetypes.

The R=4 designs produce one of the lowest repair times among archetypes subjected to DBE level ground motions. In general, R=1 designs produced the lowest repair times among archetypes subjected to MCE level ground motions. The cases with R=4 and R=1 do not have significant differences in terms of repair times where the repair time increases by 6, 14, and 6 days for 3-, 6-, and 9-story BRBFs, respectively.

Based on the above discussions, R=4 can be considered as the ideal response factor for BRBFs from an additional cost and repair time standpoint. Higher R factors were found to be problematic for tall frames which are prone to residual drifts. According to the study of Bosco and Marino (2013), R=q=4 corresponds to designs where the story drift angle is limited to 1.25% for BRBFs designed without P-Δ effects. The following section presents a complementary study on the use of self-centering systems to mitigate residual drifts in BRBFs.

CHAPTER 6

SELF-CENTERING BUCKLING RESTRAINED BRACES

BRBs have very high energy dissipation capacity and stable hysteresis performance; however, its lower stiffness after yielding commonly result in large residual deformations after a strong earthquake. In order to cope with this deficiency, researchers and engineers conduct investigations to lower residual deformations of BRBs. Christopoulos et al.(2008) proposed a self-centering energy dissipation (SCED) bracing that utilized post-tensioned (PT) aramid-fiber tendons to provide a self-centering and friction devices to dissipate energy. In this bracing system, steel tubes push end plates on both sides to extend prestressed tendons under both tension and compression. Miller et al. (2011) introduced the pre-tensioned superelastic NiTi shape memory alloy (SMA) rods into the BRB to form self-centering BRB (SC-BRB). The design was not only overcome the deficiency of the BRB but also offered slightly larger energy dissipation capacity. Because SMA is expensive and its thermal stability is poor, the necessity for research about cheaper materials arised. Zhou et al. (2015) used basalt fiber-reinforced polymers (BFRP) as a PT tendon for SC-BRB. BFRP material has low elastic elongation and high ultimate elongation capacity. Their test indicated that the brace has an obvious flag-shaped hysteresis response with a very low residual deformation. Xie et. al. (2020) conducted research on SC-BRB's equipped with friction fuse and BFRP tendons. They proposed a SC-BRB with a friction fuse (SC-BRB-FS) which introduces a friction device at the end of the brace to increase the deformation capacity of the dual-tube SCBRB. Another innovative solution was suggested by Dong et. al. (2017, 2019). They combine disk springs with conventional BRB to obtained SC-BRB. The proposed SC-BRB is applied to a reinforced concrete double-column bridge pier and their results show that SC-BRB showed much smaller residual displacement compared to the piers equipped with conventional BRB and SCB systems. Chou et. al. (2016) proposed a

dual core self-centering sandwiched BRB which essentially a dual core self-centering brace that is positioned concentrically with a sandwich BRB. For self-centering behavior ASTM A416 Grade 270 steel tendons were used as tensioning elements. Their test program concluded that proposed SC-BRB provides appreciable energy dissipation, self-centering behavior and large deformation capacity. Xu et. al. (2016, 2017) proposed pre-pressed spring self-centering energy dissipation (PS-SCED) bracing system that combines friction energy dissipation devices tube members with a mechanism of pre-pressed disc springs. Nazarimofrad and Shokrgozar (2019) conducted analyses on self-centering BRB frames to assess performance of BRBs whose ductility are improved by utilizing SMA. They investigated the behavior of the two frames with four and eight stories under different ground motion records. Their results showed that SC-BRB's resulted in increasing ductility of the structure and decreasing residual displacements. Xu et. al. (2018) designed and tested a self-centering brace with magnetorheological fluid energy dissipating system and disk spring self-centering. The cyclic test results verified that the MR–SCB can achieve full flag-shaped responses with high ultimate bearing capacity and superior energy dissipation capability. The proposed MR–SCB also achieved to eliminate 96% of residual deformation. Most of the studies are at the academic level and to the author's knowledge, these SC-BRBs have not been commercialized yet. As a part of this study, the effect of SC-BRBs on the post-earthquake performance of defined archetypes are determined and compared with conventional BRBs.

6.1 Design and Analysis

To investigate the performance of SC-BRBs, same archetype buildings were considered and the BRB members were replaced with SC-BRB members in the numerical models. The fragility curves used for conventional BRBs were used for SC-BRBs. The SC-BRBs were modeled to have the same yielding capacity as conventional BRBs and therefore the forces on the other members of SFRS do not change. This way the same SFRS members were considered for both systems except

the bracing members. The archetypes were subjected to MCE level ground motions, where significant amounts of residual drifts were reported for conventional BRBFs. The generic load versus deformation response given in Fig. 6.1 was considered. It should be mentioned that the adopted hypothetical material model provides almost complete self-centering capability and has large energy dissipation capacity. The model represents an almost perfect SC-BRB behavior and not all SC-BRBs can exhibit such excellent performance.

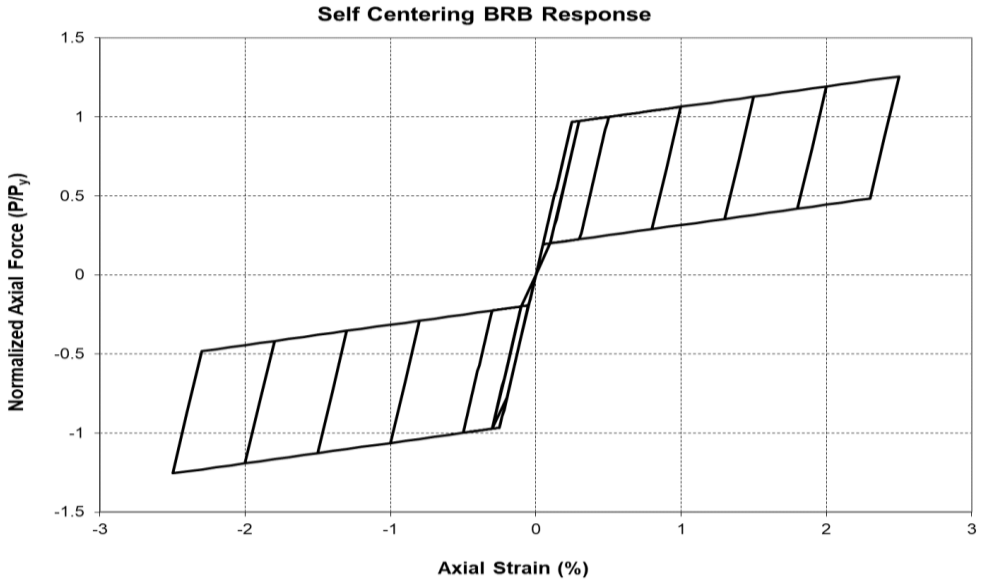

Figure 6.1. Response of Self-Centering BRB from OpenSees (Mazzoni *et al.*, 2006)

The comparisons of the engineering demand parameters are indicated in Figs 6.2 – 6.4, where results from self-centering (SC) and conventional (CONV) BRBFs are compared. In these figures, the maximum value of a demand parameter among the stories is reported. Due to the limited energy dissipation of SC-BRBs, these tend to produce higher interstory drifts when compared with conventional systems. The increase in IDR increases as the R factor is reduced. For example, the increases are 8% and 58% for 9-story archetypes designed with R=8 and R=1, respectively. As expected, very low RIDR values are reported for the SC systems indicating that the total replacement due to excessive residual drift is not a concern even after MCE level seismic events. Story accelerations also increase when SC systems are used. The increase in SA is between 3% to 23% and is less than the increase in the IDR.

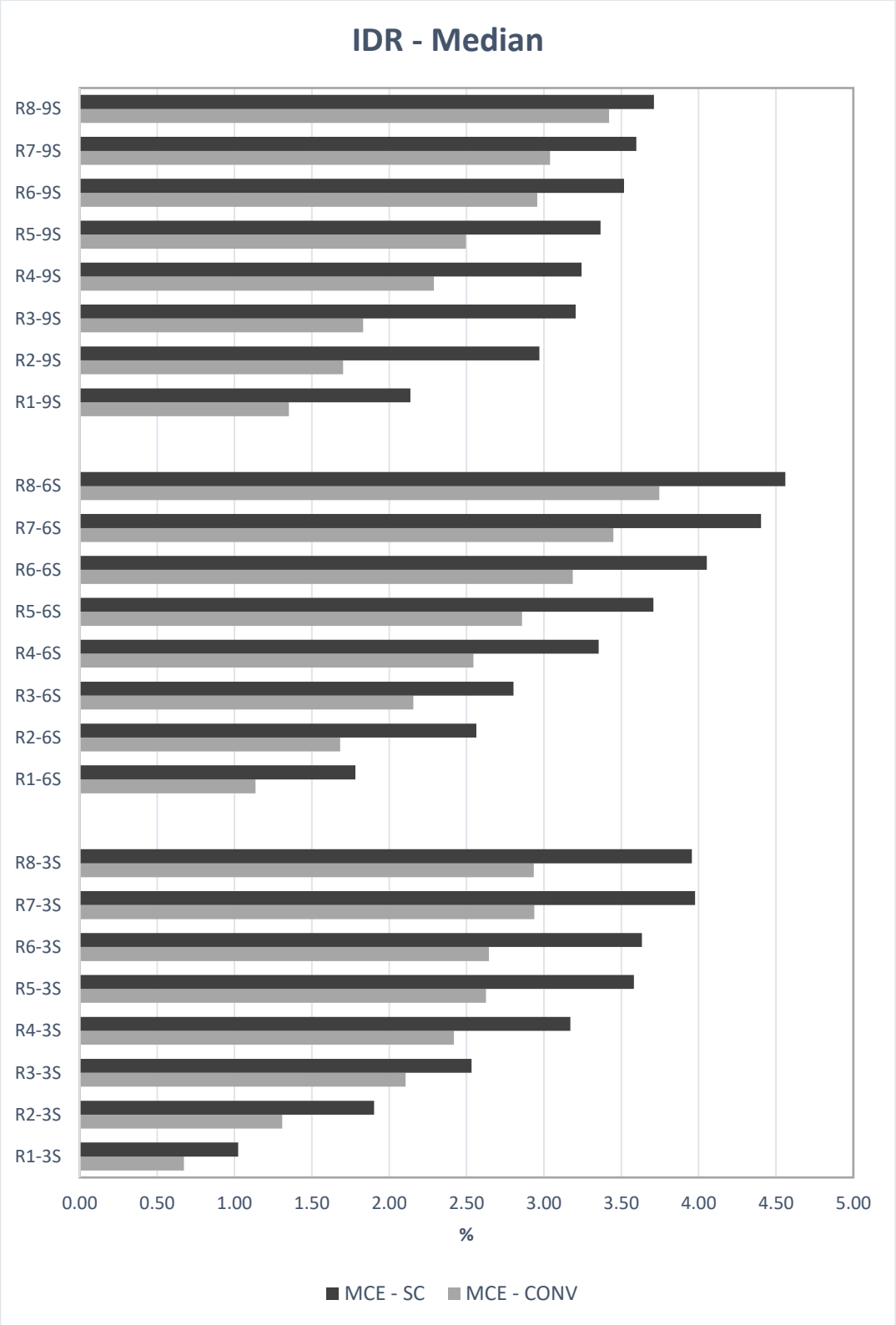

Figure 6.2. IDR Comparison of SCBRB and BRB at MCE (Max. among stories)

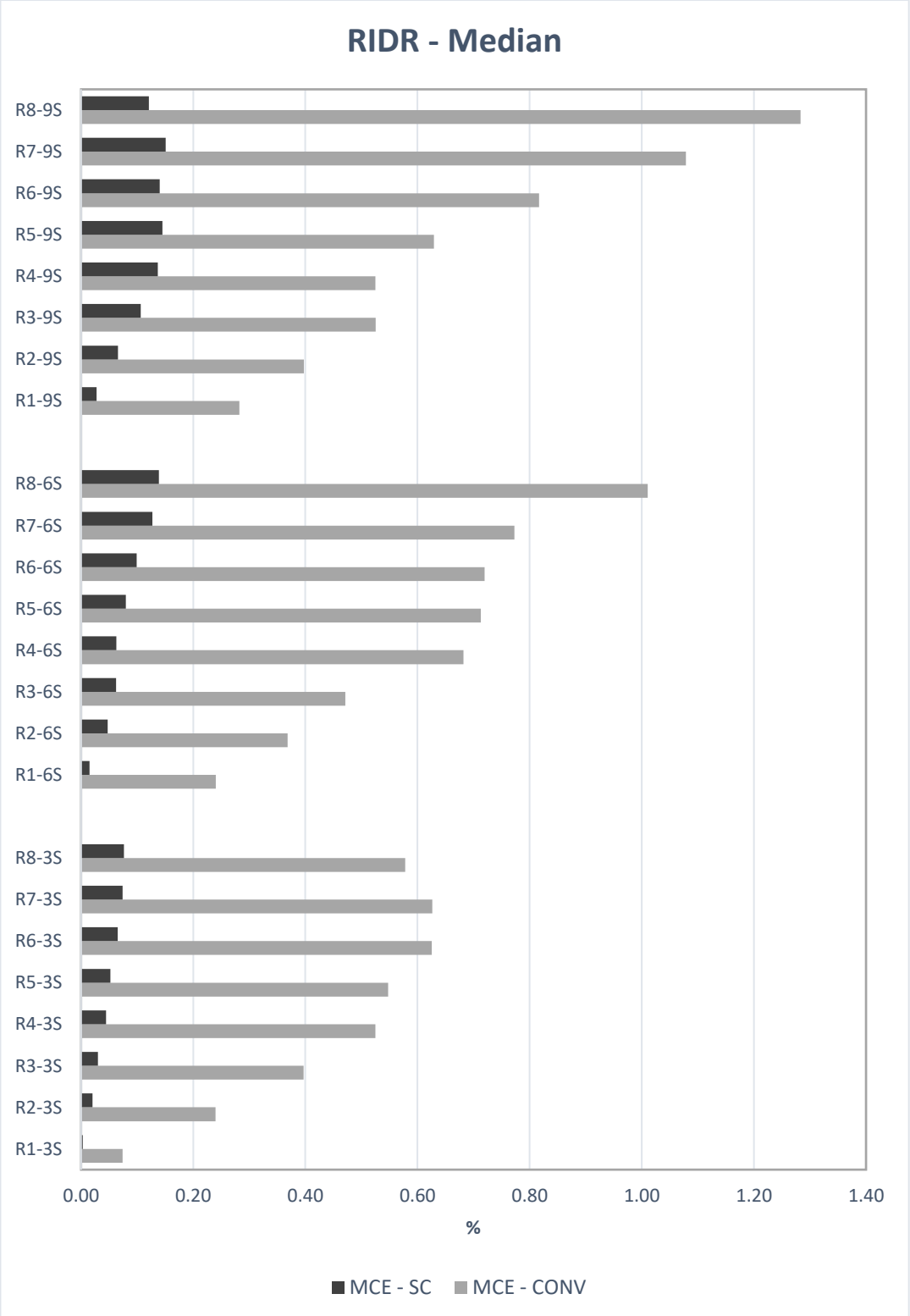

Figure 6.3. RIDR Comparison of SCBRB and BRB at MCE (Max. among stories)

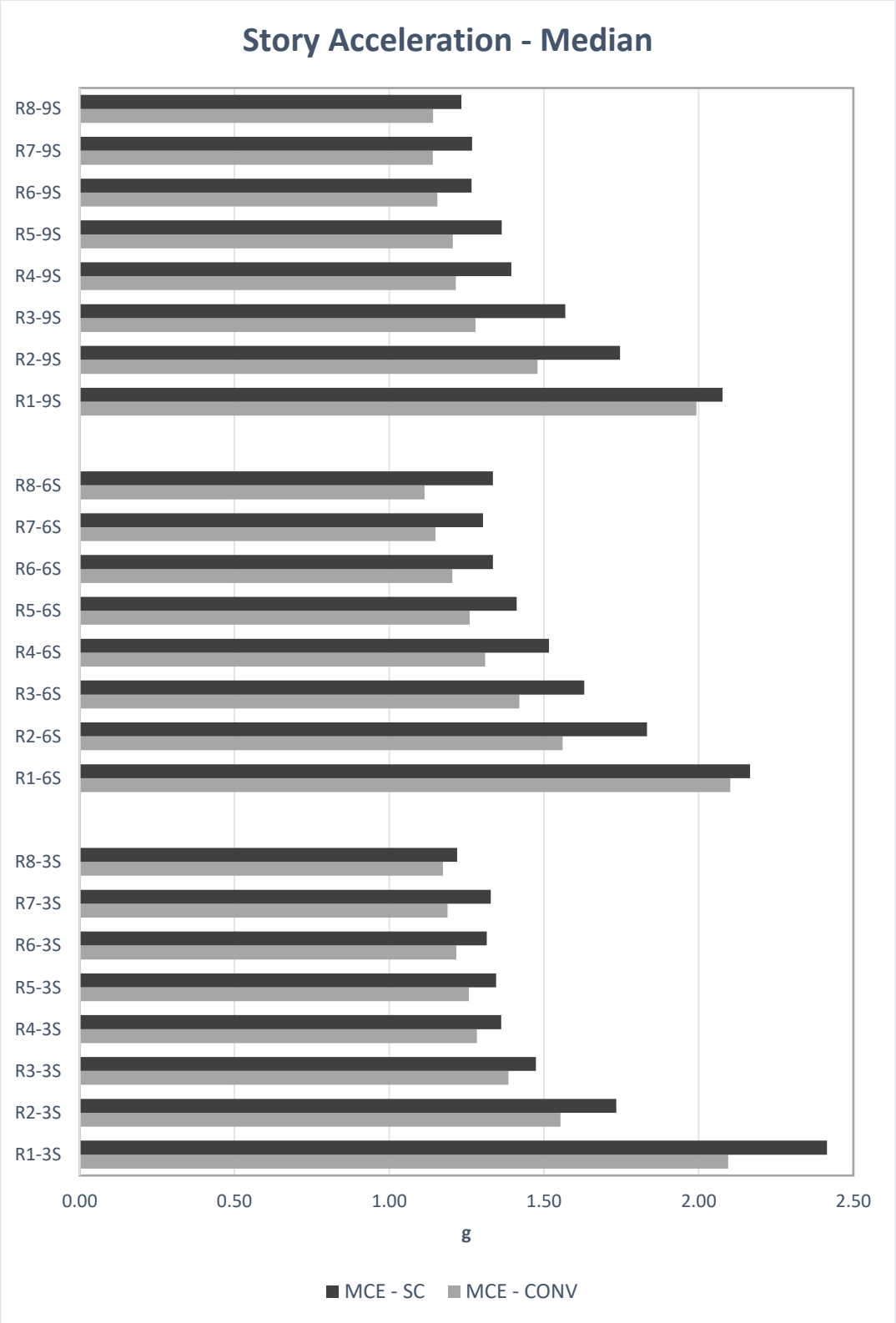

Figure 6.4. SA Comparison of SCBRB and BRB at MCE (Max. among stories)

6.2 Performance Analysis

The repair costs for SC-BRBFs were calculated by making use of the PACT tool. The ratios of the median repair cost to initial cost are reported in Figs. 6.5-6.7 and are compared with the ones for conventional BRBFs. It is evident from these figures that the use of SC-BRBs significantly reduces the repair cost for 6- and 9-story frames in which total replacement is expected. For these frames, using SC-BRBs makes R>4 designs viable.

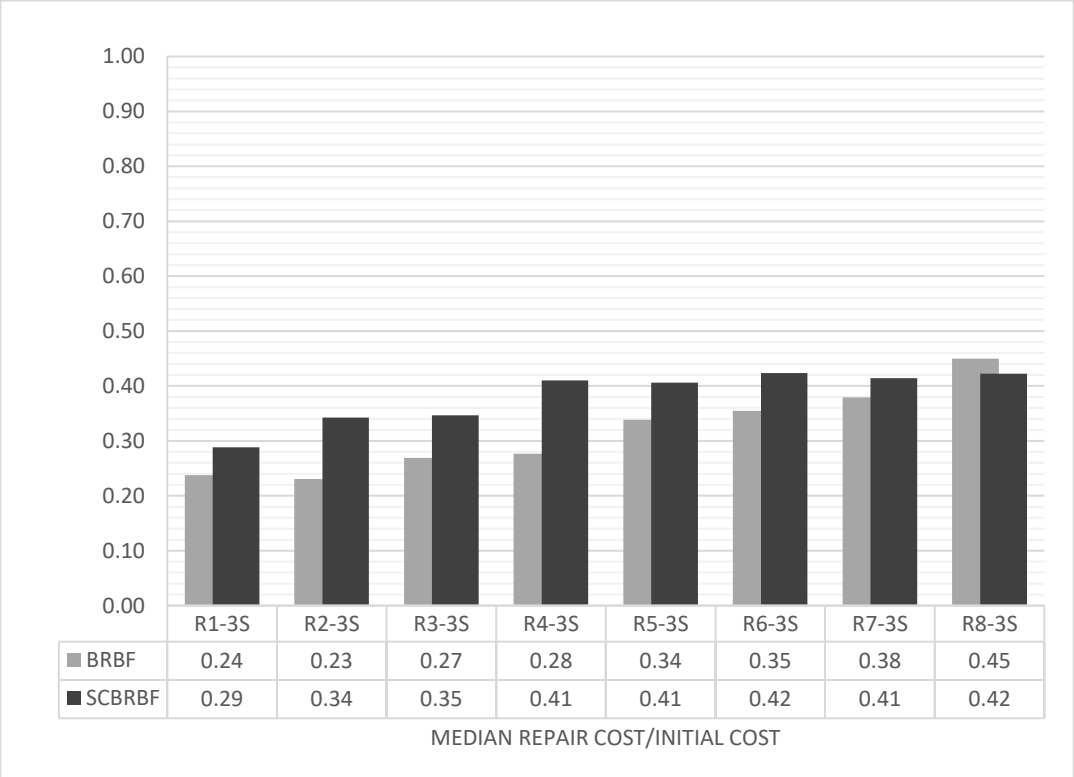

Figure 6.5. Median repair cost comparison of SCBRB and BRB (3-Story)

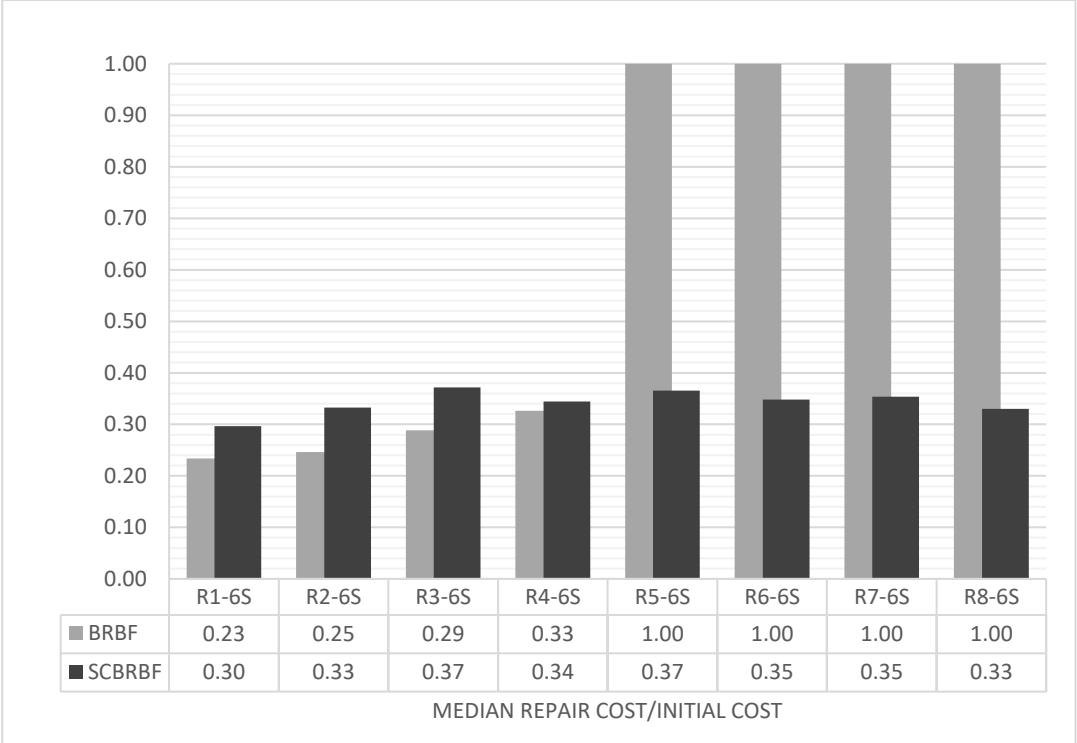

Figure 6.6. Median repair cost comparison of SCBRB and BRB (6-Story)

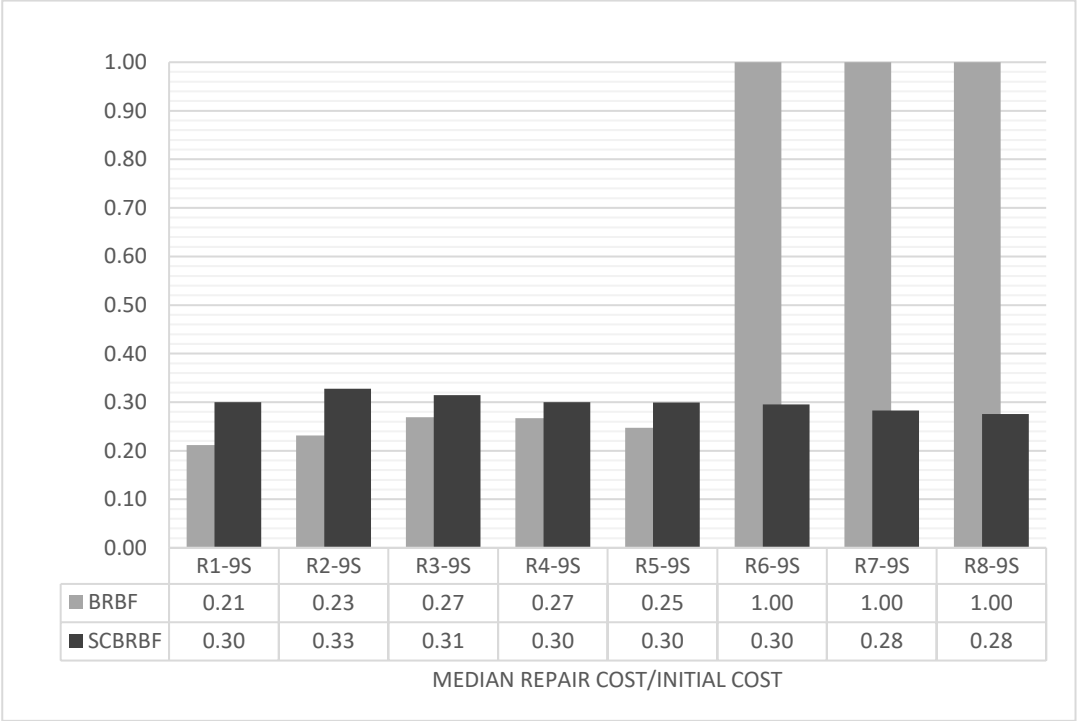

Figure 6.7. Median repair cost comparison of SCBRB and BRB (9-Story)

An additional cost analysis, similar to the one for conventional BRBs, was also conducted. The costs of SC-BRBs are not available at the time of the writing, but it is expected that these BRBs cost more than conventional BRBs due to the additional materials needed to provide self-centering behavior. In order to make a fair comparison between designs employing different R factors, the cost of SC-BRBs was considered similar to the conventional BRBs. The additional costs, which consist of the cost of repair and initial costs, are reported in Figs. 6.8-6.10 for the SC-BRBF archetypes. According to the data, R=8 presents the best solution in terms of the additional cost of 6- and 9-story archetypes. For 3-story archetypes, R=3 presents the lowest additional cost and using R=8 results in an increase of only 11%. In other words, all R≥3 cases provide similar performances. Designs employing R=8 can be recommended for SC-BRBFs considering the additional cost of repair and low initial investment as compared to designs with other R factors.

The costs associated with conventional BRBF archetypes designed with R=4 can be compared with costs associated with SC-BRBFs designed with R=8. The initial costs of these two systems are identical if the SC-BRB costs are 2.33, 2.44, 2.87 times the cost of conventional BRBs for 3-, 6-, and 9-story archetypes, respectively. The sum of the initial cost and repair cost is identical if the SC-BRB cost is 2.3 times the cost of conventional BRBs for 6- and 9-story archetypes. For the 3-story archetypes, the SC-BRBs cannot offer a cheaper solution because the repair costs of SC-BRBFs dominate over the initial costs. In other words, the sum of the repair and initial cost of SC-BRBF designed with R=8 is more than that of conventional BRBF designed with R=4.

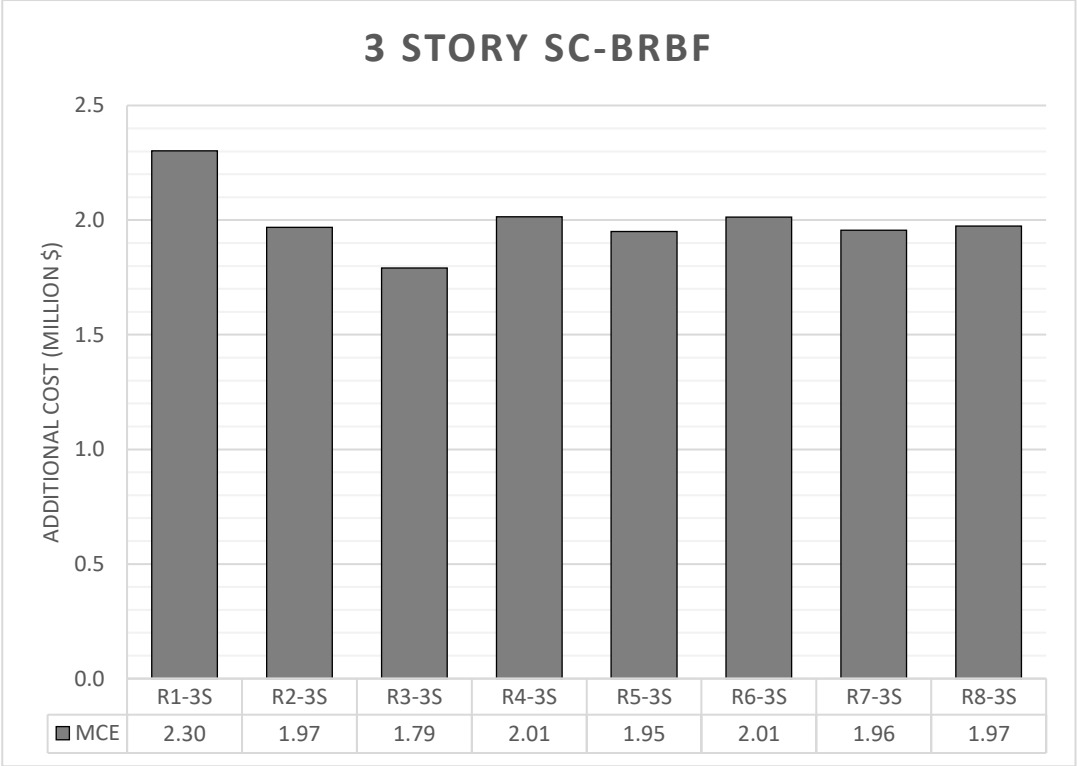

Figure 6.8. Additional Cost Analysis of 3 Story SC-BRBF Archetypes

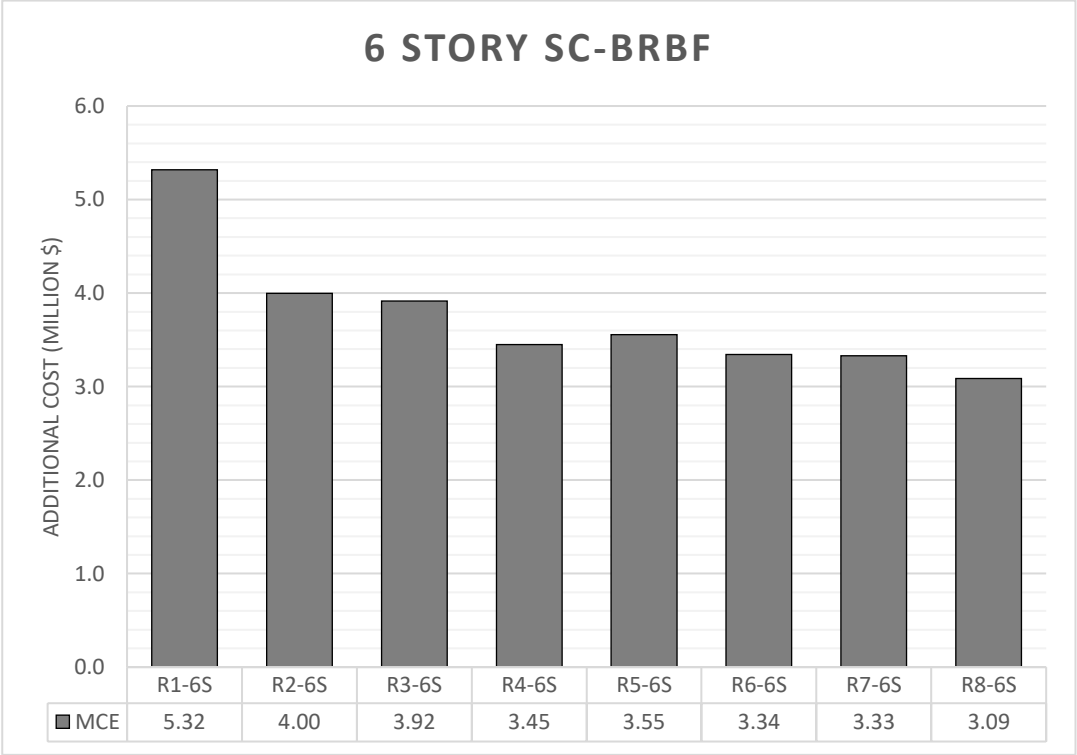

Figure 6.9. Additional Cost Analysis of 6 Story SC-BRBF Archetypes

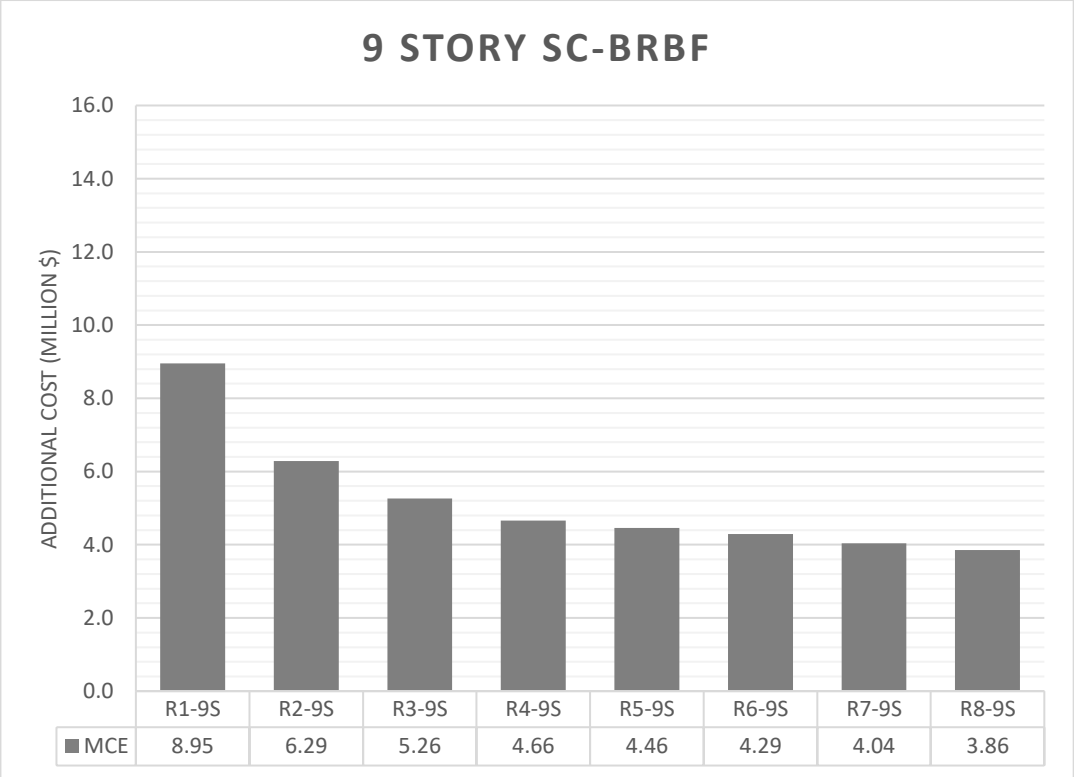

Figure 6.10. Additional Cost Analysis of 9 Story SC-BRBF Archetypes

CHAPTER 7

CONCLUSIONS

A total of 24 BRBF archetypes with the response modification factor in the range of one to eight were compared using next-generation performance evaluation procedure FEMA P-58. The archetypes, which were designed according to ASCE 7-16, AISC 341-16, and AISC 360-16, were subjected to DBE and MCE level 22 pairs of ground motions. As an input parameter of next-generation performance evaluation, nonlinear time history analyses were conducted, and results were presented in terms of story drifts, residual drifts, story velocities, and story accelerations. The results revealed that 6- and 9-story BRBFs designed with R>4 are prone to large residual drifts, which in turn result in total replacement of the building after being subjected to MCE level ground motions.

The initial construction costs of SFRS of archetypes were calculated to see the effect of changing design R-Factor on the construction stage. The results show that decreasing R-Factor to 4 increased the initial cost, only by 32%. However, decreasing R-Factor further increased the initial cost in an increased fashion as 58%, 120%, and 324% increases were observed for R=3, R=2, and R=1 archetypes, respectively.

With using PACT tool, analyses results were converted to performance parameter and performance of archetypes were compared using repair cost, repair time, irreparable residual drift probability, and unsafe placard probability. Performance assessment results showed that buildings designed using code conforming R=8, have a high chance of being in an irreparable condition, or have a significant amount of repair cost after MCE level earthquake. Furthermore, both DBE and MCE results presented that as the height of the building increase, the performance deficiency of using R=8 for design increases.

In order to obtain better performance, lower response modification factors were analyzed, and a comparative study was conducted to find optimum R-Factor in terms of post-earthquake performance and initial cost. The additional costs were calculated by summing up the additional investment cost due to the selection of R<8 and the repair costs. The results show that decreasing R-Factor increases post-earthquake performance until acceleration governed nonstructural damages dominate. However, lowering R-Factor increases initial construction costs which make the comparison harder.

Due to the nature of performance-based design, there is no specific R-Factor that gives optimum results since the post-earthquake performance of buildings depends on the initial investment and, consequently, to the investors and decision-makers. In this study, additional cost study was conducted from obtained data to propose R-Factor that can be used for more optimized buildings in compare to code-suggested ones, in terms of post-earthquake performance.

An assessment of additional costs showed that selecting R=4 (and Cd=2.5) for the design of BRBFs is the most ideal solution when performance under DBE and MCE level events are considered.

The performances of self-centering BRBFs were also investigated. The results showed that 6- and 9-story SC-BRBFs designed using R=8 do not suffer from residual drift, indicating that using these special braces can alleviate the total loss problem associated with conventional BRBs. When archetypes designed with different R factors are compared from an additional cost standpoint, selecting R=8 for the design of SC-BRBFs gives the most ideal solution.

REFERENCES

Abou-Elfath, H., Shamel Fahmy, A. and Mohamed Khalifa, K. (2018) 'Response modification factors of buckling-restrained braced frames designed according to the Egyptian code', *Alexandria Engineering Journal*. Faculty of Engineering, Alexandria University, 57(4), pp. 2851–2864.

American Institute of Steel Construction (1994) *Load & Resıstance Factor Desıgn*. Second Edition. Chicago, Illinois: AISC.

American Institute of Steel Construction (2012) *Seismic Design Manual*. Second edition.

American Institute of Steel Construction (2016a) *Seismic Provisions for Structural Steel Buildings, ANSI/AISC 341-16*. Chicago, Illinois: AISC.

American Institute of Steel Construction (2016b) *Specification for Structural Steel Buildings, ANSI/AISC 360-16*. Chicago, Illinois: AISC.

American Society of Civil Engineers (2005) *Minimum Design Loads for Buildings and Other Structures, ASCE/SEI 7-05*. Reston, Virginia: ASCE.

American Society of Civil Engineers (2017a) *Minimum Design Loads and Associated Criteria for Buildings and Other Structures, ASCE/SEI 7-16, Science*. Reston, Virginia: ASCE.

American Society of Civil Engineers (2017b) *Seismic Evaluation and Retrofit of Existing Buildings, ASCE/SEI 41-17*. Reston, Virginia: ASCE.

Applied Technology Research Council (1989) 'ATC-20, Procedures for Postearthquake Safety Evaluation of Buildings'. Redwood City, California.

Asgarian, B. and Shokrgozar, H. R. (2009) 'BRBF response modification factor', *Journal of Constructional Steel Research*. Elsevier Ltd, 65(2), pp. 290–298.

Black, C. J., Makris, N. and Aiken, I. D. (2004) ‘Component Testing, Seismic Evaluation and Characterization of Buckling-Restrained Braces’, *Journal of Structural Engineering*, 130(June 2004), pp. 1562–1569.

Bosco, M. and Marino, E. M. (2013) ‘Design method and behavior factor for steel frames with buckling restrained braces’, *Earthquake Engıneerıng And Structural Dynamıcs*, (42), pp. 1243–1263.

Bozkurt, M. B. and Topkaya, C. (2016) ‘Development of welded overlap core steel encased buckling-restrained braces’, *Journal of Constructional Steel Research*, 127, pp. 151–164.

Cardone, D. and Perrone, G. (2015) ‘Damage and Loss Assessment of Pre-70 RC Frame Buildings with FEMA P-58: A Case Study’, in *Second ATC & SEI Conference on Improving the Seismic Performance of Existing Buildings and Other Structures*, pp. 363–374.

Chou, C. C., Tsai, W. J. and Chung, P. T. (2016) ‘Development and validation tests of a dual-core self-centering sandwiched buckling-restrained brace (SC-SBRB) for seismic resistance’, *Engineering Structures*. Elsevier Ltd, 121, pp. 30–41.

Christopoulos, C., Pampanin, S. and Priestley, M. (2004) ‘Seismic design and response of buildings including residual deformations’, in *Proceedings of the 13th World Conference on Earthquake Engineering*.

Christopoulos, C. *et al.* (2008) ‘Self-centering energy dissipative bracing system for the seismic resistance of structures: Development and validation’, *Journal of Structural Engineering*, 134(1), pp. 96–107.

Core Brace. Available at: https://corebrace.com/ (Accessed: 9 February 2020).

Dazio, A. (2004) ‘Residual Displacements in Capacity Designed Reinforced Concrete Structures’, *Proceedings of the 13th World Conference on Earthquake Engineering*, (2399).

Dehghani, M. and Tremblay, R. (2018) ‘Design and full-scale experimental evaluation of a seismically endurant steel buckling-restrained brace system’, *Earthquake Engineering and Structural Dynamics*, 47(1), pp. 105–129.

Del Gobbo, G. M., Williams, M. S. and Blakeborough, A. (2018) ‘Seismic performance assessment of Eurocode 8-compliant concentric braced frame buildings using FEMA P-58’, *Engineering Structures*. Elsevier, 155(August 2017), pp. 192–208.

Del Vecchio, C. *et al.* (2018) ‘Repair costs of existing rc buildings damaged by the l’aquila earthquake and comparison with FEMA P-58 predictions’, *Earthquake Spectra*, 34(1), pp. 237–263.

Dong, H. *et al.* (2017) ‘Performance of an innovative self-centering buckling restrained brace for mitigating seismic responses of bridge structures with double-column piers’, *Engineering Structures*. Elsevier Ltd, 148(October), pp. 47–62.

Dong, H. *et al.* (2019) ‘Hysteretic performance of RC double-column bridge piers with self-centering buckling-restrained braces’, *Bulletin of Earthquake Engineering*. Springer Netherlands, 17(6), pp. 3255–3281.

Erochko, J. *et al.* (2011) ‘Residual drift response of SMRFs and BRB frames in steel buildings designed according to ASCE 7-05’, *Journal of Structural Engineering*, 137(5), pp. 589–599.

Eryasar, M. E. and Topkaya, C. (2010) ‘An experimental study on steel-encased buckling-restrained brace hysteretic dampers’, *Earthquake Engıneerıng And Structural Dynamıcs*, (39), pp. 561–581.

European Committee for Standardization (2004) ‘Eurocode 8, Design of structures for earthquake resistance - part 1: general rules, seismic actions and rules for buildings’, EN 1998-1.

Fahnestock, L. A., Ricles, J. M. and Sause, R. (2007) 'Experimental Evaluation of a Large-Scale Buckling-Restrained Braced Frame', *Journal of Structural Engineering, ASCE*, 133(9), pp. 1205–1214.

Fahnestock, L. A., Sause, R. and Ricles, J. M. (2007a) 'Seismic Response and Performance of Buckling-Restrained Braced Frames', *Journal of Structural Engineering, ASCE*, 133(9), pp. 1195–1204.

Fahnestock, L. A., Sause, R. and Ricles, J. M. (2007b) 'Seismic Response and Performance of Buckling-Restrained Braced Frames', *Journal of Structural Engineering, ASCE*, 133(9), pp. 1195–1204.

Federal Emergency Management Agency (2006) *Next Generation Performance-Based Seismic Design Guidelines - Program Plan for New and Existing Buildings, FEMA 445*. Washington, DC: FEMA.

Federal Emergency Management Agency (2009) *Quantification of Building Seismic Performance Factors, FEMA P695*. Washington, D.C.: FEMA.

Federal Emergency Management Agency (2018a) *Building the performance you need, FEMA P-58-7*. Washington, D.C.

Federal Emergency Management Agency (2018b) *Guidelines for Performance-Based Seismic Design of Buildings, FEMA P-58-6*. Washington, D.C.: FEMA.

Federal Emergency Management Agency (2018c) *Seismic Performance Assessment of Buildings. Volume 1 – Methodology, FEMA P-58-1*. Washington, D.C.: FEMA.

Federal Emergency Management Agency (2018d) *Seismic Performance Assessment of Buildings Volume 2 – Implementation Guide, FEMA P-58-2*. Washington, D.C.: FEMA.

Fujimoto, M. *et al.* (1990) 'Development of unbonded brace', *Quarterly Column*, 115(January 1990), pp. 91–96.

Guerrero, H. *et al.* (2017) ‘Evaluation of the economic benefits of using Buckling-Restrained Braces in hospital structures located in very soft soils’, *Engineering Structures*, 136, pp. 406–419.

Jarrett, J. A., Judd, J. P. and Charney, F. A. (2015) ‘Comparative evaluation of innovative and traditional seismic-resisting systems using the FEMA P-58 procedure’, *Journal of Constructional Steel Research*. Elsevier Ltd, 105, pp. 107–118.

Jorge Ruiz-Garcia and E. Miranda (2005) Performance-based assessment of exıstıng structures accountıng for resıdual Dısplacements. California.

Kiggins, S. and Uang, C. M. (2006) ‘Reducing residual drift of buckling-restrained braced frames as a dual system’, *Engineering Structures*, 28(11), pp. 1525–1532.

Kim, J., Park, J. and Kim, S. D. (2009) ‘Seismic behavior factors of buckling-restrained braced frames’, *Structural Engineering and Mechanics*, 33(3), pp. 261–284.

López, W. and Sabelli, R. (2004) ‘Seismic Design of Buckling-Restrained Braced Frames’, *SteelTIPS*, 33(July), pp. 1251–1260.

Mahdavipour, M. A. and Deylami, A. (2014) ‘Probabilistic assessment of strain hardening ratio effect on residual deformation demands of Buckling-Restrained Braced Frames’, *Engineering Structures*. Elsevier Ltd, 81, pp. 302–308.

Mahmoudi, M. and Zaree, M. (2013) ‘Determination the response modification factors of buckling restrained braced frames’, *Procedia Engineering*. Elsevier B.V., 54(2005), pp. 222–231.

Mazzoni, S. *et al.* (2006) ‘Open System for Earthquake Engineering Simulation (OpenSEES) User Command-Language Manual’, *Pacific Earthquake Engineering Research Center*, p. 465.

McCormick, J. *et al.* (2008) ‘Permissible Residual Deformation Levels for Building Structures Considering both Safety and Human Elements’, *The 14th World Conference on Earthquake Engineering*, p. 8.

Miller, D.J.; Fahnestock, L.A.; Eatherton, M. R. (2011) ‘Self-Centering Buckling-Restrained Braces for Advanced Seismic Performance’, *Structures Congress 2011*, pp. 960–970.

Moni, M., Moradi, S. and Alam, M. S. (2016) ‘Response modification factors for steel buckling restrained braced frames designed as per the 2010 National Building Code of Canada’, *Canadian Journal of Civil Engineering*, 43(8), pp. 702–715.

Naghavi, M. *et al.* (2019) ‘Numerical evaluation of the hysteretic behavior of concentrically braced frames and buckling restrained brace frame systems’, *Journal of Building Engineering*. Elsevier Ltd, 22(December 2018), pp. 415–428.

Nazarimofrad, E. and Shokrgozar, A. (2019) ‘Seismic performance of steel braced frames with self-centering buckling-restrained brace utilizing superelastic shape memory alloys’, *Structural Design of Tall and Special Buildings*, 28(16), pp. 1–11.

NEHRP Consultants Joint Venture (2010) ‘Evaluation of the FEMA P-695 Methodology for Quantification of Building Seismic Performance Factors (NIST GCR 10-917-8)’, *NIST*.

Özkılıç, Y. O., Bozkurt, M. B. and Topkaya, C. (2018) ‘Evaluation of seismic response factors for BRBFs using FEMA P695 methodology’, *Journal of Constructional Steel Research*, 151, pp. 41–57.

Polese, M., Di Ludovico, M. and Prota, A. (2018) ‘Post-earthquake reconstruction: A study on the factors influencing demolition decisions after 2009 L’Aquila earthquake’, *Soil Dynamics and Earthquake Engineering*. Elsevier Ltd, 105(November 2017), pp. 139–149.

Romano *et al.* (2015) ‘Components Fragility Functions and Comparative Seismic Risk Analysis of an older R / C Building based on FEMA P-58’, *XVI Convegno ANIDIS L’Aquila 2015*, (September).

RSMeans Online Square foot estimator. Available at: https://www.rsmeans.com/ (Accessed: 9 February 2020).

Sabelli, R. (2008) ‘Buckling-Restrained Braced Frames’, (March), p. 2008.

Sabelli, R., Mahin, S. and Chang, C. (2003) ‘Seismic demands on steel braced frame buildings with buckling-restrained braces’, *Engineering Structures*, 25(5), pp. 655–666.

Safiey, A. *et al.* (2019) ‘Rethinking Treatment of Irreparability in the Context of Performance-Based Earthquake Engineering’, in *Structures Congress 2019*, pp. 230–236.

Speicher, M. S. and Harris, J. L. (2018) ‘Collapse Prevention seismic performance assessment of new buckling-restrained braced frames using ASCE 41’, *Engineering Structures*. Elsevier, 164(January), pp. 274–289.

Star Seismic Europe Ltd. (2010) ‘Cost Advantages of Buckling Restrained Braced Frame Buildings’.

Star Seismic Europe Ltd. *Star Seismic Brochure - Buckling Restrained Brace*.

Takeuchi, T. and Wada, A. (2018) ‘Review of buckling-restrained brace design and application to tall buildings’, *International Journal of High-Rise Buildings*, 7(3), pp. 187–195.

Tremblay, R. *et al.* (2006) ‘Seismic testing and performance of buckling-restrained bracing systems’, *Canadian Journal of Civil Engineering*, 33(2), pp. 183–198.

Uang, C. and Nakashima, M. (2004) ‘Chapter 16: Steel Buckling- Restrained Braced Frames’, in, pp. 1–37.

Xie, Q. (2005) ‘State of the art of buckling-restrained braces in Asia’, *Journal of Constructional Steel Research*, 61(6), pp. 727–748.

Xie, Q., Zhou, Z. and Meng, S. P. (2020) ‘Experimental investigation of the hysteretic performance of self-centering buckling-restrained braces with friction fuses’, *Engineering Structures*. Elsevier, 203(October 2019), p. 109865.

Xu, L.-H., Fan, X.-W. and Li, Z.-X. (2017) ‘Cyclic behavior and failure mechanism of self-centering energy dissipation braces with pre-pressed combination disc springs’, *Earthquake Engıneerıng & Structural Dynamıcs*, (46), pp. 1065–1080.

Xu, L. H., Fan, X. W. and Li, Z. X. (2016) ‘Development and experimental verification of a pre-pressed spring self-centering energy dissipation brace’, *Engineering Structures*. Elsevier Ltd, 127, pp. 49–61.

Xu, L. H., Xie, X. S. and Li, Z. X. (2018) ‘A self-centering brace with superior energy dissipation capability: Development and experimental study’, *Smart Materials and Structures*. IOP Publishing, 27(9).

Xu, Z. *et al.* (2019) ‘A prediction method of building seismic loss based on BIM and FEMA P-58’, *Automation in Construction*, 102(February), pp. 245–257.

Yazgan, U. (2010) The use of post-earthquake residual displacements as a performance indicator in seismic assessment, IBK Bericht.

Zeng, X. *et al.* (2016) ‘Application of the FEMA-P58 methodology for regional earthquake loss prediction’, *Natural Hazards*.Springer Netherlands, 83, pp.177–192.

Zhou, Z. *et al.* (2015) ‘Experimental Investigation of the Hysteretic Performance of Dual-Tube Self-Centering Buckling-Restrained Braces with Composite Tendons’, *Journal of Composites for Construction*, 19(6), pp. 1–13.

Zona, A. and Dall’Asta, A. (2012) ‘Elastoplastic model for steel buckling-restrained braces’, *Journal of Constructional Steel Research*. Elsevier Ltd, 68(1), pp. 118–125.